NTNU
Norwegian University of
Science and Technology

Dynamic Simulation of Gas Expansion in Marine Risers

Naveen Velmurugan

Petroleum Engineering
Submission date: June 2016
Supervisor: John-Morten Godhavn, IPT
Co-supervisor: Espen Hauge, Statoil

Norwegian University of Science and Technology
Department of Petroleum Engineering and Applied Geophysics

Dynamic Simulation of Gas Migration in Marine Risers

Naveen Velmurugan

June 17, 2016

To my parents and brother

Abstract

The main objective of the work is to study the dynamic behavior of gas expansion in marine risers. In case of well control situations in deep and ultra deep waters, gas influx shows no warnings if not little, making it difficult to handle the gas. It can be observed that the gas is completely soluble in the base oil of the drilling mud leaving no signs of the incident as observed from the surface. The dissolved gas starts to flash from the liquid when it experiences a reduction in pressure below the bubble point pressure of the system during circulation. Owing to the depth of the risers, gas may be trapped within the marine risers after successful shut-in of blow our preventers at the sea bed. Circulating the contaminated mud poses a major threat of explosive riser unloading when the gas expands rapidly when the hydrostatic pressure is not sufficient to contain the gas. This forms the basis of study of riser equilibrium point, above which a slight movement of gas can lead to riser unloading. Explicit and implicit models have been created to understand the dynamics of gas expansion during the circulation. Specific case of oil based mud when the gas is completely dissolved in the base oil is considered. To capture the time varying dynamics of the multiphase flow, drift flux models have been created for both water based and oil based mud. Effect of choke pressure and pressure losses due to friction and acceleration have been successfully investigated. Based on the study, a minimum threshold back pressure is recommended to be able to circulate out the contaminated mud by bypassing the riser equilibrium point and avoiding riser unloading.

Acknowledgements

I would like to thank my supervisor John-Morten Godhavn, Statoil for his timely guidance and constructive feedback while carrying out this work. I would like to thank Espen Hauge , Statoil for his time to help me through this process. I would like to thank study coordinator Lisbeth Hultmann for providing administrative assistance during the study period. I would also like to thank my friend Karthik Ragunathan for providing clarifications during this work, among others who have instigated confidence in me through support and well wishes while carrying out this work.

Contents

List of Figures

List of Tables

Chapter 1

Introduction

This chapter covers the background information that is required to follow the work carried out. This literature survey covers the basic engineering setup of the systems used in the offshore drilling so as to understand the physical nature of the components used that ensure the safety of personals and rig during offshore drilling. It covers a summary of plethora of work done to understand various well control situations during gas kick, its causes and hierarchy of mathematical models used in analysing such situations. Complexities due to the presence of multiphase flow during well control situations are discussed. Dissolution of gas in oil based mud (OBM) and related delay in noticing the influx augments the necessity to investigate this matter. The background theory paves way to understand the problem statement mentioned in the end of this chapter

1.1 Marine Riser Systems

One of the most striking difference between onshore and offshore drilling is seen when the wellhead is located in the seabed during offshore drilling, making the communication with the well-bore from the rig floor complex. A marine riser provides communication and circulation capability between the surface and the sea floor and generally used at all point of offshore drilling operations (Lyons, 2005). The riser can be connected at the sea floor to a wellhead or to a sub-sea blowout preventer stack. A diverter system is usually attached at the surface. Marine risers date from the 1950s, when they were first used to drill offshore California from barges (Sparks, 2007). An important milestone in this regard in when drilling took place from the dynamically positioned barge CUSS-1 and since early days, risers have been used for four main purposes, ie., drilling, completion/work-over, production/injection and export (Sparks, 2007). While production risers transfer hydrocarbon and production materials during the production phase of development, drilling risers transfer mud to the surface during drilling

activities (Rigzone, 2016). As stated in Sparks (2007), production risers, used form floating platforms, inevitably followed some years after drilling risers. With an initial inspiration from top-tensioned drilling risers, they have taken many other forms such as bundled risers, flexible risers, top-tensioned risers (TTR), steel catenary risers (SCR) and hybrid risers, which are a combination of steel and flexible risers. Export risers come in a variety of architectures similar to those of production/injection risers, but with large diameters and lower pressures. Different types of risers and their properties are mentioned below as stated by Sparks (2007),

1.1.1 Low-pressure Drilling Risers

The standard drilling riser today is a low-pressure riser, open to atmospheric pressure at the top end. Thus, internal pressure can never exceed that owing to the drilling mud weight. Drilling risers are made up of a number of *riser joints*, typically 15-23 m long. A typical drilling riser comprises a central tube of 21 inches nominal diameter and is equipped with a number of peripheral lines. Kill and choke lines are used to circulate fluid in the event of gas kick, during which blowout preventer (BOP) is closed; booster line is used to inject fluid at the lower end of the riser; and a small diameter hydraulic line to power the sub-sea BOP. To reduce weight in water, the riser joints are equipped with synthetic foam buoyancy modules as can be seen in figure 1.2. Drilling risers are generally quipped with such modules over the upper part of their length. In past, air-can buoyancy units have been used with an advantage of adjusting the buoyancy optimally for each drilling scenario, but they posed additional complexities. To prevent the riser from collapsing under its own weight, it must be held in tension (Lyons, 2005). This can be accomplished by mechanical tensioning devices as shown in figure 1.1. As stated by Lyons (2005), many drilling operators drill the conductor hole (around 1000 ft) without using a riser. The drilling program is accomplished by circulating the returns to the sea floor. Once the conductor hole is drilled, casing is run and a subsea wellhead installed, the marine riser can be attached and used to drill the reminder of the well.

Another feature of the riser joint is the connector which are of different types like breechblock connector, flanged connector, etc. Peripheral lines are usually attached to the main tube by several guides and they are carefully designed to prevent the lines from buckling under the effect of internal pressure. Vertical motion of the floating vessel is compensated by adding a telescoping (slip) joint at the surface. This joint will usually allow upto 50 ft of vertical motion and lateral motion is compensated for by the use of ball/flexi joint connections at the sea floor and surface (Lyons, 2005). Figure 1.3 show drilling risers deployed below a drill ship and semi submersible, which are generally called mobile offshore drilling units (MODUs) and below tension leg platforms (TLPs) and spars. In case of emergency, the seabed

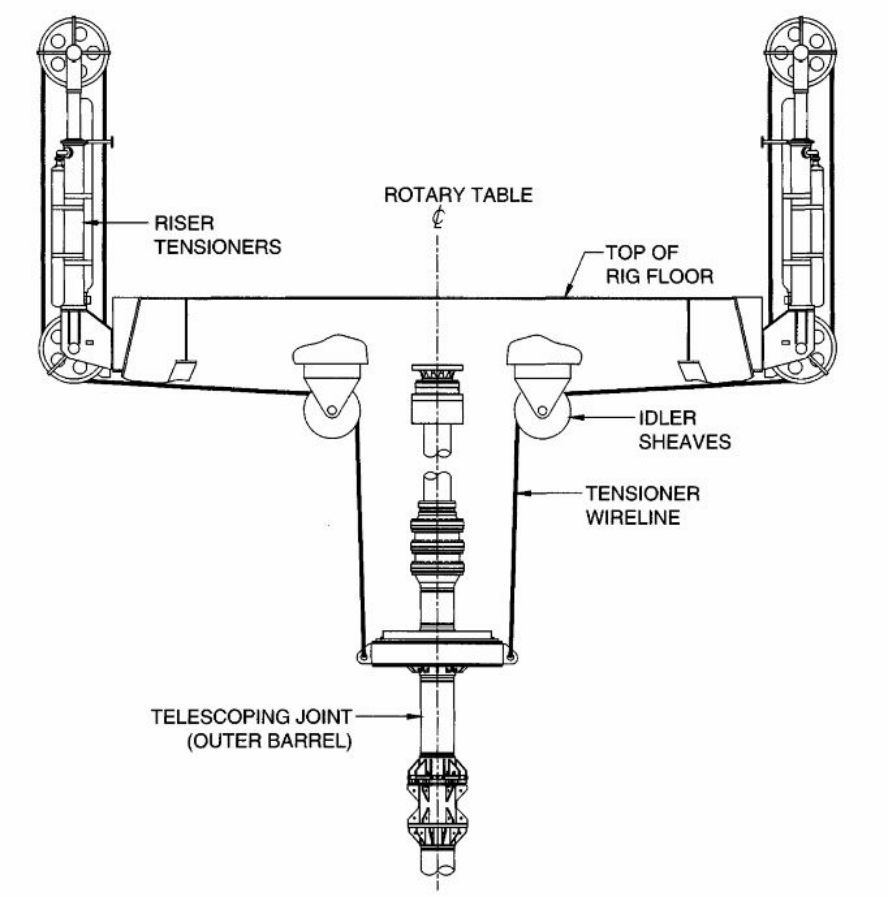

Figure 1.1: Mechanical riser tensioning device

BOP will allow the drill string to be cut and well to be closed and the lower marine riser package (LMRP) then allows the riser to be disconnected. A flex joint at the junction between the riser and the LMRP allows limited rotation of the riser. Weights of the BOP and LMRP depend on the design pressure, but are on the order of 100-300 tonnes for the BOP and 50-100 tonnes for the LMRP.

1.1.2 High-pressure Drilling Risers

When the BOP is located at the surface, a high pressure drilling riser is required. This riser has a much simpler architecture than a low-pressure riser since it does not require kill and choke lines. In event of a gas influx, the BOP is closed at the surface and thus the riser has to be designed for the full well pressure. Potentially this poses more risk when drilling with surface BOP, unless an adequate seabed disconnection system can be provided in case of an emergency. With a long history of usage of high-pressure riser

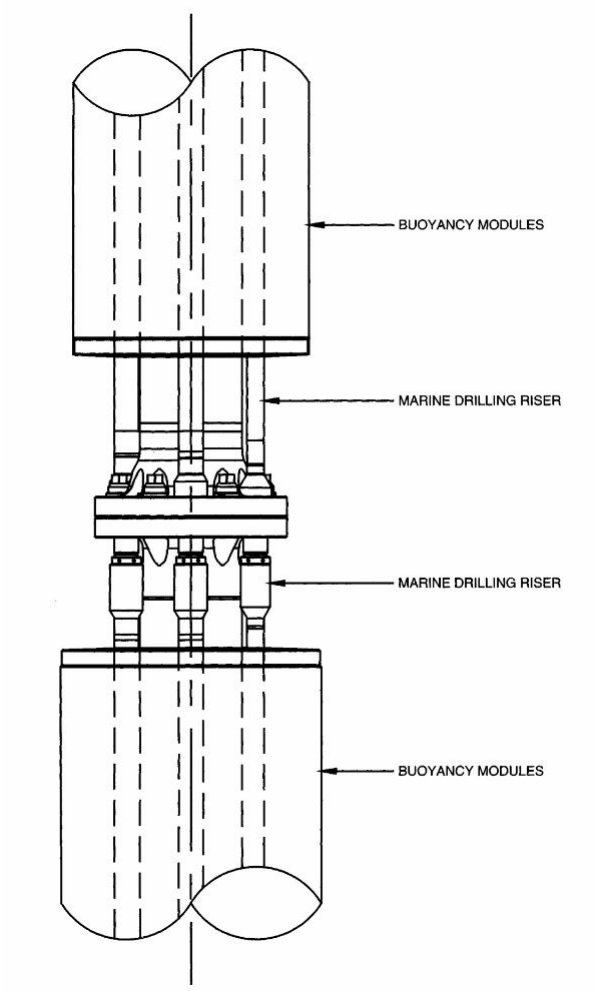

Figure 1.2: Buoyant riser tensioning device

with surface BOPs especially from semisubmersibles in moderate environmental conditions, the concept continues to be developed for deeper water and harsher environments. The problem that we focus on is related to low pressure risers only since we assume a sub-sea BOP stack is in place.

1.1.3 Completion/Workover Risers

Completion/ workover risers are similar to that of high and low pressure risers. They usually feature a high-pressure design with the wellhead on the platform and thus do not require kill and choke lines. A riser safety package (RSP) on the seabed would allow the well to be closed and an emergency disconnect package (EDP) allows the disconnection, in case of the need of emergency disconnect. Umbilical attached to the riser provides power to

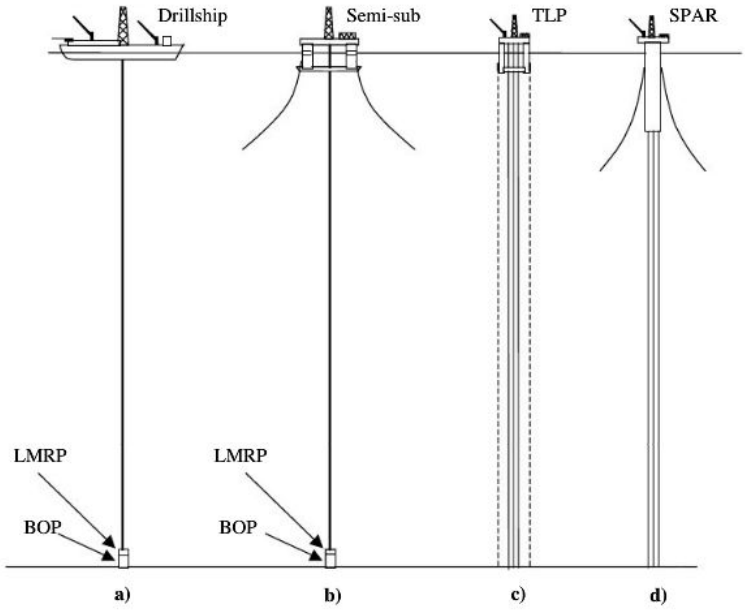

Figure 1.3: Types of marine risers

these packages. Further types include bundled risers which is a combination of several different riser architectures. Some may contain a core pipe, which also served as the export riser, with a number of satellite risers around it. Riser towers are in place, which are used in association with floating production, storage and off-loading platforms (FPSOs). Flexible risers are found to be suitable for being production, export risers and flow lines and not as a drilling riser due to the challenges posed in development of a safe system for closing the well in case of a blowout (Sparks, 2007). They are found to be useful in normal environments while using in the free-hanging mode and are not suitable for severe environments due to the large variation of the induced tension in the pipe.

1.1.4 Individual Top Tensioned Risers

Individual risers that rely on a top tension in excess of their apparent (wet) weight for stability are generally termed as individual top tensioned risers (TTRs), although all risers require top tension. TTR production/injection risers are generally designed to give direct access to the well and the riser must be designed to contain a tubing leak or a failure. Connection to the seabed is by a stress joint and with a kneel joint in case of spars, to relieve bending stresses. In general TLP uses risers with tensioners, whereas spar risers are tensioned by air cans. In case of tensioners, the top tension in-

creases with platform offset because of tensioner stiffness and in case of air cans, it is slightly reduced because of the compressibility of the air or gas in the cans. They are further divided into single barrier and dual barrier risers, where the latter are usually of larger diameters and heavy, since the annular area between the two riser casings is generally filled with drilling mud and is designed to kill the well in case of failure of the inner riser casing (Sparks, 2007).

1.1.5 Steel Caternary Risers

Steel caternary risers (SCRs) were initially used as export lines on fixed platforms and they have been lately used as export risers and production/injection risers in large numbers. SCRs and free hanging flexible risers share the same disadvantage of failure in handling large tension induced by fluctuations.

1.2 Subsea BOP

Owing to the operational nature of floating drilling, the operator does not always have the option of placing the blowout preventer stack at the surface and by placing it in the sea floor and communicating with the well through detachable marine riser, a well can be shut in at the sea floor (Lyons, 2005). This action eases the responsibility for drilling vessel of maintaining the surface position at all times. A typical BOP stack is shown in figure 1.4 and the choke and kill lines allow fluids to pass through the well, bypassing the marine riser. Functioning of a BOP is very crucial during the emergency situation which usually arises when there is a gas influx. There can be as many as six emergency systems in a BOP to operate critical functions in case of loss of the primary control, which the barrier provided by the hydrostatic head of the drilling mud. They can be briefed as

- **Emergency Disconnect Sequence (EDS)** - In case a dynamically positioning (DP) rig has lost the station keeping ability, EDS is an one button system that allows the wellbore to be secured by closing the shear rams. The subsea BOP stack is hydraulically activated to separate LMRP from the stack by unlatching the connector. An overpull is preset on the riser tensioners and the LMRP lifts from the BOP stack. A riser recoil system prevents a sling shot effect. The total sequence takes about 55 seconds utmost since the time it has been triggered.
- **Acoustic systems** - A limited number of emergency functions like activating the shear rams and disengaging LMRP connector can be operated from the rig using a hydrophone transmitting to transducers

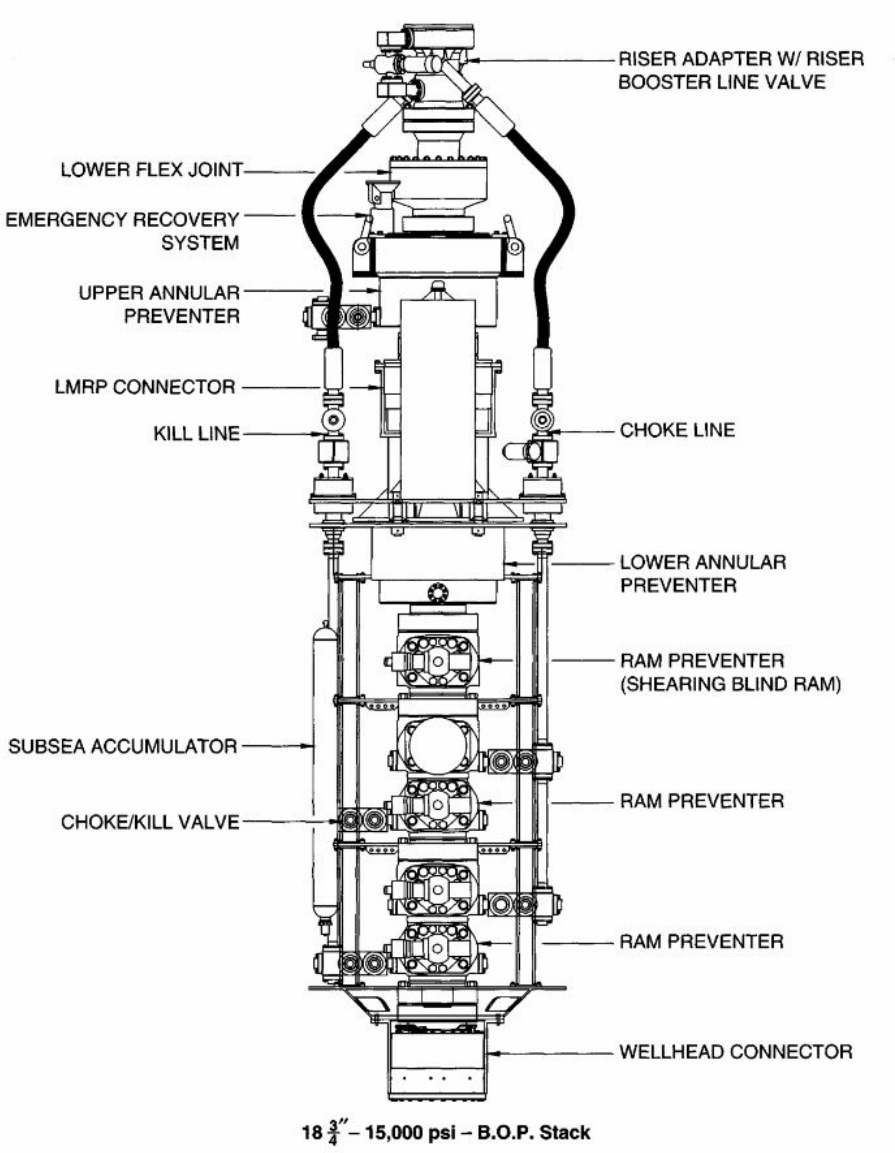

Figure 1.4: Subsea BOP stack

on the BOP. In case of a well control situation, these systems are unreliable due to the significant noise generated from the flow in wellbore.

- **Remote Operated Vehicles (ROV)** have pumps which can operate function through a 'hot stab' plugged into a dedicated receptacle in panel. The main limitation of an ROV is the time to deploy form the rig to the sea bed and the limited flow rate of their pumps.
- **Dead Man Systems** will close the shear rams in the event all hy-

draulic and electric control is lost on the BOP. This would typically happen if the riser string parted. In such situation, the hydrostatic pressure of the mud would be reduced as it is replaced by sea water and 'riser margin' is considered while calculating the required mud density to consider the possibility of such situations. Closing the shear rams secures the well in such cases.

- **Automatic Disconnect System** closes the shear rams when the lower flex joint reaches a present angle.
- **Autoshear** closes the shear rams in the event of unintentional disconnection of LMRP.

1.3 Diverter Systems

Shallow gas hazards are a common potential danger offshore with a risk of encountering shallow gas flow with insufficient casing in the well to allow a shut-in (Lyons, 2005). In such instance, diverter system is a mean of safety measure allowing the well to flow and subside by natural means which in many cases provides enough time to evacuate the rig (Lyons, 2005). A

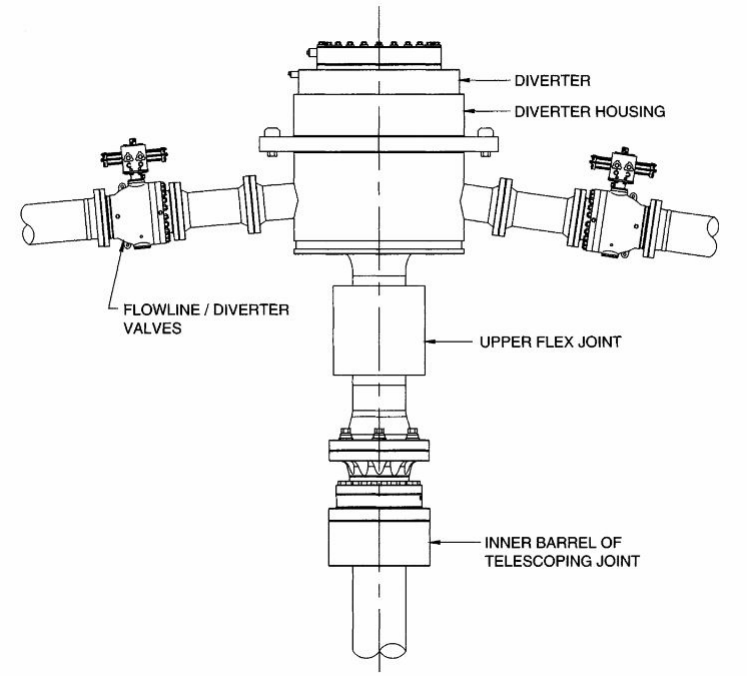

Figure 1.5: Diverter System

typical diverter system setup is shown in figure 1.5 and the components of

the system are the annular-type preventer, vent lines, the control system and the conductor or structural casing. As mentioned in Lyons (2005), the major operational consideration when using a diverter system is to make sure that the valves on the vent lines are fully open before the annular-type preventers are closed and when drilling the conductor or surface hole, shutting in the well may cause a subsurface blowout that is likely to broach to the surface. Sufficient conductor casing depth is also very important in preventing a subsurface blowout. The Minerals Management Service requires a minimum of 10 inches-diameter diverter vent line, but usage of as large as 16 inches-diameter vent lines are more usual now (Lyons, 2005). While a bottom-supported vessel must divert when shallow gas is encountered, a floating vessel has the additional option of simply abandoning the well which led to the use of riser-less systems when drilling the surface hole (Lyons, 2005).

1.4 Abnormal Pressure and Kick

Abnormal pressure is a term used to describe pressures in well-bores that are greater than the expected, naturally occurring hydrostatic pressure (of Drilling Contractors , IADC). Normal pressure is equivalent to the hydrostatic pressure generated by a column of seawater that has the normal chloride content for a specified geological region. Normal pressure is also often expressed in terms of a "normal pressure gradient". A normal pressure gradient could be between 0.433 to 0.468 psi per foot, depending on area. As stated in of Drilling Contractors (IADC), common drilling indicators that may indicate that an abnormal pressure region is being approached include,

- Increase in background and especially connection gas units
- Drilling break, that is increase or decrease of rate of penetration (depending on the type of drill bit)
- Decrease in pump pressure or Pressure While Drilling (PWD)
- Increase in stroke rate corresponding to decrease in pump pressure
- Sudden torque increase
- Change in mud chlorides
- Change in mud properties, especially viscosity
- Distinct change in cuttings - shape, size, volume
- Increase in BOP stack temperature (if equipped with sensor)
- Change in resistivity or change in sonic velocity (if LWD tools are in the string)

- Other indicators that can be calculated by pore pressure experts

Indicators above are not false proof and observing one or more of these indicators mat be sufficient to justify a flow check. Detecting abnormal pressure indicators can be complicated in deep water due to increase in lag time for gas units and cuttings reduces the timeliness of this data for detection purposes, surface flow-line temperature may not be an effective tool due to colling effect of long riser and down hole, real-time monitoring tools installed in the bottom hole assembly (BHA) can greatly assist in overall determination of the equivalent mud weight (EMW) and pore pressure where the tools include Pressure While Drilling (PWD); Logging While Drilling (LWD) and real-time pore pressure measurement for actual pore pressure identification (of Drilling Contractors , IADC). Pit Volume totalizer can be implemented to sense the pit level gain and among the multiple signs of a kick only three are positive indicators (of Drilling Contractors , IADC) and they are,

- Increase in flow out while drilling or continues flow during connections after the pumps are shut off
- Increase in surface pit level/ volume while drilling or improper hole fill while tripping
- Positive flow check

The threat of encountering an unexpected high-pressure gas is ever present as mentioned in Johnson and White (1993) and such influx into a well is known as a gas kick. Failure to take an action to contain and/or mitigate the influx would allow the gas to expand as it rises upwards, thereby reducing the hydrostatic head in the well, which in turn will cause more gas to enter the wellbore as stated in Hauge (2013). Such situations are prominent in case of deep and ultra deep wells which are of generally high pressure and/or high temperature (HPHT). Some of the special challenges that are posed in such situation are mentioned in Rommetveit et al. (2003) as follows,

- High pressure and temperatures impact mud properties in a dynamic way, and can have effects on well control.
- The conditions are above the critical point for the gas/oil/condensate influx, allowing the hydrocarbon influx to be infinitely soluble in the base oil of the mud.
- Free gas is released when it is pumped upwards in the well due to pressure reduction. This free gas will expand according to the real gas law. Bubble point of the mixture will govern where in the well one will have free gas flashing from the mud. An illustration of this is given in figure 1.6.

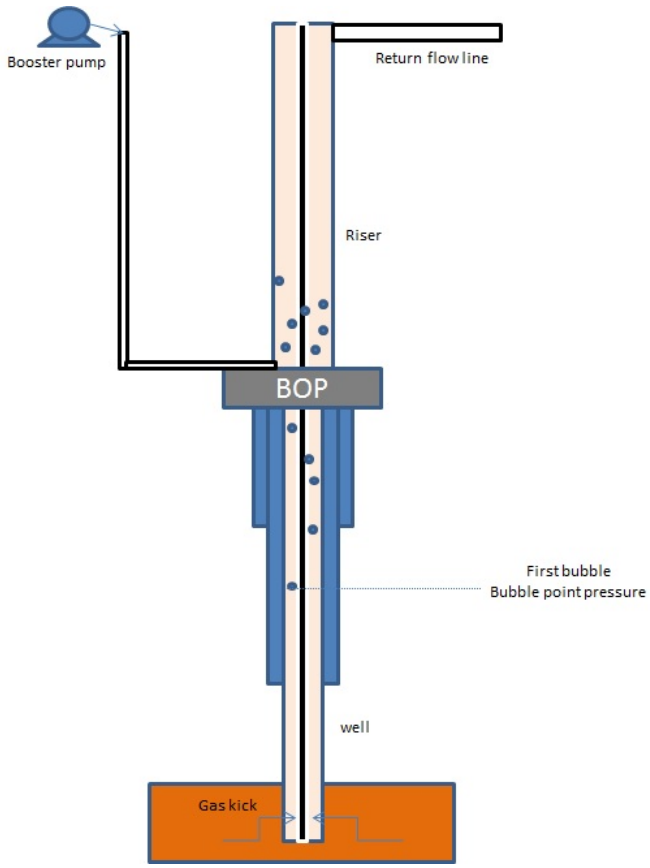

Figure 1.6: Schematic of typical gas kick situation in offshore drilling

This dissolution of gas during kick will lead to swelling of mud which may be observed at the surface as pit gain though very less and is severe in oil based mud, experimental studies have been carried out by O'Bryan et al. (1987) whereas the amount of gas that can be dissolved in the oil-based drilling fluids at different pressure and temperature conditions is given by O'Bryan et al. (1988), Thomas et al. (1984) and Berthezene et al. (1999). Similar cases in other types of drilling fluids, like invert emulsion drilling fluid is explained by Swanson et al. (1988), explaining the experimental results to the surface observations and N-Paraffin based drilling fluids is explained by Galves et al. (2014). PVT properties of these systems of gas-drilling fluid is studied by Monteiro et al. (2008), with its application to well control. Flatabø et al. (2015), carried out experiments to understand gas absorption in petroleum fluids at HPHT conditions. General methods to handle drilled gas which may develop as a kick over time if unnoticed is provided by O'Bryan et al. (1989).

Once the free gas starts to exist, different flow regimes may exist as

discussed in section 1.9 and it becomes important to understand the slip velocity of the gas bubble. Detailed mathematical model is discussed in section 1.10. Several experiments have been carried out to understand the gas rise in one such situation as discussed in this section. Some of the notable experiments were carried out by Tarvin et al. (1994), Tarvin et al. (1991), Johnson et al. (1995) and Johnson et al. (1991). Through extensive experimental measurements, Johnson and White (1993), gives an overview of the dependency of flow regimes over void fraction specific to the cases discussed in this section. Some of the results have been incorporated into a computer model for kicks in water and oil based drilling fluids developed by White et al. (1990). Impact on gas distribution within the wellbore during the process is considered in Swanson et al. (1988), Rader et al. (1975) and Hauge et al. (2012), where a triangular distribution for the void fraction is considered. There are specific cases such as in Skalle et al. (1991), where the effect of gas rise velocity on the bottom hole pressure in a vertical well is experimentally studied and in Johnson et al. (1993), where the gas rise velocities are studied in deviated wells.

Knowledge regarding the fluid mechanics of bubbles in general is provided by Subramanian et al. (2002) and those specific to viscous liquids is given by Bhaga and Weber (1981). Numerical simulation schemes to model bubble rising in shear-thinning fluids is given by Zhang et al. (2010) and the same for viscous liquid is given by Hua and Lou (2007).

1.5 Hierarchy of Mathematical Models

It is easy to understand that in order to study such situations, robust mathematical models are required. Ability of the model to predict such situations with the desired accuracy is very much important for a safe and reliable drilling operation and well control measures. A comparison of various mathematical models to understand these multiphase situations are very well described in Aarsnes et al. (2015). Among the variety of options available, for any model the three components of a complete simulation model are mathematical structure, closure relations and numerical scheme. Various options available to form the desired combination are stated in table 1.1.All the models found in the literature can be split into three broad categories as reviewed in Aarsnes et al. (2015) and given as

1.5.1 High Fidelity Models

This category of models are robust and are designed to be highly accurate and have a high degree of predictive power over a wide range of application scenarios. They are more general in training, analysis and planning of operations and have an overall prospective of the problem. In one space dimension, the PDE formulation of dynamic distributed models may be

Table 1.1: Three components of a complete simulation model

Mathematical Structure	Closure Relations	Numerical Scheme
PDE or ODE	Slip law	Numerical accuracy
Hyperbolic or Parabolic PDE	Equation of state	Numerical stability/robustness
Number of equations	Frictional pressure loss	Implementation complexity
Stiffness	Other source terms	Solution speed

written as

$$\frac{\partial \mathbf{U}}{\partial t} + \mathbf{A}(\mathbf{U}, x, t)\frac{\partial \mathbf{U}}{\partial x} = \mathbf{D}(\mathbf{U}, x, t)\frac{\partial^2 \mathbf{U}}{\partial x^2} + \mathbf{Q}(\mathbf{U}, x, t) \tag{1.1}$$

Each term affect the mathematical structure of the model in its own way and they represent the following,

- **U**(x,t) represents the vector of unknowns which are the independent variables of the physical state at each point in space and time. It can be observed that the dimension of this vector **U** depends on the complexity of the model.
- **A** contains information that propagates with a finite speed across the computational domain representing effects such as convection or momentum transfer through pressure.
- **D** represents irreversible diffusive effects in the flow direction such as viscosity or heat or mass diffusion.
- **Q** represents source terms, that is exchanges between the state and the environment. Interactions with the environment include friction, gravity terms. Exchange terms may include heat, volume, mass and momentum transfer.

1.5.2 Drift Flux Models

This is the most widely used model to represent two phase flow in drilling engineering applications. The 3-PDE drift flux model may be described as

$$\frac{\partial(\alpha_g \rho_g)}{\partial t} + \frac{\partial(\alpha_g \rho_g \nu_g)}{\partial x} = \Gamma \tag{1.2}$$

$$\frac{\partial(\alpha_l \rho_l)}{\partial t} + \frac{\partial(\alpha_l \rho_l \nu_l)}{\partial x} = -\Gamma \tag{1.3}$$

$$\frac{\partial(\alpha_l \rho_l \nu_l + \alpha_g \rho_g \nu_g)}{\partial t} + \frac{\partial(\alpha_l \rho_l \nu_l^2 + \alpha_g \rho_g \nu_g^2) + P}{\partial x} = -F - G \tag{1.4}$$

The mass transfer term Γ is proportional to the difference in concentration of the component in the two phases and the proportionality constant is know as

the mass transfer coefficient. In most of the models it is often assumed to be zero. It is so for the case when water based mud is considered whereas a finite mass transfer is considered in the case of oil based mud due to the dissolution of gas in the base oil. This is discussed further in section (cite section). Gravitational pressure loss is $G = \rho_M g sin\theta$ and viscous pressure loss which is the frictional term F may take various form depending on the flow regime and the conduit. Frictional modelling is discussed in brief in section (cite section). Apart from the source and mass transfer definitions, several *closure laws* that establishes relation between the various states considered must be presented in order to solve the drift flux model. One such is the *slip relation*, which is a general relation between the velocity of the liquid and the gas phase due to averaging and external interactions. It is given by equation 1.8 and other closure laws usually used in conjunction are (Udegbunam et al., 2015),

$$\alpha_l + \alpha_g = 1 \tag{1.5}$$

$$\rho_l = \rho_{l,0} + \frac{P - P_0}{a_l^2} \tag{1.6}$$

$$\rho_g = \frac{P}{a_g^2} \tag{1.7}$$

$$\nu_g = K\nu_m + S \tag{1.8}$$

In the liquid density relation (equation 1.6), $a_l = 1500m/s$ which is the velocity of sound in the liquid (water) phase. When the liquid considered is water, the constants $\rho_{l,0}$ and P_0 are assumed to be $1000kg/m^3$ and 1 bar respectively. In the gas density relation (equation 1.7), $a_g = 446m/s$ which is the velocity of sound in gas when methane is considered in the gas phase.These estimations can be further extended to consider real gas behaviour, etc. which is covered in section (cite the section). In attempting to reduce the complexity of the two-phase flow models, reduced drift flux models are used where the distributed pressure dynamics are relaxed thus neglecting the fast pressure waves while keeping the dynamics of slow gas propagation (Aarsnes et al., 2015).

1.5.3 Simplified ODE Models

These ODE models do not attempt to capture the complete dynamics of the system whereas use very few of them over certain control volumes. They are most often fit-for-purpose models. Various types of models that fall under this category are 1 phase model which is a simple, liquid only model of the drilling hydraulics; Lagrangian model which is a simple ODE model representing the effect of gas liquid flow of a single bubble in the annulus. Next comes the low order lumped models which have been successful in modelling for control for severe slugging in two phase production risers.

When deriving two phase models from the first principle is highly complex, black box or step response models are good alternative. This allows to derive at the ODE models from identification techniques.

1.6 Friction Modelling

Fluid flow is classified as external and internal, depending on whether the fluid is forced to flow over a surface or in a conduit. Internal flow is considered here where the conduit is completely filled with the fluid and the flow is driven primarily by a pressure difference. The fluid velocity in a pipe changes from zero at the surface because of the no-slip conditions to a maximum at the pipe center. In fluid flow, it is convenient to work with average velocity, V_{avg}, which remains constant in incompressible flow when the cross sectional area of the pipe is constant. The friction between the fluid particles in a pipe does cause a slight rise in fluid temperature as a result of conversion of mechanical energy to thermal energy but is convenient to ignore it since the increase in temperature is too small to affect the accuracy of the calculation. In general, the flow properties are averaged over a particular temperature unless a significant heat transfer is present. In case of the riser systems that are considered here, the flow is assumed to occur at an averaged temperature in the riser. One can identify three components that can define the pressure difference that is required for a fluid flow as hydrostatic pressure loss, frictional pressure loss and kinetic pressure loss. In most of the cases, kinetic losses are minimal and can be ignored. But the consequence of ignoring and considering the kinetic losses are discussed in chapter **??**. Considering a flow between two points A and B, the minimum basic parameters that are required to design the piping system include, but are not limited to, the following,

- The characteristics and physical properties of the fluid
- The desired mass flow rate (or volume) of the fluid to be transported
- The pressure, temperature and elevation at point A
- The pressure, temperature and elevation at point B
- The distance between point A and point B (or length the fluid must travel) and equivalent length (pressure losses) introduced by valves and fittings.

1.6.1 Bernoulli Equation

The basic equation developed to represent steady-state fluid flow is the Bernoulli equation which assumes that the total mechanical energy is conserved for steady, incompressible, inviscid, isothermal flow with no heat

transfer. The equation by considering two position '1' and '2' of the fluid flow is given by (when considered in field units mentioned below),

$$Z_1 + \frac{144P_1}{\rho_1} + \frac{V_1^2}{2g} = Z_2 + \frac{144P_2}{\rho_2} + \frac{V_2^2}{2g} + H_L \tag{1.9}$$

Darcy's equation further expresses head loss as,

$$H_L = \frac{fLV^2}{2Dg} \tag{1.10}$$

and

$$\Delta P = 0.0013\frac{f\rho LV^2}{d} \tag{1.11}$$

where,

Z = Elevation head, ft
P = Pressure, psi
ρ = Density, lbm/ft^3
V = Velocity, ft/sec
g = gravitational constant, ft/sec^2
H_L = Head loss, ft
f = Moody friction factor, dimensionless
L = Length of pipe, ft
D = Diameter of pipe, ft
d = Inside diameter of pipe, in
ΔP = Pressure drop, psi

1.6.2 Reynolds number and Moody friction factor

Reynolds number is a dimensionless parameter that is useful in characterizing the degree of turbulence in the flow regime and is needed to determine the Moody friction factor. It can be defined as the ratio between the internal forces to the viscous forces in the fluid.

$$Re = \frac{\text{Internal forces}}{\text{Viscous forces}} = \frac{V_{avg}D}{\nu} = \frac{\rho V_{avg}D}{\mu} \tag{1.12}$$

Kinematic viscosity, ν, can be viewed as *viscous diffusivity* or *diffusivity for momentum*. At large Reynolds numbers, the inertial forces, which are proportional to the fluid density and the square of the fluid velocity, are large relative to the viscous forces and thus the viscous forces cannot prevent the random and rapid fluctuations of the fluid. At small or moderate Reynolds numbers, the viscous forces are large enough to suppress these fluctuations

and to keep the fluid 'in line. Thus the flow is turbulent in the first case which is characterized by velocity fluctuations and highly disordered motion and the latter is the laminar flow which is characterized by smooth streamlines and highly ordered motion. Under most practical conditions, the flow regime in a circular pipe can be categorized using Reynolds number as,

$$\begin{aligned} Re &\leq 2300 \quad \text{Laminar flow} \\ 2300 \leq Re &\leq 4000 \quad \text{Transistional flow} \\ Re &\geq 4000 \quad \text{Turbulent flow} \end{aligned}$$

Re-writing equation 1.11 for any flow regime in terms of SI units,

$$\Delta P_L = f \frac{L}{D} \frac{\rho V_{avg}^2}{2} \tag{1.13}$$

where $\rho V_{avg}^2/2$ is the dynamic pressure f is the **Darcy friction factor**,

$$f = \frac{8\tau_w}{\rho V_{avg}^2} \tag{1.14}$$

It can also be found that the pressure loss for a laminar flow in pipe is given by,

$$\Delta P = P_1 - P_2 = \frac{8\mu L V_{avg}}{R^2} = \frac{32\mu L V_{avg}}{D^2} \tag{1.15}$$

By equating equation 1.15 to the general pressure loss equation 1.13 and solving for f gives the friction factor for fully developed laminar flow in a circular pipe,

$$f = \frac{64\mu}{\rho D V_{avg}} = \frac{64}{Re} \tag{1.16}$$

This equation shows that in laminar flow, the friction factor is a function of the Reynolds number only and is independent of the roughness of the pipe surface. It can be observed that the equivalent liquid height for the corresponding loss in equation 1.13 is defined by the head loss given in equation 1.10. Frictional losses for various flow regimes when a non-Newtonian fluid such as the drilling mud is considered is given in Skalle et al. (1991). For the purpose of usage in drift flux models as discussed later in chapter **??**, the frictional part of the source term is given by Udegbunam et al. (2015), to be used in all flow patterns as,

$$F_w = \frac{2f\rho_m \nu_m abs(\nu_m)}{d_o - d_i} \tag{1.17}$$

To calculate the friction factor, f, Reynolds number is required and is given by,

$$N_{Re} = \frac{\rho_m abs(\nu_m)(d_o - d_i)}{\mu_m} \tag{1.18}$$

For $N_{Re} \geq 3000$, the flow is considered turbulent and the friction factor is defined as,

$$f = 0.052(N_{Re})^{-0.19} \tag{1.19}$$

For $N_{Re} \leq 2000$, the flow is laminar and the frcition factor is given by,

$$f = \frac{24}{N_{Re}} \tag{1.20}$$

Equation 1.19 is a Blasius-type equation for calculating friction factor in turbulent flow and interpolation is used in calculating friction factor for the intermittent flow regime in which 2000 $<N_{Re}<$3000 (Udegbunam et al., 2015). And a more generalised frictional force term for a drift flux model is given in Evje and Fjelde (2002) as,

$$F_w = \frac{32\nu_{mix}\mu_{mix}}{d^2} \tag{1.21}$$

And this simple model is used in the drift flux models considered in this work and in general, for the system that is studied here, flow of the fluid is generally maintained in the laminar flow regime making it appropriate to use the simplified general model mentioned above.

1.7 Numerical Schemes

Due to increased complexity of finding an analytical solution to Ordinary Differential Equations (ODEs) and Partial Differential Equations (PDEs), several numerical schemes are available to derive a solution which varies on the type of ODEs and PDEs that are required to be solved. For any case, they are required to be discretized to carry out the solution procedure. More general spatial discretization methods, among many are, Finite Difference Method (FDM) - method using point-value solution; Finite Volume Method (FVM) - method using cell-average solution and Finite Element Method (FEM). Practical evaluation criteria of numerical schemes for PDEs include **solution accuracy** quantifying the numerical error, which is the difference between the numerical solutions and the exact solutions. It depends on the initial data and boundary condition treatment in consistent with the order of accuracy of the numerical schemes and the preservation of the physical properties of the continuum PDEs like conservation laws (mass, momentum, energy); **efficiency** which is measured by the computer CPU time used to calculate numerical solutions and **algorithm robustness**. Replacing the derivatives by finite differences form the basis of finite difference schemes and they can be achieved by (Li and Li, 2016),

- **Taylor series expansion**: The most common method and as the name suggests, it uses the Taylor series to replace the derivative.

- **Polynomial fitting or interpolation**: Little less intensive mathematical operation that is generally used. Taylor series is a subset of this method.

- **Control volume approach**: This method is also called finite volume method (FVM). The equations are solved in integral form rather than the differential form. For cartesian grids, FVM = FDM. Solving Differential Algebraic Equations (DAEs) or semi-discrete equations of the PDEs using Method of Line (MOL) approach and more modern techniques like flux splitting schemes are part of this method.

Considering a simplest case of linear advection equation given below, assuming $a > 0$,

$$u_t + au_x = 0 \tag{1.22}$$

$$u(x, 0) = u_0(x) \tag{1.23}$$

Among the various schemes available in combining the spatial and temporal discretization together such as Lax-Freidrichs scheme, Lax-Wendroff scheme, Beam-Warming scheme, leapfrog in time central space, etc., Upwind (first-order) is described as,

$$\frac{u_i^{n+1} - u_i^n}{k} + a\frac{u_i^n - u_{i-1}^n}{h} = 0 \tag{1.24}$$

where k and h are the step size of the temporal and spacial variations respectively. Quantitative properties of finite difference schemes are studied by a method's,

- **Consistency**: A finite difference discretization of a PDE is consistent if the finite-difference equations converge to the PDE. Error approached zero when the grid spacing and time step tend to zero.

- **Stability**: The errors from any source will not grow unbounded with time. This is taken care by Courant-Fridrichs-Levy (CFL) condition which states that the following condition must hold in order for the method to be stable. Else the scheme will be divergent and unbounded.

$$0 \leq \frac{ak}{h} \leq 1 \tag{1.25}$$

- **Convergence**: The ability of the finite difference equations solution to converge to the true solution of the PDE.

1.7.1 Method of Lines

Among the various methods available and discussed above to solve PDEs, the method adapted in this work, which is MOL is described in brief in this part of the section. MOL is a semi-analytical method for the analysis of transmission lines, waveguide structures and scattering problems. It is regarded as a special finite difference method but more effective with respect to accuracy and computation time than the regular finite difference method (Sadiku and Obiozor, 2000). As stated by Sadiku and Obiozor (2000), the MOL has the following properties that makes it efficient,

- **Computational efficiency:** the semi-analytical character of the formulation leas to a simple and compact algorithm, resulting in less computational efforts compared to other techniques.
- **Numerical stability:** By separating discretization of space and time, it is easy to establish stability and convergence for a wide range of problems.
- **Reduced programming effort:** By making use of the already available and reliable ODE solvers, programming effort can be substantially reduced. In-built MATLAB solver, *ode15s*, has been used in this work, since the equations are stiff in nature.
- **Reduced computational time:** Since only a small amount of discretization lines are necessary in the computation, there is no need to solve a large system of equations; hence computing time is small.

For wave equation $u_t + au_x = 0$, using central differencing in space in MOL method results in the following equation which can be directly solved by the ODE solvers in MATLAB,

$$\frac{\mathrm{d}u_i}{\mathrm{d}t} + a\frac{u_{i+1} - u_{i-1}}{2h} = 0 \tag{1.26}$$

1.7.2 Modern Schemes for Conservation Laws

Most of these are FVM methods and can be classified into two categories, **flux-splitting methods**, in which a switch is added such that the scheme becomes first order near discontinuity and remains high order in the smooth region and **high order Godunov methods** which includes, piecewise parabolic method (PPM), essentially non-oscillatory (ENO) schemes and wave propagation method of Leveque. Interesting works related to such systems have been carried out in Evje and Fjelde (2002) which concerns the extension of an FVS type scheme, a Van Leer type scheme and an advection upstream splitting method (AUSM) type scheme to a two phase model. The

mentioned FVS scheme is elaborated in Van Leer (1982). Briley and McDonald (2001) provides an overview of the implicit algorithms that are used in solving Navier-Stokes equation. General theory on FVS and the widely used Riemann solvers are discussed in Toro (2009).Edwards (1997) provides details about low diffusive scheme for Navier-Stokes equations.

1.8 Drilling Fluids

A key requirement in any drilling process is to maintain the hydrostatic head required for drilling the formation and serve as a means to remove cuttings amongst various other uses discussed shortly. Early drilling operations used water to achieve this, with the use of continuous water circulation systems reported as early as 1845 Health and Safety Laboratory (2000). Over period of time, with advent of technology and with an effort to reach greater depths, water has been replaced by drilling mud, which is a complex blend of chemicals and weighing agents in a base fluid which may be water, oil or gas. Drilling fluids are categorized based on the type of base fluid used. In offshore drilling, due to the larger depth of the wells and higher pressure that are encountered, it is usual to use water or oil based mud and thus only they are discussed here. Nevertheless, any type of drilling fluid fulfils the following requirements or functions as stated by Darley and Gray (1988).

- Carry cuttings from beneath the bit, transport them up the annulus and permit their separation at the surface.
- Cool and clean the bit.
- Reduce friction between the drilling string and sides of the hole.
- Maintain the stability of the uncased sections of the borehole.
- Prevent the inflow of fluids - oil, gas or water - from permeable rocks penetrated.
- Form a thin, low permeable filter cake which seals pores and other openings in formations penetrated by the bit.
- Assist in collection and interpretation of information available from drill cuttings, cores and electrical logs.

It is further stated in Darley and Gray (1988) that in conjunction with the above functions, certain limitations are placed on the drilling fluid as follows,

- Not injure drilling personnel nor be damaging or offensive to the environment.
- Not require unusual or expensive methods of completion of the drilled hole.

- Not interfere with the normal productivity of the fluid-bearing formation.
- Not corrode or cause excessive wear of drilling equipment.

Composition

In order to make this blend of chemicals in base fluid fully functional, various additives like weighting agents, gelling products, viscosifiers, salinity chemicals, alkaline chemicals, lost circulation material, defoamers, biocides, corrosion inhibitors, scale inhibitors, drilling lubricants, pipe release agents, emulsifiers, shale inhibitors, thinners, dispersant, polymers, detergents, etc are added and their description are stated in Health and Safety Laboratory (2000). The typical composition of a water based drilling mud to make up a density of 1300 kg/m^3 is shown in table 1.2 and the constituents are added to a barrel of water whereas a similar data for an oil based mud is shown in table 1.3 and the constituents are combined to give a total volume of one barrel, whose density is 1318 kg/m^3, salinity 22.5% and oil to water ratio 65:35 Health and Safety Laboratory (2000).

Table 1.2: Composition of a typical bentonite gel water based mud, density 1300 kg/m^3.

Component	Quantity	Mass (Kg)	Volume (litres)	% Mass	% Volume
Water	1 bbl	159	158.99	65.33	84.92
Bentonite	20 ppb	9.1	9.07	3.73	4.85
Caustic Soda	0.5 ppb	0.23	0.22	0.09	0.12
Soda Ash	0.5 ppb	0.23	0.10	0.09	0.05
High viscosity CMC	1.5 ppb	0.68	0.47	0.28	0.25
Low viscosity CMC	3.5 ppb	1.59	1.09	0.65	0.58
Barite	160 ppb	72.58	17.28	29.82	9.23

Rheology

For efficient functioning of a tailored drilling mud for a specific well-bore conditions, it is required to test its flow characteristics. several models have been developed to characterise a fluid flow. Fluids are categorized as Newtonian and non-Newtonian fluids. A fluid that has a constant viscosity at all shear rates at a constant temperature and pressure and can be described by a one-parameter rheological model are defined as Newtonian fluids and a fluid whose viscosity is not constant at all shear rates and does not behave

Table 1.3: Composition of a typical oil based mud, density 1318 kg/m^3

Component	Quantity	Mass (Kg)	Volume (litres)	% Mass	% Volume
Base fluid	0.52 bbl	63.64	83.31	30.37	52.40
Viscosifier	5 ppb	2.26	1.40	1.08	0.88
Emulsifier 1	0.8 gpb	2.89	3.02	1.38	1.90
Emulsifier 2	0.4 gpb	1.49	1.51	0.71	0.95
Lime	5 ppb	2.26	1.00	1.08	0.63
Water	0.30 ppb	47.15	47.22	22.50	29.70
$CaCl_2$	30.2 ppb	13.70	3.35	6.54	2.11
Barite	167.9 ppb	76.15	18.16	36.34	11.42

like a Newtonian fluid are defined as non-Newtonian fluids Schlumberger (2015). Basic rheology of oil-base mud and their dependencies on pressure and temperature is shown in Houwen et al. (1986).

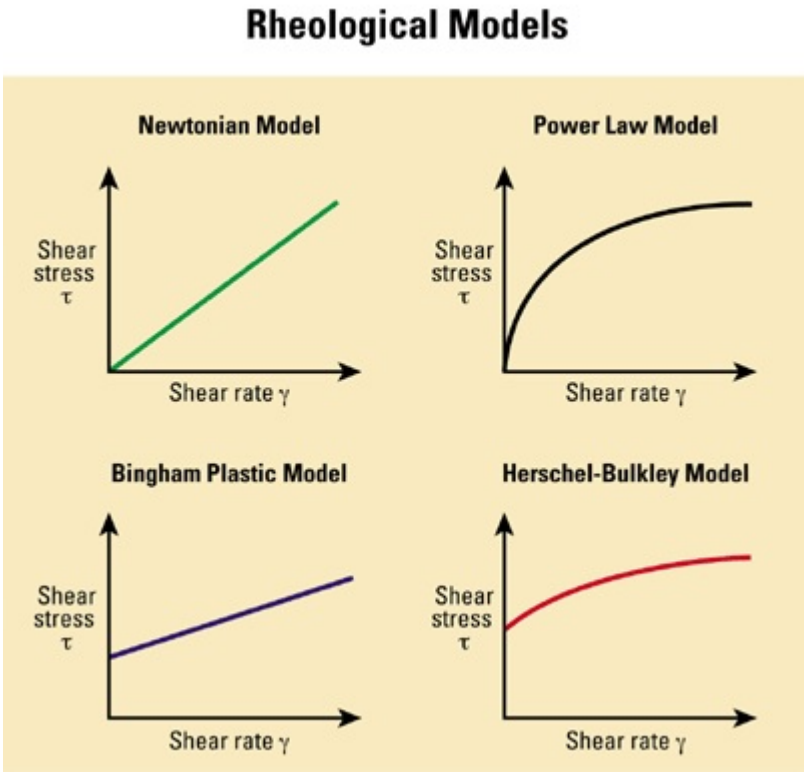

Figure 1.7: Different rheology models

Behavioural patters of different rheological models are shown in figure

1.7. They are described by the following equations Skalle (2010),

$$\begin{aligned} \text{Newtonian:} \quad & \tau = \mu\gamma \\ \text{Bingham Plastic:} \quad & \tau = \tau_y + \mu_{pl}\gamma \\ \text{Power law:} \quad & \tau = K\gamma^n \\ \text{Herschel Buckley:} \quad & \tau = \tau_y + K\gamma^n \end{aligned}$$

Most of the successful drilling fluids are non-Newtonian and thus understanding the behaviour of gas migration in non-Newtonian fluids is important.

1.9 Multiphase flows

Multiphase flows are characterized as presence of more than one phase during a fluid flow. Multiphase flows are encountered at different situation in petroleum industry during various operations ranging from drilling to transportation of refined products. In this section, different regimes of multiphase flow and the requirements to differentiate them are discussed. A brief introduction to such application in drilling is also given.

Flow regimes

One of the most common encounter of multiphase flow in petroleum industry is during the production phase, where gas and liquid are produced together in the same tubing. Plethora of work has been done to calculate the pressure drop in such scenarios. One of the most accepted work has been provided by Aziz et al. (1972). Griffith et al. (1984) reviewed works on multiphase flow and categorized the books to be referred according to the main focus of the flow regime which can be visualized as shown in figure 1.8 for vertical flow regimes and figure 1.9 for horizontal flow regimes.

Different flow regimes exists depending on the amount of different phases available in the flow area or in other terms denoted by void fraction, ϵ or its compliment liquid fraction.

$$\epsilon = \frac{\text{Volume occupied by gas}}{\text{Total volume of the test cell}} \tag{1.27}$$

Usage of void fraction to determine the flow regime is shown later in this chapter while it can also be determined based on the superficial velocities of different phases. Superficial velocity of a phase may be defined as an imaginary velocity of that phase through the same flow area in absence of the other phase. Several flow regime maps are available through various experiments at different conditions. A flow regime map for air and water in

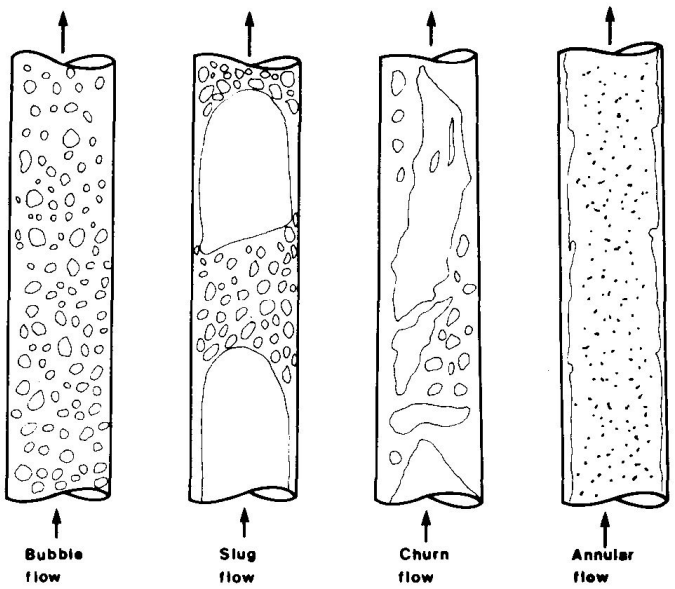

Figure 1.8: Vertical multiphase flow regimes

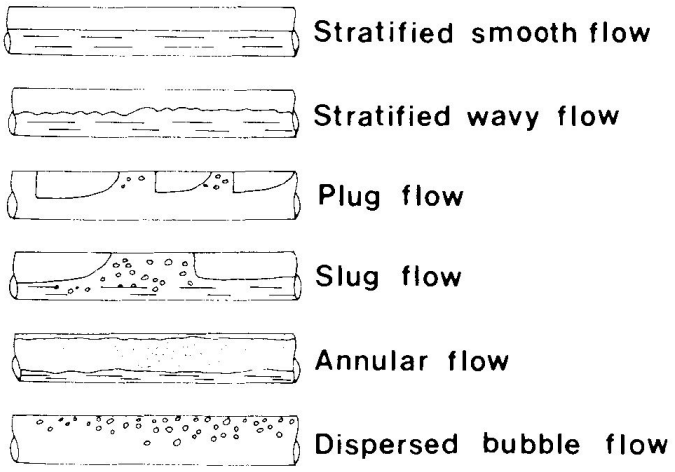

Figure 1.9: Horizontal multiphase flow regimes

a vertical up flow at 75°F and 1 atm, that is adapted from Griffith et al. (1984) is shown in figure 1.10.

A good review for the flow due to severe slug formation in pipeline or riser pipe system and other flows during the production phase of the well is provided by Brill et al. (1987). As the void fraction increases, the pressure drop is majorly contributed by friction across the flow area. One such

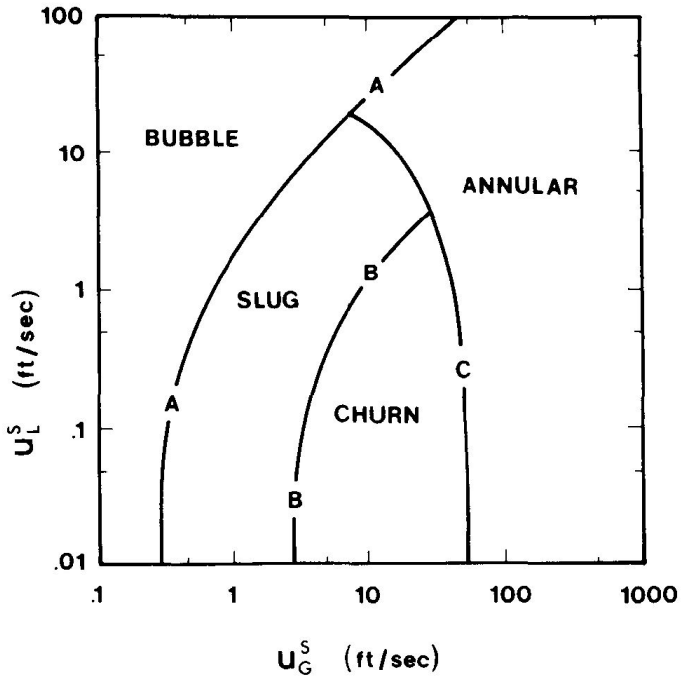

Figure 1.10: Flow regime map for air and water in vertical upflow

model for a gas-liquid slug flow is given by Orell and Rembrand (1986) which incorporates mass balance equations and solving them simultaneously to understand the frictional effects. Though relatively less work has been carried out to understand these flows in annular region, a notable work is done by Yu et al. (2010). Similarly, study of two phase flow in inclined pipes is done by Beggs et al. (1973) and investigation of gas bubbles rising in closed pipe is done by Al-Darmaki et al. (2008).

1.10 Gas Rise Velocity

It has been discussed in section 1.9 that though various parameters are available to identify flow regimes in multiphase flow, we are resorted to use void fraction as defined by equation 1.27. Plethora of work had been done in regards to the horizontal multiphase flow as compared to that of vertical flow. Although, from (Johnson and White, 1993) it is observed that for $\epsilon < 0.15$ is considered as bubbly flow and $\epsilon > 0.30$ is considered as slug flow and the flow is transitional in between. Based on the flow regime, bubble rise velocities in the medium varies. A general relation of velocities is stated as in (Johnson et al., 1991),

$$V_G = C_o V_h + V_{rel} \tag{1.28}$$

where C_o is constant, v_rel is the relative velocity of the gas bubble and the homogeneous velocity, v_h is defined as

$$v_h = v_{GS} + v_{LS} = \frac{Q_G}{A} + \frac{Q_L}{A} \tag{1.29}$$

v_{GS} and v_{LS} are the gas and liquid superficial velocity respectively, A is the cross sectional area of the flow and Q_G and Q_L are the volumetric flow rates of gas and liquid respectively. A correlation for experimental data describing the rise of single bubble as a function of density and inter facial tension. The bubble rise velocity given by this correlation as stated in (Johnson et al., 1991),

$$v_{rel} = 1.53\Big[\frac{g(\rho_L - \rho_G)\sigma}{\rho_L^2}\Big] \tag{1.30}$$

where ρ_L and ρ_G are the liquid and gas densities respectively, σ is the inter-facial tension generally between 38-60 $dynes/cm^2$ (Rader et al., 1975). An average value is considered in this report. As void fraction, ϵ_{CH_4} increases, due to hindrance from other bubbles, the velocity is reduced and is stated in (Johnson and White, 1993) as,

$$v_{rel} = v_{rel0}(1 - \epsilon)^c \tag{1.31}$$

where, v_{rel0} is the velocity of isolated bubble and c is a constant ranging from 0-3 depending on the bubble size. v_{rel0} is given by the above equation and c of 1.5 is considered in this work. For higher void fractions, > 0.30, flow regime is considered as slug flow and Taylor(1950) gave the equation for slip velocity of gas bubble in slug flow as,

$$v_{rel} = 0.35\sqrt{\frac{g(\rho_L - \rho_G)D}{\rho_L}} \tag{1.32}$$

where D is the diameter of the pipe. In case of annulus, as in the riser region, this is replaced by D_{eff} which is defined as follows,

$$D_{\text{eff}} = \frac{1}{2}\Big[\frac{\pi(D_o + D_i)}{2} + \frac{D_o - D_i}{2}\Big] \tag{1.33}$$

where D_o and D_i are in the outer and inner diameter of the annulus, respectively. Since the annular capacity is known effective diameter, D_{eff} is calculated accordingly. It has also been found by Johnson et al. (1991) through various experiments that the background void fraction of 0.02 is always suspended in the solution due to the yield stress and gelling etc., which plays an important role in the frictional pressure drops. It has been considered in this work that, 0.02% of the free gas is always suspended in the solution and only the rest is available for expansion.

1.10.1 Real Gas Approximation

In this section of the chapter, mathematical models and correlations for the liquid and gas expansion considering real gas behaviour are shown. Real gas behaviour and the required model is very well depicted by Whitson et al. (2000) and the required shall be discussed here. To be as close as possible to the real model, Peng Robinson equation of states (EOS) is used in this work, which can be described as follows,

$$p = \frac{RT}{v-b} - \frac{a}{v(v-b)+b(v-b)} \tag{1.34}$$

or, in terms of Z-factor,

$$Z^3 - (1-B)Z^2 + (A - 3B^2 - 2B)Z - (AB - B^2 - B^3) = 0 \tag{1.35}$$

Rearranging equation 1.34 in terms of v,

$$PV^3 + (Pb - RT)V^2 - (RT - 3b^2P - 2bRT + a)V + (RTb^2 + Pb^3 - ab) = 0 \tag{1.36}$$

The EOS constants are given by,

$$A = a\frac{P}{(RT)^2}$$
$$B = b\frac{P}{RT}$$
$$a = \Omega_a^0 \frac{R^2T_c^2}{p_c}\alpha$$

where $\Omega_a^0 = 0.45724$;

$$b = \Omega_b^0 \frac{RT_c}{p_c}$$

where $\Omega_b^0 = 0.07780$;

$$\alpha = [1 + m(1 - \sqrt{T_r})]^2$$

and $m = 0.37464 + 1.54226\omega - 0.26992\omega^2$ where ω is the accentric factor for a component.

1.11 Problem statement

Having discussed the general approach to address various complex multi-phase flow situations, this part of the section provides an overview of the specific problem that is attempted to address in the work of this report. The case is similar to the situation shown in the figure 1.6 but the riser is considered to be more lengthier in such a way that the free gas evolves out of the solution somewhere along the length of the riser.

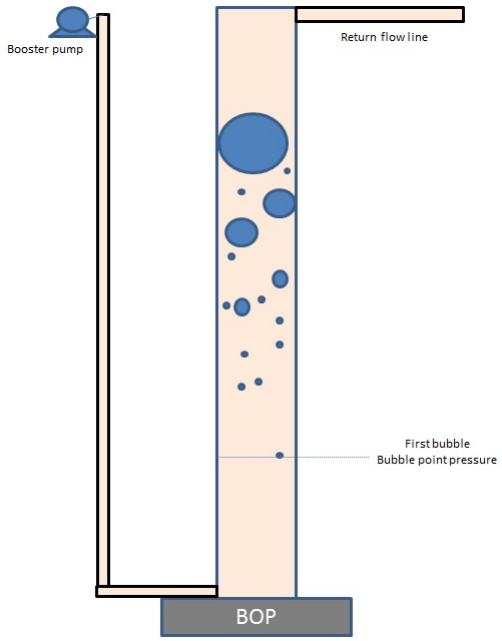

Figure 1.11: Schematic of the gas expansion in marine risers

Another fact that differentiates from the previous situation is that there is no continuous supply of gas from the formation since it is assumed that the surface indications have been shut in successfully. A schematic of one such system is shown in figure 1.11 where the bubble point pressure of the system is within the range of hydrostatic pressure experienced within the riser system. The gas would start flashing out once the contaminated mud experiences reduction in pressure due to circulation. Rapid expansion of gas bubble accompanied by the circulation and slip velocities, near the top of the riser would assist in expelling most of the mud out of the riser and this process is called *riser unloading*. A particular point can be defined within the riser region, above which a slightest expansion of the gas will lead to riser unloading since the hydrostatic pressure of the mud will be no longer sufficient to contain the gas. The work in this thesis attempts to understand and identify the riser equilibrium point and propose a way to circulate the mud out without experiencing unloading of riser. This can be achieved by understanding the expansion dynamics of gas in such systems. Aim of this work is to formulate mathematical models of various schemes and try capture the dynamics of this system. The methodology for achieving that is discussed in the later sections.

Chapter 2

Mathematical Formulation

2.1 Analytical Solution - Explicit WBM

It is always necessary to look for analytical solutions for system of equations which are the most accurate and exact answers. But owing to the complexity of mathematical models that are developed to capture the distributed dynamics of the physical systems, it is not easy to arrive at an analytical solution whereas look for numerical schemes to solve the same with a defined accuracy. This section of the chapter covers the most ideal case that can be considered for the system in question and depicts the explicit scheme adapted to get an analytical solutions. The components considered here are water based mud (WBM) and methane without any chemical interaction between them with no dissolution. The gas is assumed to behave ideally in this section. Schematic of the system that is followed throughout this section is shown in figure 2.1. The dimensions of the riser are described in terms of capacity, *cap*, which is the ratio of volume contained to the respective height occupied. It can be represented as in equation 2.1 and is usually represented in terms of bbl/ft.

$$\text{Capacity}, cap = \frac{\text{Volume of liquid in riser}}{\text{Height occupied for the respective volume}} \tag{2.1}$$

2.1.1 Ideal situation

Apart from the initial assumptions considered, ideal situation means that there are no frictional and acceleration losses resulting from the flow of mud and the expansion of gas. The variables mentioned in the figure 2.1 mean

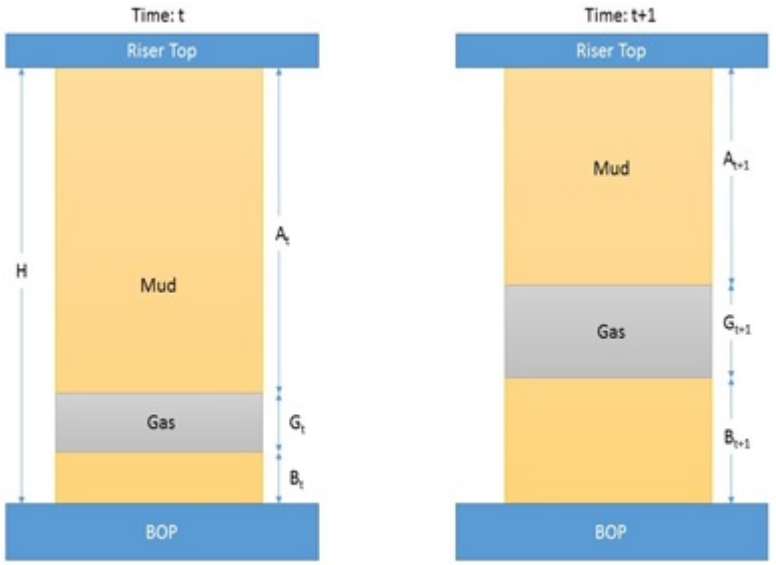

Figure 2.1: Schematic of the gas expansion for an analytical solution in case of WBM

the following,

A_n = Height of the pure mud above the gas bubble at time, n
B_n = Height of the pure mud below the gas bubble at time, n
G_n = Height of the gas bubble at time, n
H = Total height of the riser

Considering the situation and the variables stated in figure 2.1 mud height at a given time, $t+1$ is equal to sum of all the portions and can be written as,

$$A_{t+1} = H - B_{t+1} - G_{t+1} \tag{2.2}$$

Using equation 2.1 in equation 2.2,

$$A_{t+1} = H - B_{t+1} - \frac{V_{t+1}}{cap} \tag{2.3}$$

Considering ideal gas behaviour which is governed by the *ideal gas law*,

$$PV = nRT \tag{2.4}$$

Assuming that the temperature is constant throughout the riser length, gas properties at two different conditions 1 and 2 can be related as

$$P_1V_1 = P_2V_2 \tag{2.5}$$

Rewriting equation 2.3 using equation 2.5,

$$A_{t+1} = H - B_{t+1} - \frac{1}{cap}\frac{P_t V_t}{P_{t+1}} \tag{2.6}$$

As we know that pressure at any instant n in this case, P_n, is due to the hydrostatic height of the mud at that instant A_n and is given by

$$P_n = \rho g A_n \tag{2.7}$$

Using this relation in the equation 2.6,

$$A_{t+1} = H - B_{t+1} - \frac{1}{cap}\frac{\rho g A_t V_t}{\rho g A_{t+1}}$$

Since we are assuming that the fluid is incompressible, its density is constant and is independent of pressure. Using equation 2.1,

$$A_{t+1} = H - B_{t+1} - \frac{A_t G_t}{A_{t+1}}$$

Rearranging, we get the following quadratic equation

$$A_{t+1}^2 - (H - B_{t+1})A_{t+1} + A_t G_t = 0 \tag{2.8}$$

Now, the mud height above the gas bubble at any time can be found by solving the equation 2.8 for which the roots of A_{t+1} is given by

$$A_{t+1} = \frac{-b \pm \sqrt{b^2 - 4ac}}{2a}$$

where,

$$\begin{aligned} a &= 1 \\ b &= -(H - B_{t+1}) \\ c &= A_t H_t \end{aligned}$$

when the roots are obtained for the quadratic equation 2.8, the root that has a decreasing locus function, ie., $\frac{-b + \sqrt{b^2 - 4ac}}{2}$ is the height of the mud above the gas bubble and the root of increasing locus function, ie., $\frac{-b - \sqrt{b^2 - 4ac}}{2}$ is the height of the gas bubble. As per the general rules of roots for quadratic equation, there exists no real roots when, $b^2 < 4ac$. when there exists no physical solution of mud or gas bubble height for a given gas bubble or mud height respectively, that point may possibly be considered as *riser equilibrium.*

Note: The case described above is for a fully open choke or in other words, when the pressure experienced at any point is due to the hydrostatic head without a back pressure from the choke. In case the choke is considered, and the choke pressure, P_{choke} is assumed to be constant throughout the process, then at time, $t = 1$, equation 2.7 would become as follows,

$$P_1 = \rho g A_1 + P_{choke}$$

and this would in turn, affect the initial gas height and solution for the mud height above the gas for further time steps will be taken care implicitly in this simulation. Whereas, when a varying choke pressure is to be included, then the equation 2.7 would have to be represented as,

$$P_n = \rho g A_n + P_{choke,n} \tag{2.9}$$

and the derivation of the above equations would be modified to incorporate this time varying parameter. This would allow the reformulation of equation 2.7 to equation 2.9 and thus in equation 2.6,

$$P_{t+1} = \rho g A_{t+1} + P_{choke,t+1} \tag{2.10}$$

Defining the known constants and user defined variables as,

$$M = H - B_{t+1}$$
$$N = P_t G_t$$

Equation 2.6 can be re-written as

$$A_{t+1} = M - \frac{N}{\rho g A_{t+1} + P_{choke,t+1}} \tag{2.11}$$

$$A_{t+1}(\rho g A_{t+1} + P_{choke,t+1}) = M\rho g A_{t+1} + P_{choke,t+1} - N \tag{2.12}$$

$$\rho g A_{t+1}^2 + (P_{choke,t+1} - M\rho g)A_{t+1} - M P_{choke,t+1} + N = 0 \tag{2.13}$$

To solve this quadratic equation, the solution method mentioned above is used while the coefficients are changed as,

$$a = \rho g$$
$$b = P_{choke,t+1} - M\rho g$$
$$c = M P_{choke,t+1} + N$$

2.1.2 Including Frictional Loss

Though other assumptions for the given case still holds as described in this section, following scheme is an attempt to relax one of those assumptions. Frictional losses due to the flow of mud and gas expansion is considered

here. Frictional loss due to the expansion of gas, in particular, is very less and is neglected. Taking P_{choke} into account at all time steps paves way to the possibility of studying varying choke pressure over time. Starting from 2.6, which can be re-written as,

$$A_{t+1} = H - B_{t+1} - \frac{P_t G_t}{P_{t+1}} \tag{2.14}$$

At time, $t+1$, due to the displacement of mud above the gas bubble as a result of circulation and gas expansion, the pressure experienced by the gas bubble would be (from equation 2.9),

$$P_{t+1} = \rho g A_{t+1} + |\Delta P_{fric}| + P_{choke,t+1} \tag{2.15}$$

It must be noted here that the displacement of the mud above would result in decrease in hydrostatic head (since $A_{t+1} < A_t$) with an absolute additive of the frictional term since the flow is vertical and the frictional force will be experienced against the flow direction. Elaborating the terms in equation 2.15 and considering the frictional loss as described in section 1.6

$$\begin{aligned} P_{t+1} &= \rho g A_{t+1} + |\Delta P_{fric}| + P_{choke,t+1} \\ &= \rho g A_{t+1} + \left| \frac{32\mu\nu}{d^2} \Delta H \right| + P_{choke,t+1} \end{aligned}$$

Since velocity is described as ratio of distance to time, ν can be represented as $\dfrac{|A_{t+1} - A_t|}{\Delta t}$,

$$P_{t+1} = \rho g A_{t+1} + \left| \frac{32\mu}{d^2} \frac{A_{t+1} - A_t}{\Delta t} \big(A_{t+1} - A_t\big) \right| + P_{choke,t+1} \tag{2.16}$$

$$P_{t+1} = \rho g A_{t+1} + K\big(A_{t+1} - A_t\big)^2 + P_{choke,t+1} \tag{2.17}$$

Defining known values in equations 2.1.3 and 2.16 as,

$$\begin{aligned} K &= \frac{32\mu}{\Delta t d^2} \\ M &= H - B_{t+1} \end{aligned}$$

and re-writing equation 2.1.3

$$A_{t+1} = M - \frac{P_t G_t}{\rho g A_{t+1} + K\big(A_{t+1} - A_t\big)^2 + P_{choke,t+1}} \tag{2.18}$$

$$\begin{aligned} &A_{t+1}\big(\rho g A_{t+1} + K\big(A_{t+1} - A_t\big)^2 + P_{choke,t+1}\big) \\ &\qquad = M\big(\rho g A_{t+1} + K\big(A_{t+1} - A_t\big)^2 + P_{choke,t+1}\big) - P_t G_t \end{aligned} \tag{2.19}$$

$$A_{t+1}\big(\rho g A_{t+1} + K\big(A_{t+1}^2 - A_t^2 - 2A_t At + 1\big) + P_{choke,t+1}\big) = M\big(\rho g A_{t+1} + K\big(A_{t+1}^2 - A_t^2 - 2A_t At + 1\big) + P_{choke,t+1}\big) - P_t G_t \quad (2.20)$$

$$KA_{t+1}^3 + \big(\rho g - 2KA_t - KM\big)A_{t+1}^2 + \big(KA_t^2 - M\rho g + 2KMA_t + P_{choke,t+1}\big)A_{t+1} - KMA_t^2 + P_t G_t - MP_{choke,t+1} = 0 \quad (2.21)$$

2.1.3 Including Frictional and Acceleration Losses

As mentioned in the section 2.1.2, all the assumptions are carried forward and that the frictional and acceleration losses for the gas phase is negligible as compared to the liquid phase and thus it is not considered in this model. Similar to the frictional loss, kinetic or the acceleration loss is also additive in nature for each time step since it acts opposite to the direction of the flow of the fluids. One such model is adapted from the section 1.6. By including choke pressure, P_{choke} at every instant to account for a varying choke pressure, beginning with equation 2.1.3,

$$A_{t+1} = H - B_{t+1} - \frac{P_t G_t}{P_{t+1}}$$

At time, $t+1$, due to the displacement of mud above the gas bubble as a result of circulation and gas expansion, the pressure experienced by the gas bubble would be (from equation 2.9),

$$P_{t+1} = \rho g A_{t+1} + |\Delta P_{fric}| + |\Delta P_{acc}| + P_{choke,t+1} \quad (2.22)$$

$$= \rho g A_{t+1} + \left|\frac{32\mu\nu}{d^2}\Delta H\right| + \frac{\rho}{2\Delta t^2}\big(\nu_2^2 - \nu_1^2\big) + P_{choke,t+1} \quad (2.23)$$

where, ν_1 and ν_2 are the velocities at time t and $t+1$ respectively. Representing them in terms of the height of the mud above, A,

$$P_{t+1} = \rho g A_{t+1} + \left|\frac{32\mu\nu}{d^2}\Delta H\right| + \frac{\rho}{2\Delta t^2}\big[\big(A_{t+1} - A_t\big)^2 - \big(A_t - A_{t-1}\big)^2\big] + P_{choke,t+1} \quad (2.24)$$

Defining the constants and/or user defined variables as,

$$K = \frac{32\mu}{\Delta t d^2}$$
$$M = \frac{\rho}{2\Delta t^2}$$
$$N = \big(A_t - A_{t+1}\big)^2$$
$$S = K + M$$
$$T = -MN + P_{choke,t+1}$$
$$F = H - B_{t+1}$$

Rearranging the equation 2.24, with the defined constants,

$$P_{t+1} = \rho g A_{t+1} + K\big(A_{t+1} - A_t\big)^2 + M\big[\big(A_{t+1} - A_t\big)^2 - N\big] + P_{choke,t+1} \tag{2.25}$$

$$= \rho g A_{t+1} + \big(K + M\big)\big(A_{t+1} - A_t\big)^2 - MN \tag{2.26}$$

$$= \rho g A_{t+1} + S\big(A_{t+1} - A_t\big)^2 + T \tag{2.27}$$

Using equation 2.27 in equation 2.1.3,

$$A_{t+1} = F - \frac{P_t G_t}{\rho g A_{t+1} + S\big(A_{t+1} - A_t\big)^2 + T} \tag{2.28}$$

$$\begin{aligned} &\rho g A_{t+1}^2 + S A_{t+1}\big(A_{t+1}^2 - A_t^2 - 2A_t At + 1\big) + T A_{t+1} \\ &\qquad = F\rho g A_{t+1} + FS\big(A_{t+1}^2 - A_t^2 - 2A_t At + 1\big) + FT - P_t G_t \end{aligned} \tag{2.29}$$

$$\begin{aligned} &S A_{t+1}^3 + \big(\rho g - 2SA_t - FS\big)A_{t+1}^2 + \\ &\qquad \big(SA_t^2 + T - F\rho g + 2FSA_t\big)A_{t+1} - FSA_t^2 - FT + P_t G_t = 0 \end{aligned} \tag{2.30}$$

2.1.4 Solution Characteristics

Equations 2.21 and 2.30, gives a cubic expression of A_{t+1} which can be solved in MATLAB using the built-in function *'root'*. It is important to note varying characteristics of the roots to this cubic equation.

- When the roots are a set of imaginary numbers (they are complement to each other) and a real number, the value of A_{t+1} is the real number,
- When the roots are a set of real numbers, the maximum of the non-negative value is considered as the value of A_{t+1} and
- When the roots are all negative at a particular time step, $t + 1$, it denotes that variables at time t corresponds to that of the *riser equilibrium*.

2.2 Implicit solution - WBM

Another method of obtaining the results instead of deriving an explicit equations for the mud height above the bubbles, is to solve them implicitly. This can be obtained by a proper formulation of implicit system of equations and further solved using the in-built functions such as *fsolve*, which has been used in this work. The formulations for various cases are discussed further using the variables denoted in figure 2.1,

2.2.1 No Losses

Since all the assumptions that have been considered earlier for an OBM system holds here and that it is further assumed that there are no frictional and acceleration losses but has a supply of back pressure p_c from a choke, let the states of the system be defined as,

$$\vec{X} = \begin{bmatrix} A_t \\ G_t \end{bmatrix} \tag{2.31}$$

And due to the possibility of solving implicit schemes, real gas behaviour can be considered since the z-factor calculation is also an implicit scheme at for a given pressure and temperature. The method of calculating z-factor is elaborated later, while it can be represented as z(p,T) denoted that it is a function of pressure and temperature. And the real gas law can be represented as,

$$pV = z(p + p_c, T)nRT \tag{2.32}$$

Since 'p' is the hydrostatic pressure which is due to the mud height above the bubble. As the parameter A_t is the first state, pressure can be expressed as $p(X(1))$. In case of WBM, since there are no gas dissolution in the base fluid, amount of gas that is present in the free gas is constant at all times and since the gas height can be represented as v/cap,

$$F(1) = H - X(1) - X(2) - B \tag{2.33}$$

$$F(2) = X(2) - \frac{z(p(X1) + p_c, T)nRT}{cap \times (p(x(1)) + p_c)} \tag{2.34}$$

These set of equations can be solved using the function *fsolve* in MATLAB. Initial value of B is zero, which gives the initial equilibrium condition and when this set of equations is solved continuously over an iterative loop by increasing the value of B at each time step which corresponds to the velocity of the circulation, height of the gas bubble and the height of the mud above the bubble can be obtained. When the equation fails or provides a non-unique solution (which can be known from the *exitflag* option of the solver, it is considered as the *riser equilibrium point*, above which a slight movement of the mud would lead to explosive riser unloading.

Note: One must be very cautious of the system of units that are used while solving the implicit equations. All parameters must be consistent in the units used.

2.2.2 Frictional Loss

Similar to the model described in section 2.2.1, an implicit set of equations have been generated for the case where the frictional loss due to expansion

of gas and the resulting movement of the mud above the gas bubble. In presence of a choke, the states of the system can be defined as,

$$\vec{X} = \begin{bmatrix} A_t \\ G_t \end{bmatrix} \tag{2.35}$$

And the governing equation for gas bubble is,

$$pV = z(p(X(1)) + p_c + dp_{fric}, T)nRT \tag{2.36}$$

where,

$$dp_{fric} = \frac{32\mu_{mud}\nu\Delta A}{d^2} \tag{2.37}$$

Equation 2.37 can be re-written by replacing the velocity as $\Delta A/dt$,

$$dp_{fric} = \frac{32\mu_{mud}(\Delta A)^2}{dt \times d^2} \tag{2.38}$$

And thus, set of implicit equations can be written as,

$$F(1) = H - X(1) - X(2) - B \tag{2.39}$$

$$F(2) = X(2) - \frac{z(p(X(1)) + p_c + dp_{fric}, T)nRT}{cap \times (p(X(1)) + p_c + dp_{fric})} \tag{2.40}$$

2.2.3 Frictional and Acceleration Loss

It can be observed that due to expansion of gas, the mud above the bubble accelerates in its way up. This is significant towards the top of the riser where the gas expansion is rapid. To study its effect, pressure loss due to acceleration of fluid can be defined as,

$$dp_{acc} = \frac{1}{2}\rho\nu^2 \tag{2.41}$$

Replacing the velocity in terms of displacement, equation 2.41 can be re-written as,

$$dp_{acc} = \frac{1}{2(dt)^2}\rho((\Delta A_t)^2 - (\Delta A_{t-1})^2) \tag{2.42}$$

where ΔA_n is the change in displacement as observed at time n. The states of this system can be written as,

$$\vec{X} = \begin{bmatrix} A_t \\ G_t \end{bmatrix} \tag{2.43}$$

And the governing equation for gas bubble can be written as,

$$pV = z(p(X(1)) + p_c + dp_{fric} + dp_{acc}, T)nRT \tag{2.44}$$

And thus, set of implicit equations can be written as,

$$F(1) = H - X(1) - X(2) - B \tag{2.45}$$

$$F(2) = X(2) - \frac{z(p(X(1)) + p_c + dp_{fric} + dp_{acc}, T)nRT}{cap \times (p(X(1)) + p_c + dp_{fric} + dp_{acc})} \tag{2.46}$$

2.3 Analytical solution - OBM

This section covers the mathematical formulation and solution method for a simplified case while considering gas dissolution in OBM. For the cases considered in this section, the schematic representation of the problem is given by figure 2.2. The variables in the schematic figure 2.2, denotes the

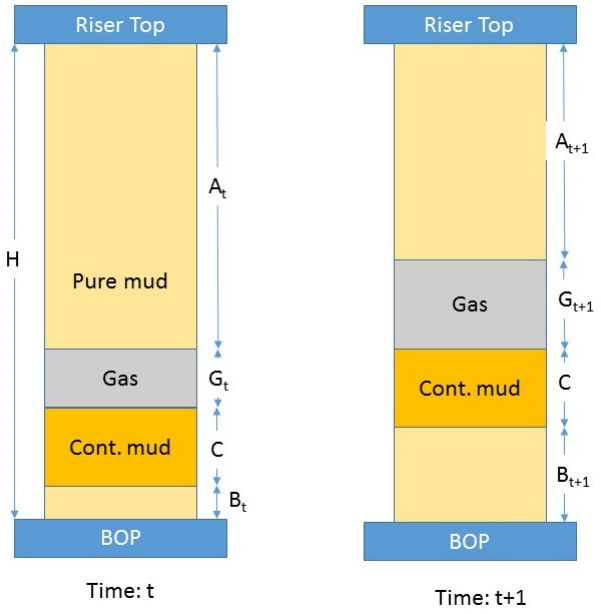

Figure 2.2: Schematic of the gas expansion for an analytical solution in case of OBM

following,

A_n = Height of the pure mud above the gas bubble at time, n
B_n = Height of the pure mud below the gas bubble at time, n
G_n = Height of the gas bubble at time, n
C = Height of the contaminated mud (Constant)
H = Total height of the riser

To formulate a mathematical structure for the given situation with OBM, the following are assumed,

- Amount of gas present is completely dissolved only in the base oil of the OBM at the initial condition and the gas flashes out as the circulation is started.

- To achieve such situation, the system of contaminated mud is just at its bubble point pressure.
- Volume of the contaminated mud is constant throughout the circulation period.
- Due to lack of proper estimate of dynamic value of formation volume factor (B_o) of the oil, based on the calculation shown further it is assumed to be 1.7 (see later part of this section).
- No diffusion of fluid from the oil phase to the mud above and below the contamination is considered.
- No chemical reaction takes place between the base oil, mud and methane.
- Pressure in the contaminated mud is considered constant throughout its volume and is always a function of the hydrostatic head of the pure mud above it.

2.3.1 Fluid solubility

In order to understand the solubility of gas in a particular system, estimation of the parameters such as bubble point pressure, solution gas oil ratio and formation volume factor are necessary. Definition and the estimation methods adapted in this work are as follows,

Bubble Point Pressure

A system in which the gas is completely dissolved in the solution, when exposed to reduction in pressure, the pressure at which the first bubble boils out of the solution to exist as a free gas is termed as bubble point pressure. This is generally a tricky parameter to estimate and is usually measure through experimental work since the bubble point pressure varies with the composition of gas within the dissolved system and is very sensitive to the proportion of gas component dissolved in it. Among various works, O'Bryan et al. (1988) studied the gas solubility in oil based drilling fluids and compared the results between that of various base oils focusing on the solution gas oil ratio to estimate the amount of gas that is soluble at a particular pressure. Thomas et al. (1984) studied the effect of gas solubility in kick detection and carried out experimental studies for diesel oil system and oil based mud system with main focus on estimating bubble point pressure. Comparison of methane solubilities in various systems of synthetic oil based drilling muds was carried out by Berthezene et al. (1999), of which diesel oil system is one among them. The experimental solubility data obtained by Berthezene et al. (1999) at $90^{\circ}C$ is given in table 2.2. It is important to note that among the conservative list of base constituents of an OBM, which are

water, oil and emulsifier, major fraction of gas in dissolved in the base oil as compared to the other constituents. Table 2.1 presents the total amount of gas dissolved in each of the three major constituents of the drilling fluid, in the proportion needed for a 1 liter formulation that gives a stable emulsion as mentioned in (Berthezene et al., 1999). It can be noted from the data in

Table 2.1: Experimental methane solubility data in base components of drilling fluid

	Base Constituents		
	Water	Emulsifier	Oil
Amount of liquid (for 729 g of emulsion)	120	13	596
Total gas absorbed (g) as measured	0.38	0.93	53.16

Table 2.2: Experimental methane solubility data in diesel oil at 90 °C

Pressure bar	w_{CH_4}	x_{CH_4}
350	0.1188	0.6510
300	0.0986	0.6021
250	0.0801	0.5467
200	0.0633	0.4835
150	0.0468	0.4046

table 2.1 that amount of gas that is dissolved in the base oil is around 97.6% of the total amount of gas that is dissolved in the liquid. This justifies the assumption made earlier that the gas is dissolved only in the base oil of the drilling fluid. The terms mass fraction, w_{CH_4} and mole fraction χ_{CH_4} are defined as,

$$w_{CH_4} = \frac{m_{CH_4}}{m_{liquid} + m_{CH_4}} \tag{2.47}$$

$$\chi_{CH_4} = \frac{n_{CH_4}}{n_{liquid} + n_{CH_4}} \tag{2.48}$$

Using the data in table 2.2, bubble point pressures are extrapolated as a function of mass fraction, w_{CH_4} and mole fraction, χ_{CH_4} of methane in the diesel oil and are given by equations,

$$P_b = 2 \times 10^6 w_{CH_4} - 727450 w_{CH_4}^3 + 85273 w_{CH_4}^2 - 1134.5 w_{CH_4} + 80.773 \tag{2.49}$$

$$P_b = 37.589 e^{(3.446 \chi_{CH_4})} \tag{2.50}$$

where,

P is pressure in bars

m_x is the mass of component 'x', Kg

n_x is the number of moles of component 'x', Kmol

The experimental measurements for the methane and diesel oil system as reported in Thomas et al. (1984) is given in table 2.3

Table 2.3: Experimental measurements for methane/diesel oil system

Methane ($mole\%$)	Bubblepoint pressure at $100°F$ (psia)
19.08	805
23.92	1000
28.76	1320
34.28	1682
39.01	2065
44.24	2405
54.26	3635
61.23	4820
66.45	5790

The equation that extrapolates the data in table 2.3 to find the bubble point pressure as a function of mole percent of methane is,

$$P_b = 0.0257x_{CH_4}^3 - 1.5717x_{CH_4}^2 + 85.11x_{CH_4} - 444.21 \tag{2.51}$$

where,

P is pressure in psia

x_{CH_4} is the mole percent of CH_4, %

To have a consistent system to compare both the systems, mole composition is chosen as an obvious choice as it is the common parameter that is available for both the system. A plot of bubblepoint pressure for various mole fraction, with proper unit conversions, can be seen in figure 2.3 which states that 2.50 is a better predictor of bubblepoint pressure, since that provides a more realistic values as compared to the extrapolation in equation 2.51, which shows a negative or unrealistic bubble point pressure at lower mole fractions.

Solution gas oil ratio

Solution gas oil ratio, R_s, can be defined as the amount of gas that can be dissolved in 1 STB of oil. It is usually expressed in the units of scf/STB.

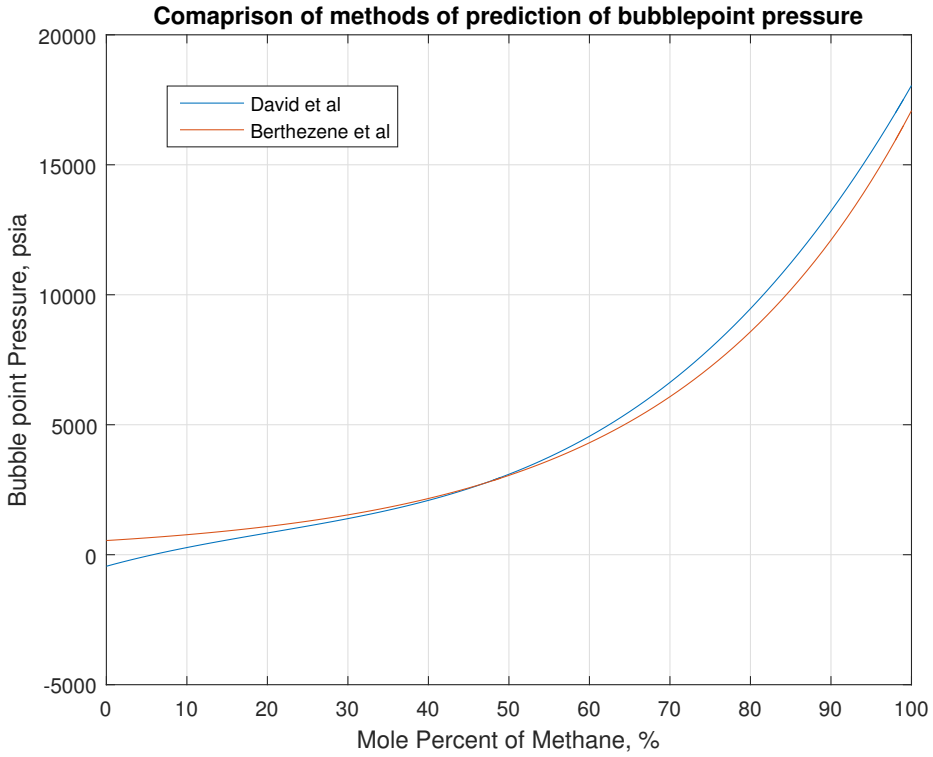

Figure 2.3: Comparison of methods of prediction of bubble point pressure

Among several ways to calculate the R_s, O'Bryan et al. (1988) carried out several experiments to calculated this ratio for various components of the drilling fluid. According to the assumption justified earlier, that the dissolution of gas in considered only in the base oil, the R_s relation is given as (O'Bryan et al., 1988),

$$R_s = (\frac{P}{aT^b})^n \tag{2.52}$$

where for this particular system,

R_s solution gas oil ratio, scf/STB

P pressure in psi

T temperature in F

$a = 1.922$

$b = 0.2552$

γ_g = specific gravity of gas

$$n = 0.3576 + 1.168\gamma_g + (0.0027 - 0.00492\gamma_g)T - (4.51\times10^{-6} - 8.198\times10^{-6}\gamma_g)T^2$$

The most commonly used correlation for prediction of R_s for most of the petroleum systems is given by Vazquez and Beggs correlation and is stated as (Vazquez et al., 1980),

$$R_s = C_1 \gamma_{gs} p^{c_2} exp C_3 (\frac{\gamma_o}{T + 460}) \tag{2.53}$$

$$\gamma_{gs} = \gamma_{gp}[1 + 1.5912 \times 10^{-5} (\gamma_o) T log(p/114.7)] \tag{2.54}$$

where

γ_{gs} = gas gravity resulting from 100 psig
γ_{gp} = gas gravity at separator conditions, P and T
p = actual separator pressure, psia
T = actual separator temperature, F
γ_o = oil gravity, $^\circ$ API

and the values of coefficients are given in table 2.4 It is important to note

Table 2.4: Values of coefficient for R_s calculations

coefficient	$\gamma_o \leq 30$	$\gamma_o > 30$
C_1	0.0362	0.0178
C_2	1.0937	1.1870
C_3	25.7240	23.9310

here that the equation 2.50 is also an indirect measure of R_s since its gives the amount of gas that can be dissolved in a system at a given pressure and vice-versa which is also denoted by equation 2.53 and 2.52 but in different units. A comparison between these correlations have been done so as to use it in the current study and is represented in figure 2.5. The standard for the comparison is obtained from Thomas et al. (1984), which shows the solubility of methane in No.2 Diesel fuel at variety of pressure and temperatures. The data has been digitized (see figure 2.4) and extrapolated by fitting a polynomial of fourth order given by equation 2.3.1

$$R_s = (2.48 \times 10^{-15} p^4 - 2.37 \times 10^{-11} p^3 + 9.75 \times 10^{-8} p^2 + 0.000027 p + 0.015) * 1000 \tag{2.55}$$

where,

R_s = Solution gas oil ratio, scf/STB
p = pressure, psia

As can be seen from the figure 2.5, various correlation estimate the value of solution gas oil ratio similarly at lower pressures whereas they deviate too

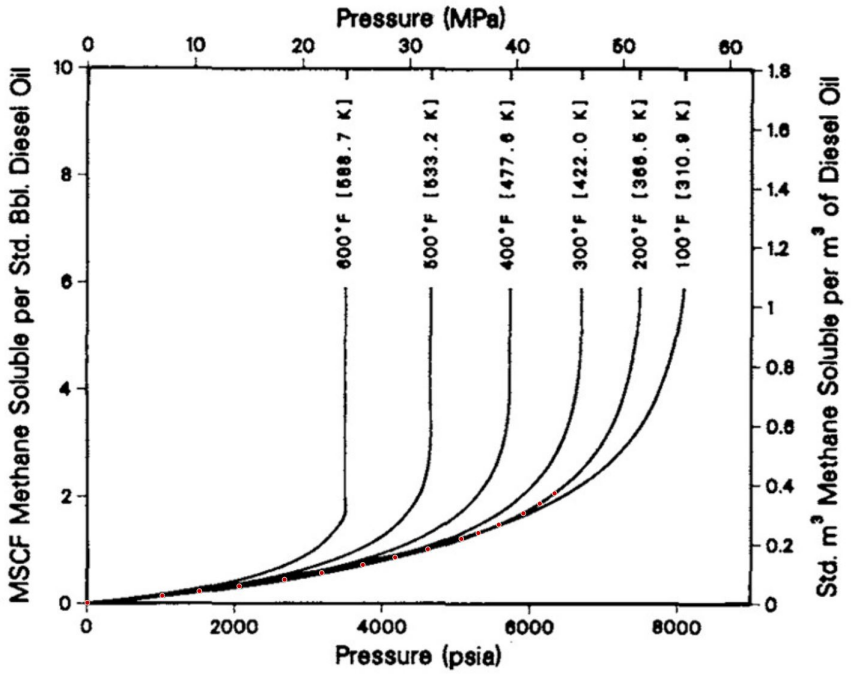

Figure 2.4: Digitized plot for a standard comparison of R_s

much from the standard data at higher pressures. It has been observed that the fit of the standard data is much more reliable since the values coincide with the experimental data obtained at higher pressures of the system and thus the standard fit is the reliable correlation to calculate R_s. It must be noted that once the bubble point pressure is found, R_s is constant for the pressures above bubblepoint.

Formation Volume Factor

Due to release of gas from the solution when introduced to reduction in pressure, oil shrinks as more gas is released. The extent of shrinkage is provided by formation volume factor, B_o which can be defined as,

$$B_o = \frac{\text{Volume of oil in reservoir conditions, bbl}}{\text{Volume of oil at standard conditions, STB}} \tag{2.56}$$

One particular method of estimating B_o for pressures below bubblepoint is given by Vazquez et al. (1980) as,

$$B_o = 1 + C_1 R_s + C_2(T - 60)(\gamma_o/\gamma_{gs}) + C_3 R_s(T - 60)(\gamma_o/\gamma_{gs}) \tag{2.57}$$

and the value of coefficients to evaluate B_o is given in table 2.5

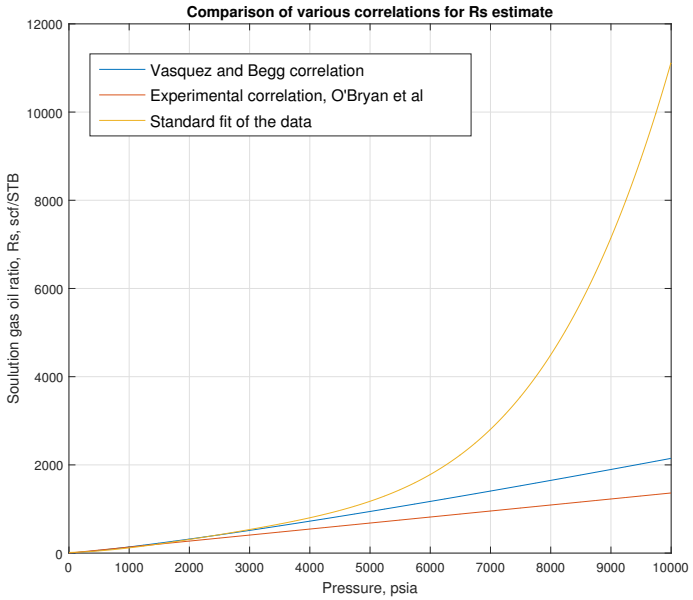

Figure 2.5: Comparison of various correlations for R_s estimate

Table 2.5: Values of coefficient for B_o calculations

coefficient	$\gamma_o \leq 30$	$\gamma_o > 30$
C_1	4.677×10^{-4}	4.677×10^{-4}
C_2	1.751×10^{-5}	1.100×10^{-5}
C_3	-1.811×10^{-8}	1.377×10^{-9}

The variation of B_o with respect to various values of R_s is shown in figure 2.6. Since the maximum value of R_s for the given system can be around $2000 scf/STB$, the avoid complications in the implicit schemes, it can be assumed that the value of B_o is an average value of the extremes, which is 1.7

2.3.2 Implicit Scheme

Due to various interdependency of parameters that are to be considered in case of OBM, formulating an implicit scheme to solve the set of equations can be efficient in obtaining the model as close to reality. Apart from the assumptions already considered for an OBM system, it is important to note that the volume of the contaminated base oil is considered constant and is found from the initial equilibrium condition when the system is at its bubblepoint pressure just before the circulation starts.

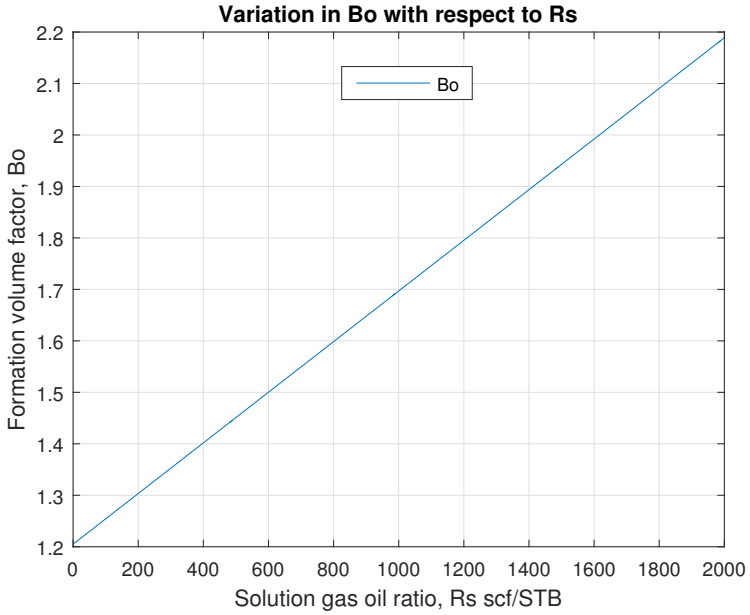

Figure 2.6: Variation of B_o with change in R_s

No Losses

The very first step is to consider the case where the frictional and acceleration losses are ignored but a back pressure, p_c, from the choke is considered. As discussed from the previous section, equation 2.50 is considered to be the primary relation establishing the connection between the pressure and the amount of gas that is dissolved in the system at the particular pressure. As discussed in section 2.2, real gas equation in considered. States of the system can be defined as,

$$\vec{X} = \begin{bmatrix} A_t \\ G_t \\ \chi_{CH_4} \end{bmatrix} \tag{2.58}$$

And the govening equation for gas bubble can be written as,

$$pV = z(p(X(1)) + p_c, T)nRT \tag{2.59}$$

To find the number of moles of gas that is dissolved at a given pressure from the value of mole fraction of the gas, χ_{CH_4}, the following rearrangement can

be done,

$$\chi_{CH_4} = \frac{n_{CH_4,diss}}{n_{CH_4,diss} + n_{liq}} \tag{2.60}$$

$$n_{CH_4,diss} = n_{liq}\frac{\chi_{CH_4}}{1-\chi_{CH_4}} \tag{2.61}$$

$$n_{CH_4,free} = n_{CH_4,tot} - n_{CH_4,diss} \tag{2.62}$$

$$n_{CH_4,free} = n_{CH_4,tot} - n_{liq}\frac{\chi_{CH_4}}{1-\chi_{CH_4}} \tag{2.63}$$

$$n_{CH_4,free}(X(3)) = n_{CH_4,tot} - n_{liq}\frac{X(3)}{1-X(3)} \tag{2.64}$$

$$n_{liq} = cap \times C\rho_{mud}/M_{liq} \tag{2.65}$$

And thus, set of implicit equations can be written as,

$$F(1) = H - X(1) - X(2) - B - C \tag{2.66}$$

$$F(2) = X(2) - \frac{z(p(X(1)) + p_c, T)n_{CH_4,free}(X(3))RT}{cap \times (p(X(1)) + p_c)} \tag{2.67}$$

$$F(3) = 37.589e^{3.4446X(3)} - (p(X(1)) + p_c) \tag{2.68}$$

To find the value of the contamination height of the mud, a function F(C) is solved by equating the bubble point pressure from equation 2.50 and pressure due to the mud above whose height will be $H - C$. The solution at $F(C) = 0$ gives the initial values of the contamination so that the system is at the bubble point pressure just before the circulation. As mentioned earlier, this system of equations can be solved by using the function *fsolve* in MATLAB and solving them over an iterative loop will help identify the *riser equilibrium point* for this system. The step increment of 'B' is defined by the velocity of circulation of mud through the booster pump.

Frictional loss

Due to the expansion of gas and circulation of mud, the system experiences certain frictional loss. Frictional loss due to gas is considered too small and thus ignored. In such cases, the states of the system are,

$$\vec{X} = \begin{bmatrix} A_t \\ G_t \\ \chi_{CH_4} \end{bmatrix} \tag{2.69}$$

And the govening equation for gas bubble can be written as,

$$pV = z(p(X(1)) + p_c + dp_{fric}, T)nRT \tag{2.70}$$

And thus, set of implicit equations can be written as,

$$F(1) = H - X(1) - X(2) - B - C \tag{2.71}$$

$$F(2) = X(2) - \frac{z(p(X(1)) + p_c + dp_{fric}, T) n_{CH_4,free}(X(3)) RT}{cap \times (p(X(1)) + p_c + dp_{fric})} \tag{2.72}$$

$$F(3) = 37.589 e^{3.4446 X(3)} - (p(X(1)) + p_c + dp_{fric}) \tag{2.73}$$

dp_{fric} is equal to as defined in equation 2.38.

Acceleration loss

In case of OBM, due to continuous increase in the availability of free gas as the mud is being circulated, it can be expected that acceleration losses can be quite signification. Though it may be quite less at the initial time period since there is no or very less free gas available to affect the expansion and thus acceleration. The system of equations can be modified as,

$$\vec{X} = \begin{bmatrix} A_t \\ G_t \\ \chi_{CH_4} \end{bmatrix} \tag{2.74}$$

And the govening equation for gas bubble can be written as,

$$pV = z(p(X(1)) + p_c + dp_{fric} + dp_{acc}, T) nRT \tag{2.75}$$

And thus, set of implicit equations can be written as,

$$F(1) = H - X(1) - X(2) - B - C \tag{2.76}$$

$$F(2) = X(2) - \frac{z(p(X(1)) + p_c + dp_{fric} + dp_{acc}, T) n_{CH_4,free}(X(3)) RT}{cap \times (p(X(1)) + p_c + dp_{fric} + dp_{acc})} \tag{2.77}$$

$$F(3) = 37.589 e^{3.4446 X(3)} - (p(X(1)) + p_c + dp_{fric} + dp_{acc}) \tag{2.78}$$

dp_{acc} is equal to as defined in equation 2.42.

Chapter 3

Drift Flux Model

As mentioned in the section 1.5.2, we use a similar drift flux model here for the vertical flow with a chosen set of closure laws described separately for different cases. It can be noted that the frictional source is an additive function and gravitational source is a decremental function along the flow direction.

$$\frac{\partial(\alpha_g \rho_g)}{\partial t} + \frac{\partial(\alpha_g \rho_g \nu_g)}{\partial x} = \Gamma \tag{3.1}$$

$$\frac{\partial(\alpha_l \rho_l)}{\partial t} + \frac{\partial(\alpha_l \rho_l \nu_l)}{\partial x} = -\Gamma \tag{3.2}$$

$$\frac{\partial(\alpha_l \rho_l \nu_l + \alpha_g \rho_g \nu_g)}{\partial t} + \frac{\partial(\alpha_l \rho_l \nu_l^2 + \alpha_g \rho_g \nu_g^2) + P}{\partial x} = -F + G \tag{3.3}$$

3.1 Discretization

To solve the drift flux model for various cases, Method of Lines (MoL) is practiced here wherein the equations are semi discretized using finite volume method resulting in a differentiable algebraic equation (DAE). Final equation in continuous in time and discretized in space. First choice to carry on this scheme is on non-staggered grid of the system. But, to reduce the computational effort and ease of use, the riser system in discretized as a staggered grid as shown in 3.1. Here the control variables pressure P, volume fractions α and densities ρ are defined at the nodes of the control volume and phase velocities ν at the faces. In finite volume method (FVM) of discretization, the flow domain is discretized by volume of finite size and difference equations representing the balances of flux across the finite volume faces are obtained (Fahad Matovu, 2014). We assume that volumes and faces across which fluxes propagate of control volumes are equal. They can be represented as,

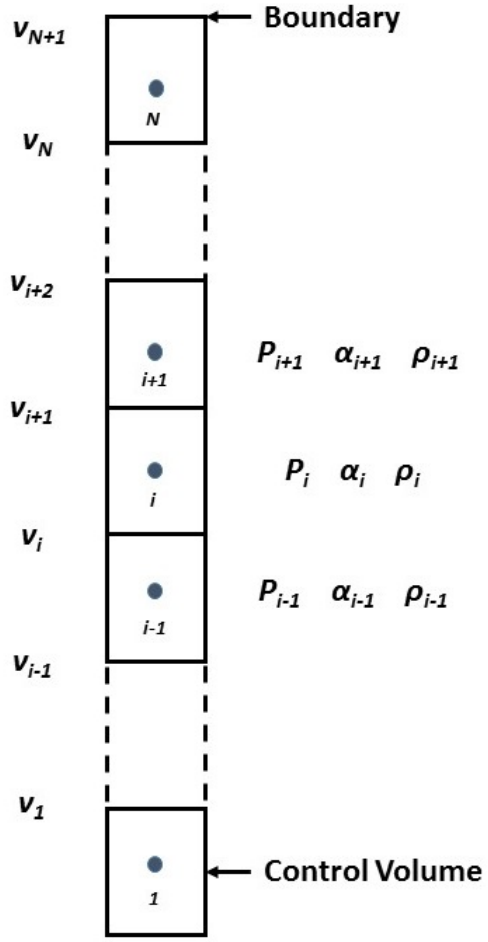

Figure 3.1: Staggered grid discretization of riser

For liquid phase,

$$\oint_{CV} \frac{\partial(\alpha_l \rho_l)}{\partial t}\, dV + \oint_{CV} \frac{\partial(\alpha_l \rho_l \nu_l)}{\partial t}\, dV = \oint_{CV} \Gamma\, dV \tag{3.4}$$

$$\frac{\mathrm{d}(\alpha_{li}\rho_{li})}{\mathrm{d}t} = \frac{(\hat{\alpha}_{li}\hat{\rho}_{li}\nu_{li} - \hat{\alpha}_{li+1}\hat{\rho}_{li+1}\nu_{li+1})}{\Delta x} + \Gamma_i \tag{3.5}$$

For gas phase,

$$\oint_{CV} \frac{\partial(\alpha_g \rho_g)}{\partial t}\, dV + \oint_{CV} \frac{\partial(\alpha_g \rho_g \nu_g)}{\partial t}\, dV = \oint_{CV} -\Gamma\, dV \tag{3.6}$$

$$\frac{\mathrm{d}(\alpha_{gi}\rho_{gi})}{\mathrm{d}t} = \frac{(\hat{\alpha}_{gi}\hat{\rho}_{gi}\nu_{gi} - \hat{\alpha}_{gi+1}\hat{\rho}_{gi+1}\nu_{gi+1})}{\Delta x} - \Gamma_i \tag{3.7}$$

For the momentum equation,

$$\oint_{CV} \frac{\partial(\alpha_l \rho_l \nu_l + \alpha_g \rho_g \nu_g)}{\partial t}\, dV + \oint_{CV} \frac{\partial(\alpha_l \rho_l \nu_l^2 + \alpha_g \rho_g \nu_g^2 + P)}{\partial t}\, dV = \oint_{CV} -\frac{32 \nu_{mix} \mu_{mix}}{d^2}\, dV + \oint_{CV} \rho_m g\, dV \quad (3.8)$$

$$\frac{\mathrm{d}(\alpha_{li} \rho_{li} \nu_{li} + \alpha_{gi} \rho_{gi} \nu_{gi})}{\mathrm{d}t} = \frac{(\hat{\alpha}_{li} \hat{\rho}_{li} \nu_{li}^2 - \hat{\alpha}_{li+1} \hat{\rho}_{li+1} \nu_{li+1}^2)}{\Delta x} + \frac{(\hat{\alpha}_{gi} \hat{\rho}_{gi} \nu_{gi}^2 - \hat{\alpha}_{gi+1} \hat{\rho}_{gi+1} \nu_{gi+1}^2)}{\Delta x} + \frac{(P_i - P_{i+1})}{\Delta x} - \frac{32 \mu_{mix,i} \nu_{mix,i}}{d^2} + \rho_m g \quad (3.9)$$

We now have the set of DAEs from equation 3.5, 3.7 and 3.9 that can be solved along with their closure laws using the *ode15* solver in MATLAB. The variables with a hat in the differential equations are variables at control volume faces and are approximated from the variable in the neighbouring nodes using the first-order upwind scheme as shown below,

$$\hat{x} = a_{i+1} x_i + (1 - a_{i+1}) x_{i+1} \quad (3.10)$$

where x is either α or ρ and a_{i+1} is given by,

$$a_{i+1} = \begin{cases} 1 & \text{if } \nu_{i+1} \geq 0 \\ 0 & \text{otherwise} \end{cases} \quad (3.11)$$

The state vector used for the simulation is shown below,

$$\vec{x} = \begin{bmatrix} \alpha_g \rho_g \\ \alpha_l \rho_l \\ \alpha_g \rho_g \nu_g + \alpha_l \rho_l \nu_l \\ \nu_l \\ \nu_g \\ \alpha_g \end{bmatrix} \quad (3.12)$$

3.2 Water Based Mud

In case of WBM, it is considered that there is no dissolution and thus the mass transfer term, Γ is zero. The gas, methane in this case is assumed to behave as an ideal gas and the main liquid component, water, is considered incompressible. The equations for this case would be,

$$\frac{\mathrm{d}(\alpha_{li} \rho_{li})}{\mathrm{d}t} = \frac{(\hat{\alpha}_{li} \hat{\rho}_{li} \nu_{li} - \hat{\alpha}_{li+1} \hat{\rho}_{li+1} \nu_{li+1})}{\Delta x} \quad (3.13)$$

$$\frac{\mathrm{d}(\alpha_{gi} \rho_{gi})}{\mathrm{d}t} = \frac{(\hat{\alpha}_{gi} \hat{\rho}_{gi} \nu_{gi} - \hat{\alpha}_{gi+1} \hat{\rho}_{gi+1} \nu_{gi+1})}{\Delta x} \quad (3.14)$$

$$\frac{\mathrm{d}(\alpha_{li}\rho_{li}\nu_{li} + \alpha_{gi}\rho_{gi}\nu_{gi})}{\mathrm{d}t} = \frac{(\hat{\alpha}_{li}\hat{\rho}_{li}\nu_{li}^2 - \hat{\alpha}_{li+1}\hat{\rho}_{li+1}\nu_{li+1}^2)}{\Delta x} + \frac{(\hat{\alpha}_{gi}\hat{\rho}_{gi}\nu_{gi}^2 - \hat{\alpha}_{gi+1}\hat{\rho}_{gi+1}\nu_{gi+1}^2)}{\Delta x} + \frac{(P_i - P_{i+1})}{\Delta x} - \frac{32\mu_{mix,i}\nu_{mix,i}}{d^2} + \rho_m g \tag{3.15}$$

Closure laws that provide the relation between the variables considered are

$$\alpha_l + \alpha_g = 1 \tag{3.16}$$

$$\rho_l = \rho_{l,0} + \frac{P - P_0}{a_l^2} \tag{3.17}$$

$$\rho_g = \frac{P}{a_g^2} \tag{3.18}$$

$$\nu_g = K\nu_{mix} + \nu_{slip} \tag{3.19}$$

Constants and parameters are defined in table () and the additional equations are defined as,

$$\nu_{mix} = \nu_{ls} + \nu_{gs} = \alpha_l\nu_l + \alpha_g\nu_g \tag{3.20}$$

$$\nu_g = \frac{K\alpha_l\nu_l + \nu_{slip}}{(1 - K\alpha_g)} \tag{3.21}$$

$$\rho_{mix} = \alpha_l\rho_l + \alpha_g\rho_g \tag{3.22}$$

$$\mu_{mix} = \alpha_l\mu_l + \alpha_g\mu_g \tag{3.23}$$

3.3 Oil Based Mud

In case of oil based mud, the principle liquid component considered is diesel oil and the gas is methane. Here the gas is considered as a real gas and the liquid is compressible ie, the density of oil varies with pressure. These characteristics of the system are captured by the closure laws. It is also considered that the gas is dissolved in the liquid component and thus gives rise to the mass transfer term in the drift flux model. Since the gas in initially completely dissolved in the base oil of OBM at high pressures, they are considered together as liquid component and later the gas flashes from the liquid phase and is present as free gas giving rise to a concentration difference for the gas component in the liquid and the gaseous phase, which explains the need to consider the mass transfer terms here. The DAEs of the drift flux model here would be,

$$\frac{\mathrm{d}(\alpha_{li}\rho_{li})}{\mathrm{d}t} = \frac{(\hat{\alpha}_{li}\hat{\rho}_{li}\nu_{li} - \hat{\alpha}_{li+1}\hat{\rho}_{li+1}\nu_{li+1})}{\Delta x} + \Gamma_i \tag{3.24}$$

$$\frac{\mathrm{d}(\alpha_{gi}\rho_{gi})}{\mathrm{d}t} = \frac{(\hat{\alpha}_{gi}\hat{\rho}_{gi}\nu_{gi} - \hat{\alpha}_{gi+1}\hat{\rho}_{gi+1}\nu_{gi+1})}{\Delta x} - \Gamma_i \tag{3.25}$$

$$\frac{\mathrm{d}(\alpha_{li}\rho_{li}\nu_{li} + \alpha_{gi}\rho_{gi}\nu_{gi})}{\mathrm{d}t} = \frac{(\hat{\alpha}_{li}\hat{\rho}_{li}\nu_{li}^2 - \hat{\alpha}_{li+1}\hat{\rho}_{li+1}\nu_{li+1}^2)}{\Delta x} + \frac{(\hat{\alpha}_{gi}\hat{\rho}_{gi}\nu_{gi}^2 - \hat{\alpha}_{gi+1}\hat{\rho}_{gi+1}\nu_{gi+1}^2)}{\Delta x} + \frac{(P_i - P_{i+1})}{\Delta x} - \frac{32\mu_{mix,i}\nu_{mix,i}}{d^2} + \rho_m g \tag{3.26}$$

where Γ_i is the gas dissolution rate from gaseous to liquid phase. *Closure laws* that provide the relation between the variables considered are

$$\alpha_l + \alpha_g = 1 \tag{3.27}$$

$$\rho_l = \rho_{l,0} + \frac{\rho_{l,0}}{\beta}(P - P_0) - \rho_0\alpha(T - T_0) \tag{3.28}$$

$$\rho_g = \frac{PM}{ZRT} \tag{3.29}$$

$$\nu_g = K\nu_{mix} + \nu_{slip} \tag{3.30}$$

Constants and parameters are defined in table () and the additional equations are defined as,

$$\nu_{mix} = \nu_{ls} + \nu_{gs} = \alpha_l\nu_l + \alpha_g\nu_g \tag{3.31}$$

$$\nu_g = \frac{K\alpha_l\nu_l + \nu_{slip}}{(1 - K\alpha_g)} \tag{3.32}$$

$$\rho_{mix} = \alpha_l\rho_l + \alpha_g\rho_g \tag{3.33}$$

$$\mu_{mix} = \alpha_l\mu_l + \alpha_g\mu_g \tag{3.34}$$

In equation 3.29, the deviation factor, Z is assumed to be an average of the values calculated at extreme ranges of the pressure encountered within the riser. The average value is assumed as 1.0097 in this case. In equation 3.28 which is a linearized approximation coined by Kaasa et al. (2012), since the temperature is assumed to be constant throughout the riser, it can be re-written as,

$$\rho_l = \rho_{l,0} + \frac{\rho_{l,0}}{\beta}(P - P_0) \tag{3.35}$$

β, called as the isothermal bulk modulus of the liquid is a complex function of pressure and is usually measure experimentally. Correlation for its dependence of bulk modulus of diesel on pressure has been studied experimentally by Lapuerta et al. (2012) and the data can be extrapolated using the following equation,

$$\beta = 774 + 22.9P + 0.433P^2 - 0.0188P^3 \tag{3.36}$$

where,

β	is bulk modulus in MPa
P	is pressure in MPa
$\rho_{l,0}$ and P_0	are the reference points for linearization

General equation for the mass transfer term can be defined as,

$$\dot{n}_A = K_c A(\Delta C_A) \tag{3.37}$$

where,

K_c	is the mass transfer coefficient [mol/(s.m^2)/mol/m^3], or m/s
$\dot{n}_A$	is the mass transfer rate [mol/s]
A	is the effective transfer area [m^2]
ΔC_A	is the driving force concentration difference [mol/m^3]

K_c is a parameter that is measured experimentally and thus leaves us to resort to make use of the correlation available to predict its value at various pressure. An approximate measure is obtained from the work done by Mohebbi and Mosayebi Behbahani (2015) related to measurement of mass transfer coefficients during gas hydrate formation where the main components are methane in the gaseous phase and water in the liquid phase. Depending upon the system and experience of the reader, this factor may be increased to tens to few hundred times since the dissolution of methane in base oil of OBM will be quite high than that happening in water. The correlation provided in the work (Mohebbi and Mosayebi Behbahani, 2015) is,

$$K_L = 10^{-4}(a + bT + cP + dTP + eP^2) \tag{3.38}$$

where

$$a = 13.6$$
$$b = -0.05108$$
$$c = 12.17$$
$$d = -0.04061$$
$$e = -0.01888$$

R^2 value for the fit = 0.92

K_L	is expressed in m/s
P	is pressure in MPa
T	is temperature in K

Having found the mass transfer coefficient, leads to examine the method to calculate the concentration difference at each time instant which is the driving force for the mass transfer to occur. Berthezene et al. (1999) carried out experimental tests to measure the methane solubility at 90°C (considered the same temperature in simulations) in synthetic OBMs and their base oils, diesel oil being one among them. Data obtained are presented in table 2.2 and the extrapolations are used to estimate the amount of gas that is dissolved and the amount of gas that is available as free gas. This difference in the concentration is the main drive for the mass transfer to occur.

Chapter 4

Simulation Results

This chapter focuses on discussing the various parameters used for simulation and the corresponding results.

4.1 Analytical model

Table 4.1 shows all the parameters that are use for the simulation in analytical models. Consistent units and parameters are used in order to compare the results as and when required. Figure 4.1 explains the situation in which we experience a riser gas in flux when the riser is filled with water based mud. At time t=0, it can be seen that gas occupies a finite height and thus a finite volume. This is because of the assumptions that have been considered relating to no dissolution of gas in WBM and that the initial system is in equilibrium. The corresponding pressure due to the remaining mud above the bubble which corresponds to the value at t=0 in figure 4.2, is the equilibrium pressure to contain the considered amount of gas. It can be seen from both the figures 4.1 and 4.2 that the gas starts expanding when the circulation is started and that results in corresponding expulsion of the mud above. The reference line shown in figure 4.2 corresponds to the level of mud that would be remaining, had the mud been expelled in the rate of velocity of circulation. But, it can be seen that more mud has been expelled at a given point of time as compared to the reference level, which is assisted due to the expansion of the gas bubble. Due to the scale of the figures 4.1 and 4.2, it becomes increasing difficult to identify the difference between the results when various pressure losses are considered. Thus, to aid investigation, a closure snapshot of the situations are shows in figures 4.3 and 4.4. It can be observed that there are no significant differences in the gas bubble height and the mud height above the bubble, when different situations of pressure losses are considered. This augments the fact that frictional and acceleration losses are minimal, at least when slower systems are considered. A minute variation in the values can be seen towards the end of the available

Table 4.1: Simulation parameters for analytical models

Parameter	Value	Units
Riser height	10000	ft
Riser capacity	0.35	bbl/ft
Temperature	194	° F
Mud density (both WBM & OBM)	11	ppg
Base oil in OBM	No. 2 Diesel fuel	
Specific gravity of Diesel (at the given temperature)	0.7825	
Molar mass of water	18.02	Kg/Kmol
Density of water	1000	Kg/m^3
Gas considered	Methane	
Amount of gas	10	Kmol
Critical Pressure of gas	667.8	psia
Critical temperature of gas	343	R
Accentric factor ω	0.0115	
Standard temperature	60	° F
Standard pressure	14.7	psia
Density of air	1.205	Kg/m^3
Mud viscosity	5×10^{-2}	Pas
Formation Volume factore	1.7	bbl/STB
Diameter of riser	0.48	m
Velocity of circulation	2	ft/s
Acceleration due to gravity,g	9.81	m/s^2

data, owing to the acceleration losses due to rapid expansion of gas towards the top of the riser column due to the fact that back pressure due to the hydrostatic head is nearly absent and the pressure is experienced only due to the choke available. In all simulation for various systems, it can be observed that there exists no solution after a point, which is the last point of the available data represented in the figure. In physical terms, it means that any slight increase in height of the gas bubble yields no corresponding mud height. This point can be understood as ***riser equilibrium point*** (REP), where the hydrostatic pressure above the gas bubble is too less to contain its expansion and thus any further circulation of this gas bubble can lead to explosive unloading of riser, which is a threat to safety of personnel and equipments on the rig. But, it can be noticed from the results that presence of frictional and acceleration losses, act opposite to the direction of flow of the fluids and thus adds up to the total back pressure experienced by the gas bubble. Rightly, presence of friction, delays the occurrence of riser equi-

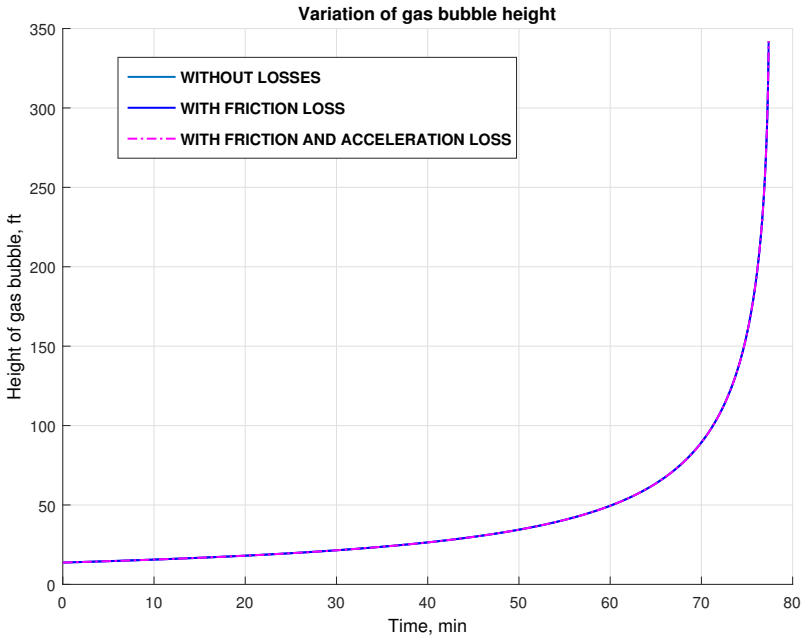

Figure 4.1: Variation of gas height in WBM with choke pressure = 14.7 psia

librium. In other words, riser equilibrium point has been shifted upwards in the riser. Corresponding final level of height of the gas bubble towards the reach of REP can be studied from figure 4.4 for various cases of pressure losses.

Figure 4.5 shows a similar situation but in the presence of additional back pressure served by the presence of choke. As can be seen from both the figures 4.5 and 4.6 that when the gas bubble experiences higher pressure either though the hydrostatic head of the mud or through the back pressure from the choke, it effectively delays the occurrence of riser unloading. Since the comparison between the consideration of different pressure losses in case of WBM has already been demonstrated, 4.5 and 4.6 shows the data when both frictional and acceleration losses are considered which is more realistic in any case. The case is completely different in the presence of oil based mud, which results in complete dissolution of gas in the base oil. As can be seen from figures 4.9, initial volume of gas at time t=0 is zero. This is due to the fact that all the gas that is considered is dissolved in the base oil which is diesel in this case. In agreement to the assumption it can be noted that such an equilibrium situation corresponds to bubble point pressure of the system. Thus any slight reduction in pressure experienced by the dissolved system, gas starts flashing out of the solution, which in this case is when the circulation is initiated. This corresponds to a situation where there is

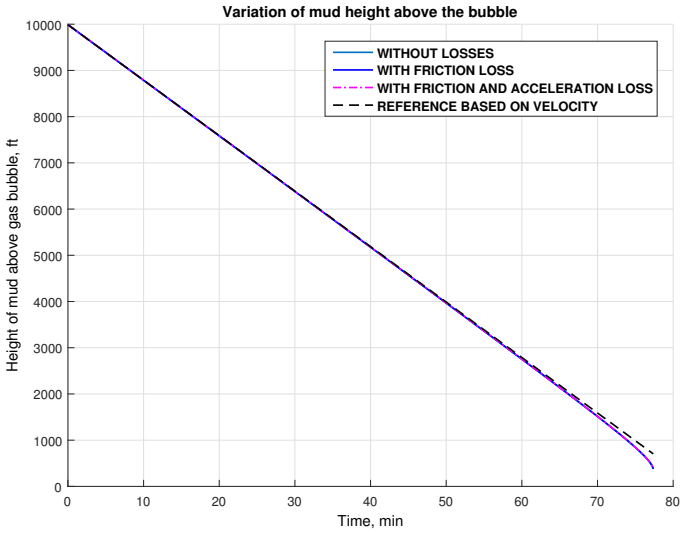

Figure 4.2: Variation in the height of the mud above the gas bubble in WBM with choke pressure = 14.7 psia

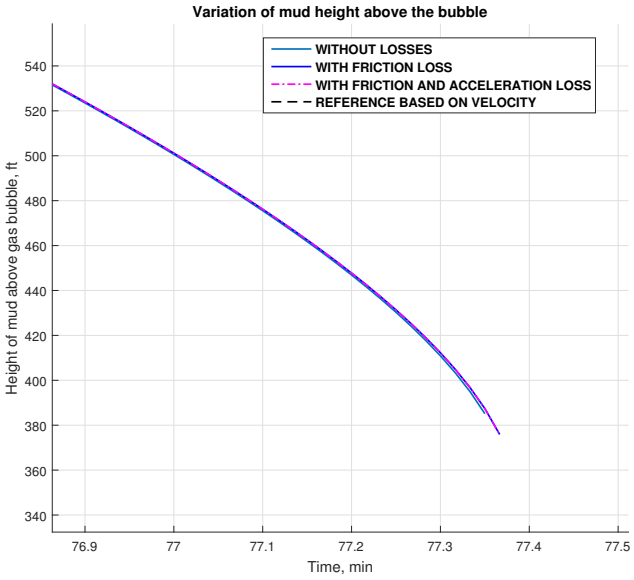

Figure 4.3: Closure snapshot of variation in mud height in WBM considering different pressure losses

a continuous supply of gas from the contaminated oil during the circulation and thus the expansion is faster due to increasing supply of free gas. This

can be clearly observed when the figure 4.9 is compared to 4.6, in which case the OBM system reaches the REP faster than an WBM system, clearly observed form the time axis of both the plots.

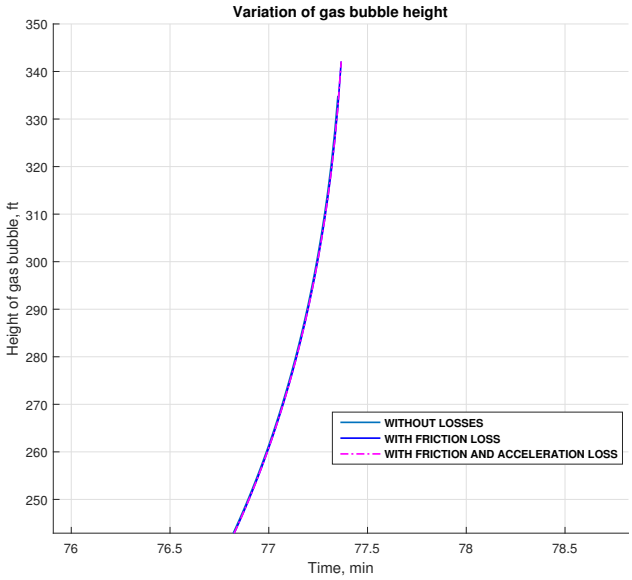

Figure 4.4: Closure snapshot of variation in height of the gas bubble in WBM considering different pressure losses

It is still in agreement that the presence of additional back pressure helps in delaying the occurrence of unloading. This can be observed from the shift of REP towards the upper end of the riser from figure 4.8. To observe the difference between consideration of various pressure losses in OBM system, figures 4.7 provides a closure snapshot of the gas height towards the end of the simulation. It can be observed that OBM system is in agreement with the fact that frictional and acceleration losses are additive in nature and helps delay riser unloading.

One important observation that can be made using these models is that increasing the back pressure allows the riser equilibrium point further up towards the top of the riser. So in that lines, it must be possible to overcome the riser equilibrium point and completely avoid any type of unloading. To find the back pressure that is required to eliminate the existence of REP within the riser length, the data given in table 4.2 with respect to the amount of back pressure and the level of REP were extrapolated. These data were obtained from the simulations and REP is identified as the point after which there exists no solution, as mentioned earlier. The equation of

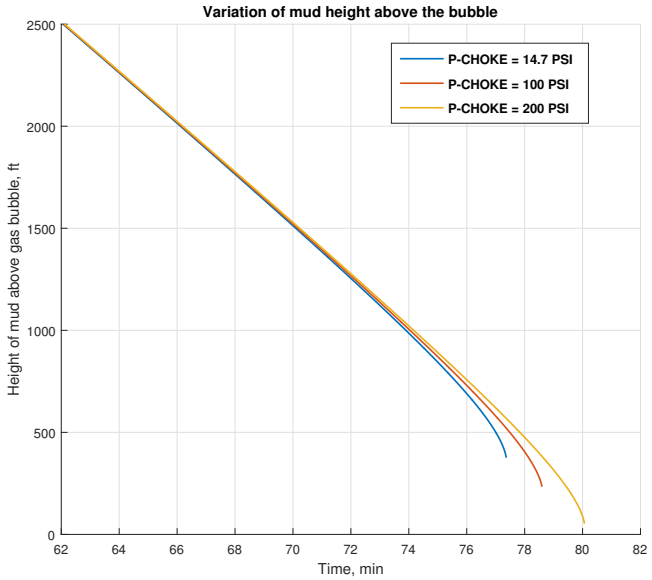

Figure 4.5: Extension of the possible riser equilibrium point in WBM case at various choke pressures

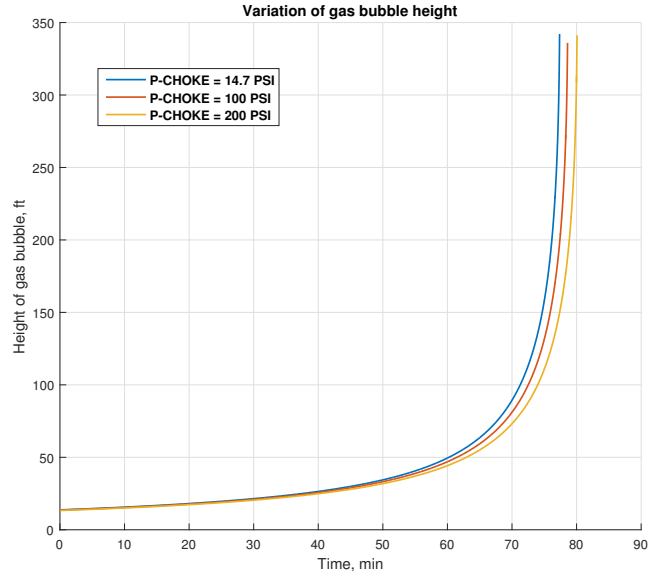

Figure 4.6: Variation in gas bubble expansion in WBM at different choke pressures

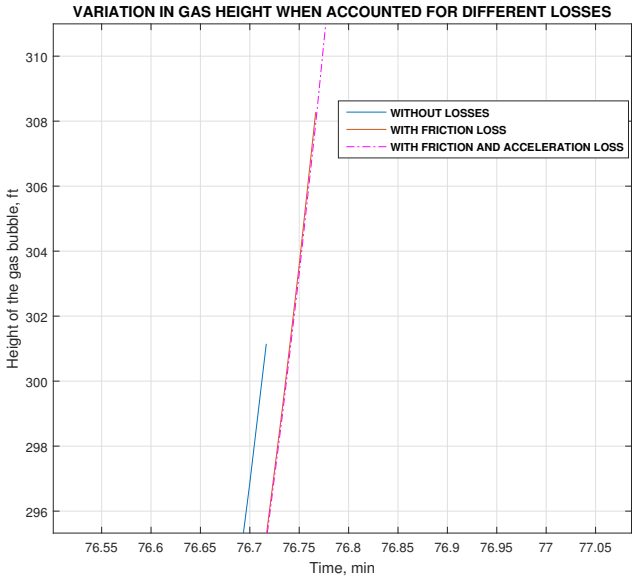

Figure 4.7: Closure snapshot of various pressure losses in OBM with choke pressure = 14.7 psia

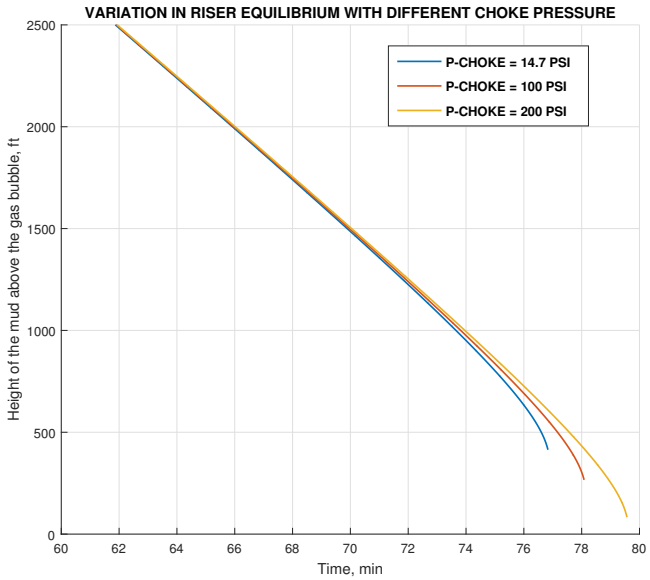

Figure 4.8: Extension of the possible riser equilibrium point in OBM at various choke pressures

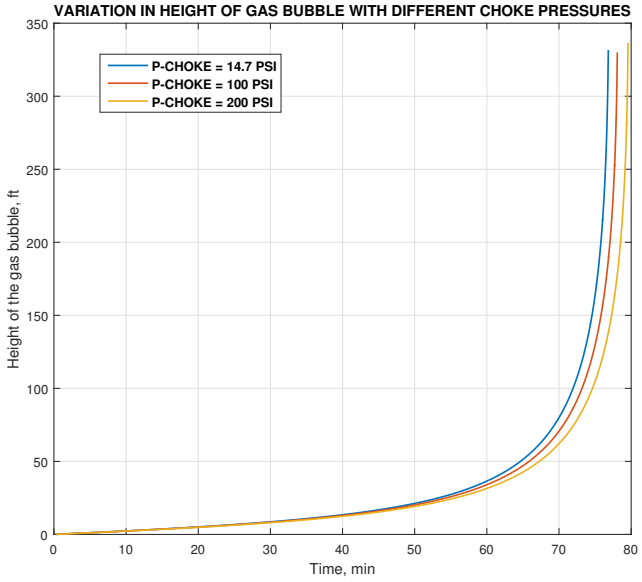

Figure 4.9: Variation in gas bubble expansion in OBM at different choke pressures

Table 4.2: Change in position of riser equilibrium point with different back pressure for WBM of 11 ppg

REP ft	Choke pressure psi
357.8494	14.7
221.0401	100
35.8104	200

the extrapolation is,

$$REP = -0.0013p_{choke}^2 - 1.4501p_{choke} + 379.46 \tag{4.1}$$

The root of the equation 4.1 is given by $p_{choke} = 218.8psi$ and thus REP can be avoided within the riser length if $p_{choke} \geq 218.8psi$. To verify, corresponding behaviour of expansion is shown in figure 4.10 when the choke pressure is set to 218.8 psi. It can be observed that the height of the mud above the bubble is very close to zero for this value of choke pressure. It is possible that with higher choke pressure than this threshold, the gas can be contained within the riser with any rapid expansion or as it is called, riser unloading. When a pressure above this threshold is maintained, the gas can be directly vented out through the mud degasser available at the surface.

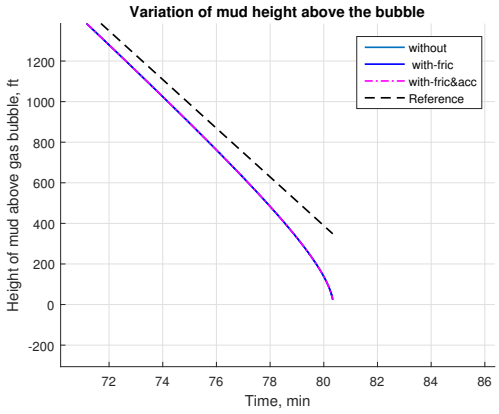

Figure 4.10: Minimum choke pressure (218.8 psi) to eliminate REP within riser for WBM (11 ppg)

Table 4.3: Change in position of riser equilibrium point with different back pressure for WBM of 11 ppg

REP ft	Choke pressure psi
403.996	14.7
254.1537	100
67.6204	200

A similar situation when OBM is used, the data can be observed to be as in table 4.3 and the equation of extrapolation is given by equation 4.2,

$$REP = -0.0006p_{choke}^2 - 1.6894p_{choke} + 428.96 \tag{4.2}$$

and the solution for the equation 4.2 is obtained at $p_{choke} = 234.4psi$. The corresponding behaviour of the mud above the bubble for this pressure is shown in figure 4.11. Similarly correlations can be derived for systems with different physical properties and an estimate of minimum back pressure can be known to eliminate the occurrence of riser unloading. It can be seen from figure 4.12 that both explicit and implicit numerical schemes can predict the behaviour similarly and the basic difference arise in the fact that implicit scheme allows to consider the real gas behaviour making it an better estimate about the practical situation.

4.2 Drift Flux Models

This section of this chapter discusses the results generated using drift flux models to study the two phase flow in the riser system. The table 4.4 sum-

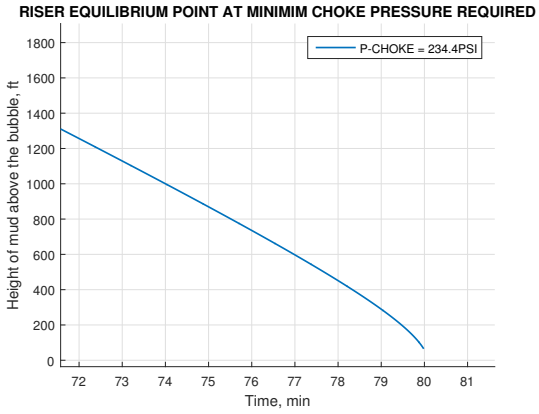

Figure 4.11: Minimum choke pressure (234.4 psi) to eliminate REP within riser for OBM (11 ppg)

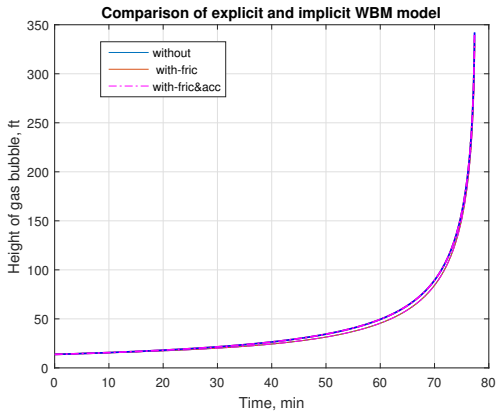

Figure 4.12: Comparison of explicit and implicit numerical schemes for WBM

marises all the parameters that were used for the drift flux model considering both WBM and OBM.

It must be noted that the parameters considered here for the drift flux model are slightly away from the real configuration of the riser system. Drift flux models predict the phase distribution and velocities of various phases when there is a continuous supply of both the phases into the system as opposed to the case for riser gas handling where the influx is shut using BOP. But studying these systems provide an better understanding of the distribution of phases and their dependence on additional pressures. The parameters have been chosen to demonstrate the usage of drift flux model for this given application while it is prone to improvements and be modified to real system by considering the quantitative parameters numerical

Table 4.4: Simulation parameters for drift flux models

Parameter	Value	Units
Riser height	3048	m
Temperature	363	K
Base oil density	782.5	kg/m^3
Water density	1000	kg/m^3
Universal gas constant	8.314	[Kpa m^3 K Kg]
C_0	1.2	
Amount of gas	10	Kmol
Number of cells	3	
Number of states	6	
Methane molar mass	16.04	Kg/kmol
Slip Velocity	0.3182	m/s
Initial gas void fraction	0.3	
Initial liquid velocity	0.1	m/s
Acceleration due to gravity,g	9.81	m/s^2
Total run time	250	sec

schemes like stability, consistency, etc. As can be seen from table 4.4, the complete riser is discretized into 3 cells. Higher the number of cells, better is the accuracy while stability of the solution must be taken care. 3 cells serve the purpose of depicting the upper, middle and lower part of the riser. Results have been presented to understand the physical variation of parameters and their sensitivity to additional back pressure for which a choke is considered. Data presented are coupled for two cases, one when open to atmosphere or the choke pressure is 1 bar and the other when the choke pressure is 100 bars. Figures 4.13 and 4.14 represent the evolution of pressure in the cell due to the gravitational and frictional losses when WBM is considered. It can be observed that the presence of back pressure helps in preventing the dissipation of pressure in the system and maintains a gradient. If the pressure is completely dissipated, the gas would expand rapidly as can be seen from the corresponding void fraction in figure 4.15 whereas presence of a back pressure reduces the the gas expansion which can be observed through the void fractions in figures 4.16. Sudden increment in the phase velocities and quickly being dominated by the gaseous flow as seen from figure 4.17 complements the earlier made claim. Multiphase flow prevails and the content moves as a mixture in presence of additional pressure. This is observed in figure 4.18. A similar trend can be observed in OBM system as well when the data are compared between the flow open to atmosphere and the flow restricted by a choke which is clearly depicted in figures 4.19 and 4.20. Continuous availability of free gas with reduction

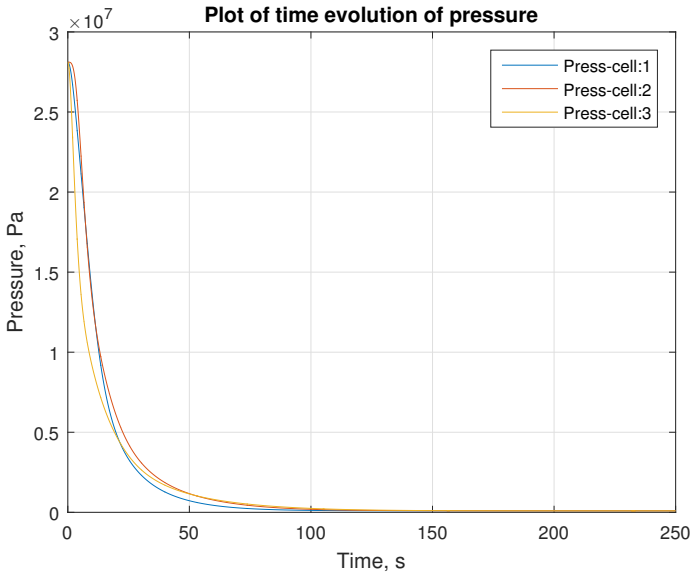

Figure 4.13: Variation in cell pressure in WBM system when choke pressure is 1 bar

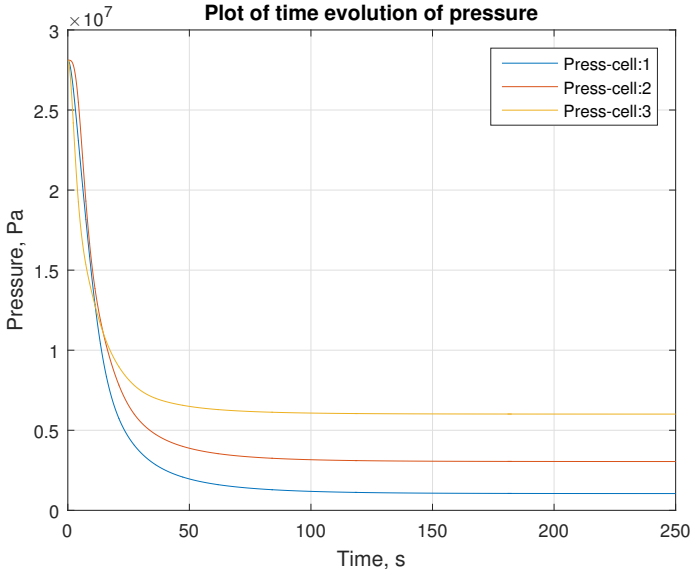

Figure 4.14: Variation in cell pressure in WBM system when choke pressure is 100 bar

in pressure, from the initially contaminated liquid makes the transition of flows and velocity changes smoother which can be observed in the plots 4.21 through 4.24. Figures 4.25 and 4.26 represents the gas exchange rate which

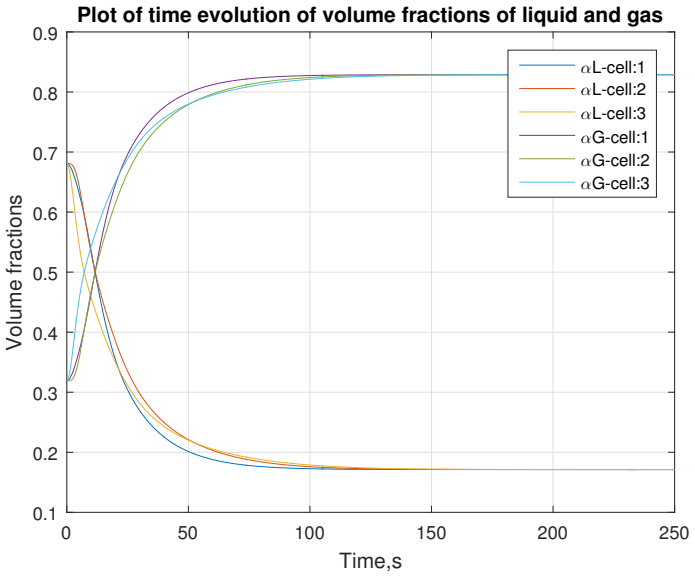

Figure 4.15: Variation in void fraction in WBM system when choke pressure is 1 bar

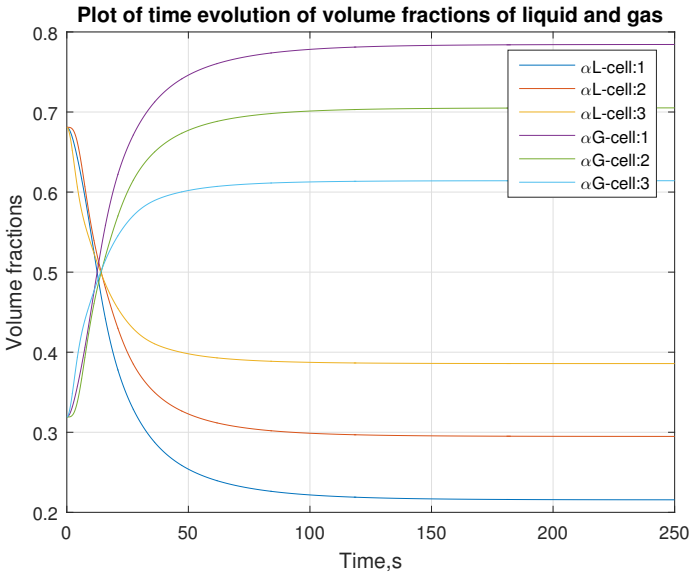

Figure 4.16: Variation in void fraction in WBM system when choke pressure is 100 bar

may be defined as the mass transfer of gas from the dissolved state to the free gas state or vice-versa depending on the gradient of the component's concentration. Component considered here is methane and it is known

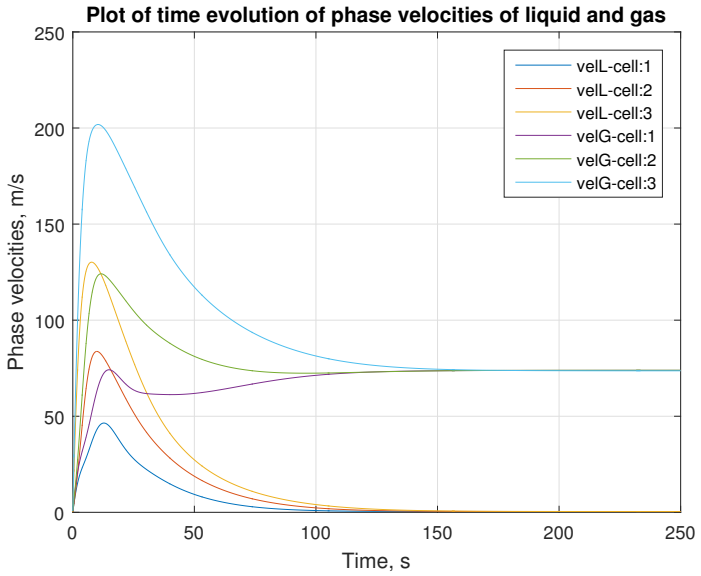

Figure 4.17: Variation in phase velocities in WBM system when choke pressure is 1 bar

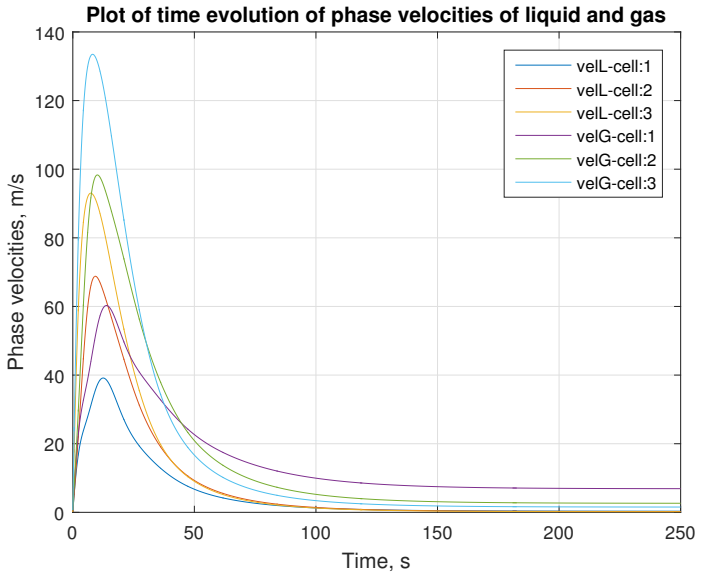

Figure 4.18: Variation in phase velocities in WBM system when choke pressure is 100 bar

that the concentration of methane is very high in the dissolved liquid and thus faster mass transfer takes place to be converted to free gas, at once the pressure is reduced. As mentioned earlier, flow open to atmosphere dis-

sipates the pressure completely and thus methane is lost from the system resulting in almost nil mass transfer once the steady flow has been achieved. Whereas in case of presence of an additional back pressure, the mass of gas in contained within the system and thus mass transfer continues to take place, though minimal, during steady state flow. In physical terms, it can be interpreted in a way that dissipation of all the pressure and gas from the system translates to a situation where the riser equilibrium has been passed and all the gas has been released due to unloading. Whereas in the presence of back pressure, gas is not allowed to expand rapidly thus preventing explosive unloading. In other words, REP has not been reached. This can be related to the previous claims and observations from the analytical models.

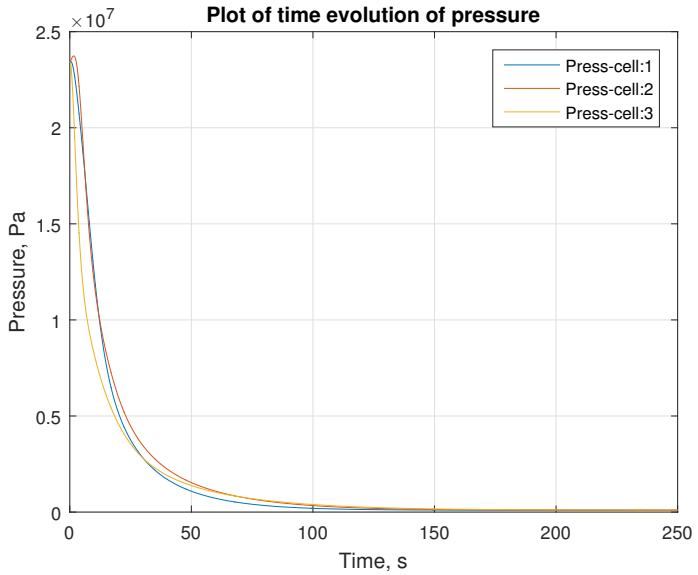

Figure 4.19: Variation in cell pressure in OBM system when choke pressure is 1 bar

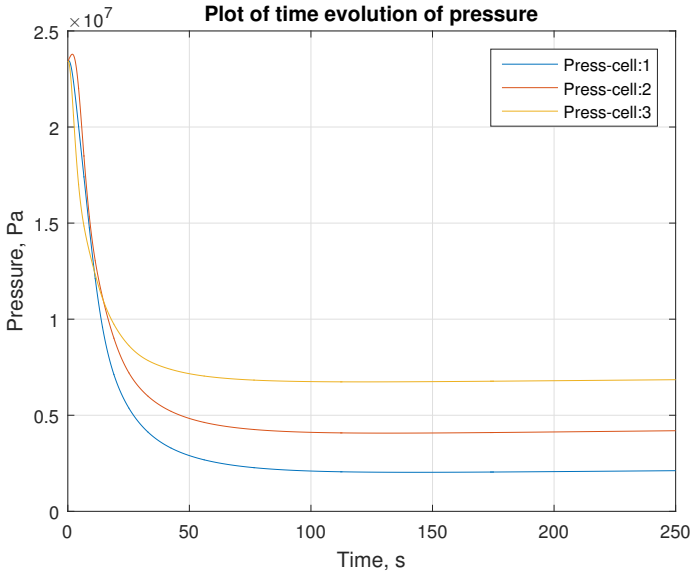

Figure 4.20: Variation in cell pressure in OBM system when choke pressure is 100 bar

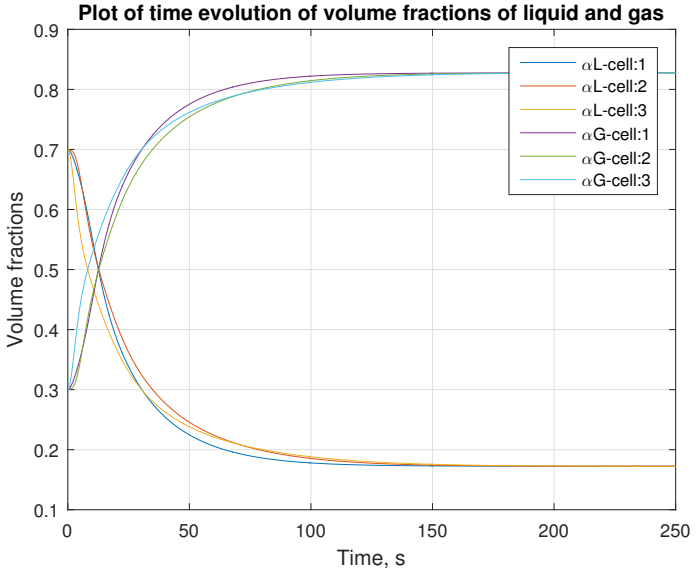

Figure 4.21: Variation in void fraction in OBM system when choke pressure is 1 bar

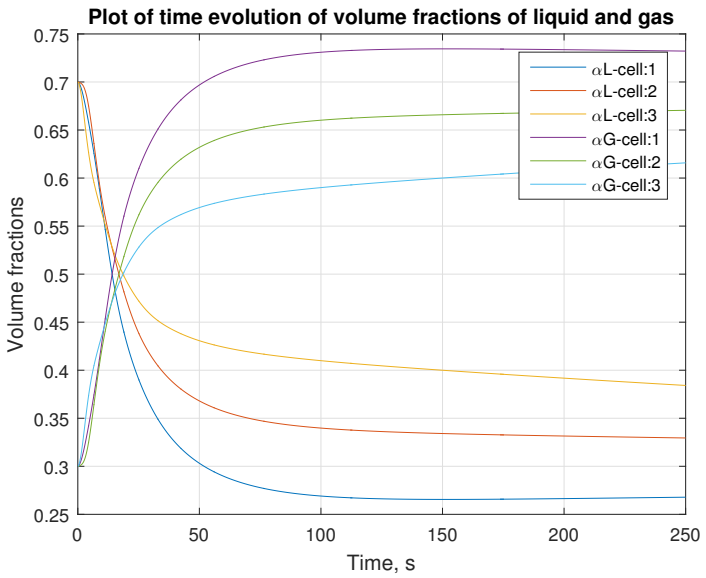

Figure 4.22: Variation in void fraction in OBM system when choke pressure is 100 bar

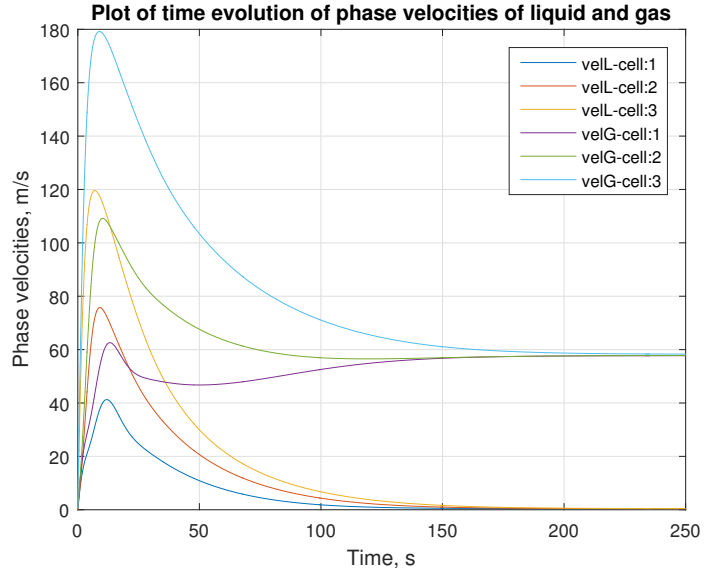

Figure 4.23: Variation in phase velocity in OBM system when choke pressure is 1 bar

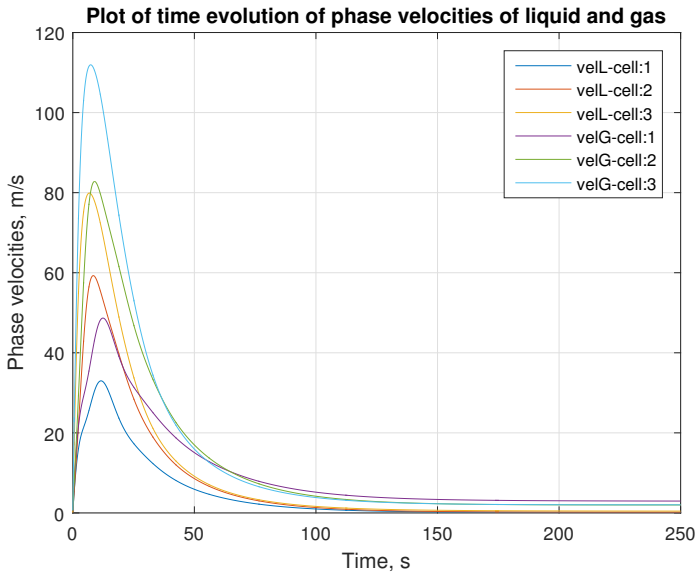

Figure 4.24: Variation in phase velocity in OBM system when choke pressure is 100 bar

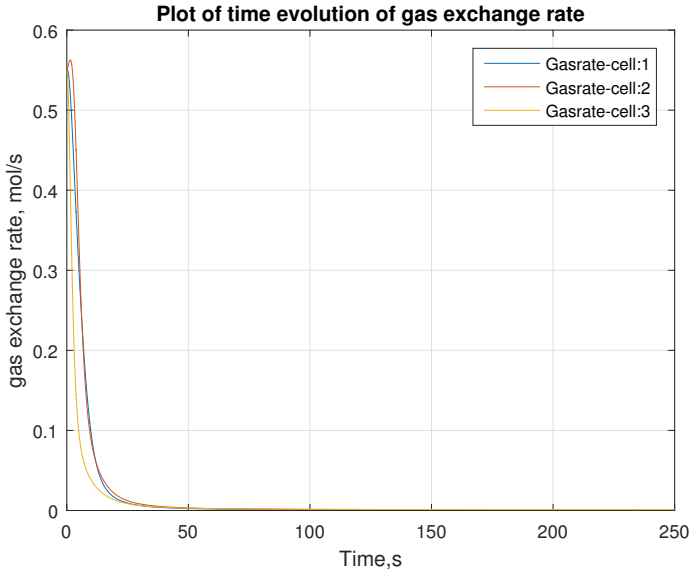

Figure 4.25: Variation in gas exchange rate in OBM system when choke pressure is 1 bar

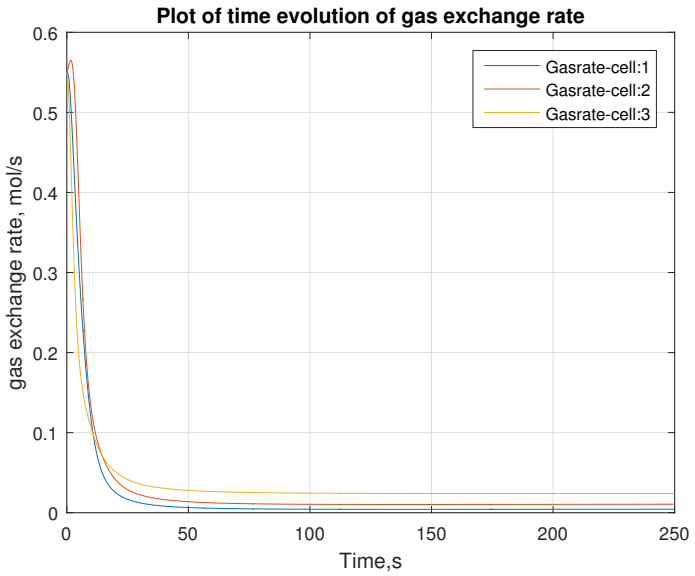

Figure 4.26: Variation in gas exchange rate in OBM system when choke pressure is 100 bar

Chapter 5

Conclusions

This chapter summarises the conclusions that can be drawn from the work carried out in this thesis. To begin with, a basic foundation of the theory required to understand the background of the work are described in chapter 1. Mathematical formulation for various analytical models such as the explicit schemes for gas bubble in water based mud and implicit schemes for gas bubble in oil based mud are discussed in chapter 2. Drift flux models and formulation of the partial differential equations pertaining to cases related to multiphase flow in riser systems are discussed in chapter 3. All the simulations that have been carried out for different cases are presented in chapter 4 and the claims are discussed thoroughly. Based on the understanding of the work done so far, the following can be concluded.

- Mathematical formulation based on explicit analytical scheme can be a good starting place to model systems such as riser gas migration but can be observed that models with higher order of accuracy and incorporating realistic behaviour are looked forward to.
- Using implicit schemes to formulate and solve riser gas systems has proven to be an better alternative than explicit schemes to model the systems close to their real behaviour. Ability to include the real gas scenario in the implicit equations is the main distinguishing factor from finding s solution through explicit equations.
- Considering frictional losses has proven to be crucial in identifying the riser equilibrium point (REP). When ignored, the error that arises in estimation of REP is in the order of 10 ft, in terms of the units predominantly used in this work.
- For most of the considered systems, pressure losses due to acceleration of fluid is too small and general assumption to ignore these losses are valid. Nevertheless, when considered, it can be noted that acceleration loss play an important role in the accurate estimation of REP. It has

been noted that, acceleration loss is significant towards the upper part of the riser, when the gas expansion is rapid in this region due to lack of enough hydrostatic pressure to contain the gas. Ignoring the acceleration losses may be responsible for an error up to an order of 10 ft in estimating the REP.

- Drift flux models provide more accurate measure of the phase distribution and velocities in the system than the static models that are considered. This is due to the ability of the partial differential equation formulation that are capable to capture the dynamic changes of the system. But, usage of such models increase the difficulty in computation owing to a trade off between the accuracy and complexity. In very conservative calculation, more accurate and robust models that make use of drift flux models may not be necessary, provided there is enough window for operational fluctuations without compromising the safety of personnel and rig.

- Significant difference in the behaviour of water based and oil based system arises due to the fact that the gas can be completely dissolved in the oil system. Considering solubility of gas only in the base oil is an acceptable assumption due to the higher fraction of solubility of gas in base oil and due to the fact that the considered models are able to capture the dynamics related to continuous flashing of gas from the dissolved solution.

- Inclusion of mass transfer terms is one of the highlighted advantage of the robustness of the drift flux models. But, better estimate of the coefficients are required, paving way to experimental prediction of these parameters for such systems.

- Major source of error in formulating most of the models is due to the lack of generalization of prediction methods for various parameters. High sensitivity of the parameters to the change in pressure and temperature is the basic reason.

- Prediction of bubble point pressure of the system of dissolved gas in a liquid is crucial in estimating other parameters related to the fluid solubility and variation in their physical properties. Methods used in this work has proven to be effective in predicting bubble point pressure, which can be observed from the initial conditions of the data obtained.

- Due to highly complex nature of solving set of partial differential equations, discretization and the numerical method adapter to solve such systems serve to be another major source of error. These errors are accounted in the form of truncation errors, stability of the solution and convergence/ consistency of the method adapted. Method of Lines

(MOL) adapted in the work proved to be efficient in estimating the variables of interest while there is a scope of improvement in terms of discretization and stability issues.

- Drift flux models considered here are more suitable when there is a continuous supply of both the phases. This can be the situation when multiphase flow regimes exist when before the influx has been identified and isolated using BOP as opposed to the riser gas situation where the gas dynamics are studied from the fixed amount of gas that has entered the riser area before successful shut-in of the BOP. Modifying the drift flux models to such situations may provide a better estimate of the variables.

- Peng-Robinson Equation of State, being a widely accepted model to estimate the real gas dynamics has proven sufficient to consider real behaviour of gas in the riser systems.

- It has been found that REP can be bypassed for a given system through proper selection of minimum back pressure that is required. If the pressure within the system is maintained above this threshold limit, the gas can be bled through the mud gas separator or poor boy degasser in the surface. In case of failure to maintain this threshold pressure by any means, riser unloading in inevitable while circulating the contaminated fluid and gas out of the riser.

- Systems using OBM require a higher threshold pressure to bypass the REP as compared to WBM system, which may be due to higher free gas acceleration towards the top of the riser, where the base oil serves as the source of free gas continuously.

- Methane solubility and the estimates for solution gas oil ratio and formation volume factor carried out in this work proves the importance of proper estimation of these parameters and that they are too sensitive to pressure and temperature variation. Proper understanding is required to seek out the appropriate estimation schemes.

Abbreviations

A – Height of mud above gas, ft

B – Height of mud below the contaminated mud, ft

B_x – Formation Volume factor of component 'x'

BOP – Blowout Preventor

C_o – Compressibility of oil, P^{-1}

cap – Riser capacity, bbl/fr

CMC – Carboxymethyl Cellulose

D_{eff} – Effective diameter, m

D_i – Inner diameter, m

D_o – Outer diameter, m

dh – Discretization step height, ft

ϵ – Void fraction

B_o – Formation Volume Factor

G – Height of free gas, ft

g – Acceleration due to gravity, $9.81 m/s^2$

m_x – Mass percent of component 'x'

μ – Viscosity, cP

$\mu_p l$ – Plastic viscosity, cP

n – Power law index / Number of moles, Kmol / Time instant

ν – Strain,s^{-1}

ν_x – Specific gravity of 'x'

Abbreviations

OBM – Oil Based Mud

ω – Accentric factor

P – Pressure, KPa, psia

P_b – Bubble point pressure, psia

R_{sbr} – Solution gas oil ratio of brine

R_{se} – solution gas oil ration of emulsion

R_{sm} – Solution gas oil ratio of mud

R_{so} – solution gas oil ratio of oil

ρ – Density, ppg,kg/m^3

s – Solid fraction in mud

T – Temperature, °F, °R

t – Time, min

τ – Shear stress, Pa

τ_y – Yield stress, Pa

${U_x}^s$ – Superficial velocity of phase 'x'

V – Volume, bbl,m^3

V_G – Velocity of gas phase, ft/sec

V_h – Homogenous velocity, ft/sec

V_{rel} – Relative velocity, ft/sec

WBM – Water Based Mud

χ_x – Mole fraction of component 'x'

$(\quad)_{std}$ – Value at standard conditions

$(\quad)_{res}$ – Value at reservoir conditions

Bibliography

Aarsnes, U. J. F., Flåtten, T., and Aamo, O. M. (2015). Models of gas-liquid two-phase flow in drilling for control and estimation applications.

Al-Darmaki, S., Falcone, G., Hale, C., Hewitt, G., et al. (2008). Experimental investigation and modeling of the effects of rising gas bubbles in a closed pipe. *SPE Journal*, 13(03):354–365.

Aziz, K., Govier, G. W., et al. (1972). Pressure drop in wells producing oil and gas. *Journal of Canadian Petroleum Technology*, 11(03).

Beggs, D. H., Brill, J. P., et al. (1973). A study of two-phase flow in inclined pipes. *Journal of Petroleum technology*, 25(05):607–617.

Berthezene, N., de Hemptinne, J.-C., Audibert, A., and Argillier, J.-F. (1999). Methane solubility in synthetic oil-based drilling muds. *Journal of Petroleum Science and Engineering*, 23(2):71–81.

Bhaga, D. and Weber, M. (1981). Bubbles in viscous liquids: shapes, wakes and velocities. *Journal of Fluid Mechanics*, 105:61–85.

Briley, W. R. and McDonald, H. (2001). An overview and generalization of implicit navier–stokes algorithms and approximate factorization. *Computers & fluids*, 30(7):807–828.

Brill, J. P. et al. (1987). Multiphase flow in wells. *Journal of petroleum technology*, 39(01):15–21.

Darley, H. C. and Gray, G. R. (1988). *Composition and properties of drilling and completion fluids*. Gulf Professional Publishing.

Edwards, J. R. (1997). A low-diffusion flux-splitting scheme for navier-stokes calculations. *Computers & Fluids*, 26(6):635–659.

Evje, S. and Fjelde, K. K. (2002). Hybrid flux-splitting schemes for a two-phase flow model. *Journal of Computational Physics*, 175(2):674 – 701.

Fahad Matovu, Heinz Preisig, J. M. (2014). Drift-flux models.

Flatabø, G. Ø., Torsvik, A., Oltedal, V. M., Bjørkvik, B., Grimstad, A.-A., Linga, H., et al. (2015). Experimental gas absorption in petroleum fluids at hpht conditions. In *SPE Bergen One Day Seminar*. Society of Petroleum Engineers.

Galves, L. V., Gandelman, R. A., and Martins, A. L. (2014). Impact of gas solubility on kick detection in n-paraffin based drilling fluids.

Griffith, P. et al. (1984). Multiphase flow in pipes. *Journal of petroleum technology*, 36(03):361–367.

Hauge, E. (2013). Automatic kick detection and handling in managed pressure drilling systems.

Hauge, E., Godhavn, J.-M., Stamnes, Ø. N., and Aamo, O. M. (2012). A dynamic model of percolating gas in an open well-bore. In *7th Vienna Conference on Mathematical Modelling (MATHMOD), Proceedings, Vienna, Austria, February*, volume 15, page 17.

Health and Safety Laboratory, U. O. D. I. (2000). "drilling fluids composition and use within the uk offshore drilling industry.

Houwen, O., Geehan, T., et al. (1986). Rheology of oil-base muds. In *SPE Annual Technical Conference and Exhibition*. Society of Petroleum Engineers.

Hua, J. and Lou, J. (2007). Numerical simulation of bubble rising in viscous liquid. *Journal of Computational Physics*, 222(2):769–795.

Johnson, A., Cooper, S., et al. (1993). Gas migration velocities during gas kicks in deviated wells. In *SPE Annual Technical Conference and Exhibition*. Society of Petroleum Engineers.

Johnson, A., Rezmer-Cooper, I., Bailey, T., McCann, D., et al. (1995). Gas migration: Fast, slow or stopped. In *SPE/IADC Drilling Conference*. Society of Petroleum Engineers.

Johnson, A. and White, D. (1993). Experimental determination of gas migration velocities with non-newtonian fluids. *International journal of multiphase flow*, 19(6):921–941.

Johnson, A., White, D., et al. (1991). Gas-rise velocities during kicks. *SPE drilling engineering*, 6(04):257–263.

Kaasa, G.-O., Stamnes, Ø. N., Aamo, O. M., Imsland, L. S., et al. (2012). Simplified hydraulics model used for intelligent estimation of downhole pressure for a managed-pressure-drilling control system. *SPE Drilling & Completion*, 27(01):127–138.

Lapuerta, M., Agudelo, J. R., Prorok, M., and Boehman, A. L. (2012). Bulk modulus of compressibility of diesel/biodiesel/hvo blends. *Energy & Fuels*, 26(2):1336–1343.

Li, S. and Li, H. (2016). Spatial discretization.

Lyons, William C., P. G. J. (2005). Elsevier.

Mohebbi, V. and Mosayebi Behbahani, R. (2015). Measurement of mass transfer coefficients of natural gas mixture during gas hydrate formation. *Iranian Journal of Oil & Gas Science and Technology*, 4(1):66–80.

Monteiro, E. N., Ribeiro, P. R., Lomba, R. F. T., et al. (2008). Study of the pvt properties of gas-synthetic drilling fluid mixtures applied to well control operations. In *SPE Annual Technical Conference and Exhibition*. Society of Petroleum Engineers.

O'Bryan, P., Bourgoyne, A., et al. (1989). Methods for handling drilled gas in oil-based drilling fluids. *SPE Drilling Engineering*, 4(03):237–246.

O'Bryan, P., Bourgoyne Jr, A., et al. (1987). Swelling of oil-base drilling fluids due to dissolved gas. In *SPE Annual Technical Conference and Exhibition*. Society of Petroleum Engineers.

O'Bryan, P. L., Bourgoyne Jr, A. T., Monger, T. G., Kopcso, D. P., et al. (1988). An experimental study of gas solubility in oil-based drilling fluids. *SPE drilling engineering*, 3(01):33–42.

of Drilling Contractors (IADC), I. A. (2015). International Association of Drilling Contractors (IADC).

Orell, A. and Rembrand, R. (1986). A model for gas-liquid slug flow in a vertical tube. *Industrial & engineering chemistry fundamentals*, 25(2):196–206.

Rader, D. W., Bourgoyne Jr, A., Ward, R., et al. (1975). Factors affecting bubble-rise velocity of gas kicks. *Journal of Petroleum Technology*, 27(05):571–584.

Rigzone (2016). How do risers work.

Rommetveit, R., Fjelde, K. K., Aas, B., Day, N. F., Low, E., Schwartz, D. H., et al. (2003). Hpht well control; an integrated approach. In *Offshore Technology Conference*. Offshore Technology Conference.

Sadiku, M. and Obiozor, C. (2000). A simple introduction to the method of lines. *International Journal of Electrical Engineering Education*, 37(3):282–296.

Schlumberger (2015). Schlumberger, oilfield glossary.

Skalle, P. (2010). *Drilling fluid engineering*. Bookboon.

Skalle, P., Podio, A., Tronvoll, J., et al. (1991). Experimental study of gas rise velocity and its effect on bottomhole pressure in a vertical well. In *Offshore Europe*. Society of Petroleum Engineers.

Sparks, C. P. (2007). PennWell.

Subramanian, R. S., Balasubramaniam, R., and Wozniak, G. (2002). 6 fluid mechanics of bubbles and drops. *Physics of Fluids in Microgravity*, page 149.

Swanson, B., Gilvary, B., McEwan, F., et al. (1988). Experimental measurement and modeling of gas solubility in invert emulsion drilling fluids explains surface observations during kicks. In *European Petroleum Conference*. Society of Petroleum Engineers.

Tarvin, J. et al. (1994). Gas rises rapidly through drilling mud. In *SPE/IADC Drilling Conference*. Society of Petroleum Engineers.

Tarvin, J., Walton, I., Wand, P., White, D., et al. (1991). Analysis of a gas kick taken in a deep well drilled with oil-based mud. In *SPE Annual Technical Conference and Exhibition*. Society of Petroleum Engineers.

Thomas, D. C., Lea Jr, J. F., Turek, E., et al. (1984). Gas solubility in oil-based drilling fluids: Effects on kick detection. *Journal of petroleum technology*, 36(06):959–968.

Toro, E. F. (2009). Flux vector splitting methods. In *Riemann Solvers and Numerical Methods for Fluid Dynamics*, pages 265–291. Springer.

Udegbunam, J. E., Fjelde, K. K., Evje, S., Nygaard, G., et al. (2015). On the advection-upstream-splitting-method hybrid scheme: A simple transient-flow model for managed-pressure-drilling and underbalanced-drilling applications. *SPE Drilling & Completion*, 30(02):98–109.

Van Leer, B. (1982). Flux-vector splitting for the euler equations. In *Eighth international conference on numerical methods in fluid dynamics*, pages 507–512. Springer.

Vazquez, M., Beggs, H. D., et al. (1980). Correlations for fluid physical property prediction. *Journal of Petroleum Technology*, 32(06):968–970.

White, D., Walton, I., et al. (1990). A computer model for kicks in water-and oil-based muds. In *SPE/IADC Drilling Conference*. Society of Petroleum Engineers.

Whitson, C. H., Brulé, M. R., et al. (2000). *Phase behavior*. Henry L. Doherty Memorial Fund of AIME, Society of Petroleum Engineers.

Yu, T., Zhang, H.-Q., Li, M., Sarica, C., et al. (2010). A mechanistic model for gas/liquid flow in upward vertical annuli. *SPE Production & Operations*, 25(03):285–295.

Zhang, L., Yang, C., and Mao, Z.-S. (2010). Numerical simulation of a bubble rising in shear-thinning fluids. *Journal of Non-Newtonian Fluid Mechanics*, 165(11):555–567.

Appendix A

MATLAB Code

This Appendix contains the MATLAB codes that are used in the analysis of the gas migration in the marine risers

A.1 Explicit formulation for WBM

```
% WATER BASED MUD
% EXPLICIT FORMULATION
% COMPARISON OF NO LOSS, FRICTION AND ACCELERATION LOSS
% IDEAL GAS BEHAVIOUR

clear all;
close all;
clc;

% unit conversion factors
ppg2si = 119.8264;      % density - ppg to kg/m3
bbl2si = 0.1589873;     % volume - bbl to m3
cuft2si = 0.02831685;   % volume - cu.ft to m3
psi2si = 6.894757;      % pressure - psia to KPa
ft2si = 0.3048;         % length - ft to m
in2si = 0.0254;         % length - in to m

% Inputs
rhom = 11;                    % mud weight, ppg
mud_den = rhom*ppg2si;        % mud weight, kg/m3
cap = 0.35;                   % annular capacity, bbl/ft
H = 10000;                    % riser height, ft
chokeline_dia = 2;            % diameter of choke line, in
riser_volume = cap*H;         % riser volume, bbl
p_choke = 218.8;              % choke pressure, psi
temp = 194;                  % temperature, F
g = 9.81;                    % acceleration due to gravity, m/s2
mu_mud = 5e-2;               % mud viscosity, Pa.s

%circulation
q_bpump = 2000;                 % velocity of boosted pump, liters/min
q_bpump = q_bpump*0.0062898;    % " " ,bbl/min

% this is only through the choke line. this must be converted to the
% flowrate into the riser using q1A1 = q2A2
% calculate area of riser using capacity
```

```
riser_area = cap*bbl2si/ft2si;     % m2, area
riser_dia = sqrt((4*riser_area)/pi);    % diameter of riser, m
chokeline_area = pi*((chokeline_dia*in2si)^2)/4;
qin_riser = 42;
%when different area(q_bpump*chokeline_area)/riser_area;
Tend = ceil(riser_volume/qin_riser);  % total time to circulate out,min

% Gas parameters
mole_gas = 10;          % amount of methane, Kmol
Mg = 16.04;             % molecular wt of methane, kg/kmol
sg_gas = Mg/28.97;      % specific gravity of gas at surface conditions

% critical parameters of methane
Pc = 667.8;             % critical pressure, psia
Pc = Pc * 6.894757;     % " " ,KPa
Tc = 343;               % critical temperature, R
Tc = Tc/1.8;            % " " ,K
omega = 0.0115;         % acentric factor
R = 8.314;              % universal gas constant (KPa, m3, K, Kg)
temp_eos = (temp + 459.67)/1.8; % temperature in K

%calculate the initial volume of 10kmol methane
guess = 35;         % initial guess for the gas height, ft
err = 1;
while abs(err)>1e-1
    mud_est = H-guess;
    press_est = (0.052*rhom*mud_est + p_choke)*psi2si;  % KPa
    vol_est = mole_gas*R*temp_eos/press_est;            % m3
    vol_est = vol_est/bbl2si;                           % bbl
    ght = vol_est/cap;                                  % ft
    err = (H - ght - mud_est);
    if err>0
        guess = guess - 0.1;
    else
        guess = guess + 0.1;
    end
end
%%
% define the arrays
Tend=Tend*60;
dt=1;
A = zeros(Tend,1);
B = zeros(Tend,1);
G = zeros(Tend,1);
P = zeros(Tend,1);
ref = zeros(Tend,1);

% initial values
G(1) = ght*ft2si; %m
A(1) = H*ft2si - G(1); %m
P(1) = mud_den*g*A(1)+ p_choke*psi2si*1e3;     % pressure in pa
ref(1) = A(1);
fin = 0;

% without friction
soln = zeros(2,1);
time = zeros(Tend,1);
for i =1:Tend %sec
    time(i) = i*dt;
    B(i+1) = B(i) + 2*ft2si;
    ref(i+1) = ref(i) -2*ft2si;

```

```
99      M = H*ft2si - B(i+1);
100     N = P(i)*G(i);
101
102     a = mud_den*g ;
103     b = p_choke*psi2si*1e3 - M*mud_den*g;
104     c = -M*p_choke*psi2si*1e3 + N;
105
106     xx = roots([a b c]);
107     soln(:,1)=xx(:);
108     if isreal(soln(:,1))
109         A(i+1) = max(soln(:,1)); %ft
110     else
111         fin = i-1;
112         break;
113     end
114
115     if A(i+1)>0
116         G(i+1) = H*ft2si - B(i+1) - A(i+1); %ft
117         P(i+1) = mud_den*g*A(i+1)+ p_choke*psi2si*1e3; %psi
118     else
119         fin=i-1;
120         break;
121     end
122 end
123 if fin == 0
124     fin = Tend;
125 end
126
127 A = A./ft2si; %ft
128 B = B./ft2si; %ft
129 G = G./ft2si; %ft
130 P = P./(psi2si*1e3); %psi
131 time = time./60; %min
132 ref = ref./ft2si; %ft
133
134 %%
135 % with friction
136 A1 = zeros(Tend,1);
137 B1 = zeros(Tend,1);
138 G1 = zeros(Tend,1);
139 P1 = zeros(Tend,1);
140 ref1 = zeros(Tend,1);
141 time1 = zeros(Tend,1);
142
143 G1(1) = ght*ft2si; %m
144 A1(1) = (H*ft2si-G1(1));%m
145 ref1(1) = A1(1); %m
146 P1(1) = mud_den*g*A1(1)+ p_choke*psi2si*1e3;     % pressure in Pa
147 fin1 = 0;
148
149 K = (32*mu_mud)/(dt*riser_dia^2);
150
151 soln = zeros(3,Tend);
152
153 for i=1:Tend %sec
154     time1(i) = i*dt;
155     B1(i+1) = B1(i) + 2*ft2si;
156     ref1(i+1) = ref1(i) - 2*ft2si;
157     M = H*ft2si -B1(i+1);
158
159     a = K;
160     b = mud_den*g - 2*A1(i)*K - K*M;
```

```
161     c = K*(A1(i)^2) - M*mud_den*g + 2*K*M*A1(i) + p_choke*psi2si*1e3;
162     d = - K*M*(A1(i)^2) + P1(i)*G1(i) - M*p_choke*psi2si*1e3;
163
164     xx = roots([a b c d]);
165     soln(:,i)=xx(:);
166     y=0;
167     for j=1:3
168         if imag(soln(j,i))~=0
169             y=y+1;
170         end
171     end
172
173     if y>0
174         for k=1:3
175             if imag(soln(k,i))==0
176                 A1(i+1)=soln(k,i);
177             end
178         end
179     else
180         A1(i+1) = max(soln(:,i));
181     end
182
183     if A1(i+1)<0
184           fin1=i-1;
185           break;
186     else
187           G1(i+1) = H*ft2si - B1(i+1) - A1(i+1);
188           P1(i+1) = mud_den*g*A1(i+1)+ p_choke*psi2si*1e3; %pa
189
190     end
191 end
192
193 if fin1 == 0
194     fin1 = Tend;
195 end
196
197 A1 = A1./ft2si; %ft
198 B1 = B1./ft2si; %ft
199 G1 = G1./ft2si; %ft
200 P1 = P1./(psi2si*1e3); %psi
201 time1 = time1./60; %min
202 ref1 = ref1./ft2si; %ft
203
204 %%
205 % with friction and acceleration
206 A2 = zeros(Tend,1);
207 B2 = zeros(Tend,1);
208 G2 = zeros(Tend,1);
209 P2 = zeros(Tend,1);
210 ref2 = zeros(Tend,1);
211 time2 = zeros(Tend,1);
212 fin2 = 0;
213
214 G2(1) = ght*ft2si; %m
215 A2(1) = (H*ft2si-G2(1));%m
216 ref2(1) = A2(1); %m
217 P2(1) = mud_den*g*A2(1)+ p_choke*psi2si*1e3;     % pressure in Pa
218
219 K = (32*mu_mud)/(dt*riser_dia^2);
220 M = mu_mud/(2*(dt^2));
221
222 soln = zeros(3,Tend);
```

```
223
224 for i=1:Tend %sec
225     time2(i) = i*dt;
226     B2(i+1) = B2(i) + 2*ft2si;
227     ref2(i+1) = ref2(i) - 2*ft2si;
228     F = H*ft2si-B2(i+1);
229
230     if i==1
231         N=0;
232     else
233         N=(A2(i) - A2(i-1))^2;
234     end
235
236     S = K+M;
237     T = -M*N + p_choke*psi2si*1e3;
238
239     a = S;
240     b = mud_den*g - 2*A2(i)*S - F*S;
241     c = S*(A2(i)^2) + T - F*mud_den*g + 2*F*S*A2(i);
242     d = - F*S*(A2(i)^2) - F*T + P2(i)*G2(i);
243
244     xx = roots([a b c d]);
245     soln(:,i)=xx(:);
246     y=0;
247     for j=1:3
248         if imag(soln(j,i))~=0
249             y=y+1;
250         end
251     end
252
253     if y>0
254         for k=1:3
255             if imag(soln(k,i))==0
256                 A2(i+1)=soln(k,i);
257             end
258         end
259     else
260         A2(i+1) = max(soln(:,i));
261     end
262
263     if A2(i+1)<0
264           fin2=i-1;
265           break;
266     else
267           G2(i+1) = H*ft2si - B2(i+1) - A2(i+1);
268           P2(i+1) = mud_den*g*A2(i+1)+ p_choke*psi2si*1e3; %pa
269
270     end
271 end
272
273 A2 = A2./ft2si; %ft
274 B2 = B2./ft2si; %ft
275 G2 = G2./ft2si; %ft
276 P2 = P2./(psi2si*1e3); %psi
277 time2 = time2./60; %min
278 ref2 = ref2./ft2si; %ft
279
280 if fin2 == 0
281     fin2 = Tend;
282 end
283 %%
284 % plotting
```

```
285
286 figure(1)
287 hold on
288 plot(time(1:fin),A(1:fin),time1(1:fin1), A1(1:fin1),'b', time2(1:fin2),...
289     A2(1:fin2),'-.m',time1(1:fin1),ref1(1:fin1),'--k','LineWidth',1.25)
290 legend ('without' ,' with-fric' ,'with-fric&acc','Reference')
291 xlabel ('Time, min','FontSize',12)
292 ylabel ('Height of mud above gas bubble, ft','FontSize',12)
293 title ('Variation of mud height above the bubble','FontSize',12)
294
295 figure(2)
296 hold on
297 plot(time(1:fin),G(1:fin),time1(1:fin1), G1(1:fin1),'b',time2(1:fin2),...
298     G2(1:fin2),'-.m','LineWidth',1.25)
299 legend ('without',' with-fric','with-fric&acc','Location','northwest')
300 xlabel ('Time, min','FontSize',12)
301 ylabel ('Height of gas bubble, ft','FontSize',12)
302 title ('Variation of gas bubble height','FontSize',12)
303 %%
304 figure(3)
305 hold on
306 plot(time2(1:fin2),A2(1:fin2),'LineWidth',1.25)
307 xlabel ('Time, min','FontSize',12)
308 ylabel ('Height of mud above gas bubble, ft','FontSize',12)
309 title ('Variation of mud height above the bubble','FontSize',12)
310 grid
311
312 figure(4)
313 hold on
314 plot(time2(1:fin2),G2(1:fin2),'LineWidth',1.25)
315 xlabel ('Time, min','FontSize',12)
316 ylabel ('Height of gas bubble, ft','FontSize',12)
317 title ('Variation of gas bubble height','FontSize',12)
318 grid
```

A.2 Implicit formulation for WBM

```
% WATER BASED MUD
% IMPLICIT CALCULATIONS
% REAL GAS BEHAVIOUR
% COMPARISON OF VARIOUS PRESSURE LOSSES

close all;
clear all;
clc;

global Pc Tc R omega

% Setup inputs
H = 10000;              % riser height, ft
cap = 0.35;             % riser annular capacity, bbl/ft

% Mud parameters
temp = 194;             % temperature, F (90 deg C)
mud_den = 11;           % density of mud, ppg from ref A
sg_oil = 0.7825;        % sp. gravity of C7+ of diesel oil,
                        %which is used as base oil at 90 degc
M_oil = 199;            % molecular weight of DIESEL OIL, kg/kmol
M_water = 18.02;        % mol wt of water, Kg/Kmol
rho_water = 1000;       % density of water at 4 deg c for sp gr
api_oil = (141.5/sg_oil)-131.5; % API gravity of base oil

% Gas parameters
mole_gas = 10;          % amount of methane, Kmol
Mg = 16.04;             % molecular wt of methane, kg/kmol
sg_gas = Mg/28.97;      % specific gravity of gas at 1 atm and 60F
mass_methane = mole_gas*Mg; %kg

% critical parameters of methane
Pc = 667.8;             % critical pressure, psia
Pc = Pc * 6.894757;     % " " ,KPa
Tc = 343;               % critical temperature, R
Tc = Tc/1.8;            % " " ,K
omega = 0.0115;         % acentric factor
R = 8.314;              % universal gas constant (KPa, m3, K, Kg)
temp_sc = 60;           % standard temperature, F
press_sc = 14.7;        % standard pressure, psia

% unit conversion factors
ppg2si = 119.8264;      % density - ppg to kg/m3
bbl2si = 0.1589873;     % volume - bbl to m3
cuft2si = 0.02831685;   % volume - cu.ft to m3
psi2si = 6.894757;      % pressure - psia to KPa
ft2si = 0.3048;         % length - ft to m
in2si = 0.0254;         % length - in to m

% calculating densities in SI units
rho_air = 1.205; % kg/m3 at 1 atm and 60F
rho_mud = mud_den*ppg2si;
rho_oil = sg_oil*rho_water;
rho_gas = sg_gas*rho_air;
mu_mud = 5e-2;              % mud viscosity, Pa.s
% unit convertions for EOS calculations
temp_eos = (temp + 459.67)/1.8;     % temperature in K
pchoke = 218.8; %psi
options = optimset('Display','off');
time = 1:1:5000;
```

```
%%
c = zeros(5000,2);
feval = zeros(5000,2);
exitflag = zeros(5000,1);
for i=1:5000
    B = (i-1)*2;

F2 = @(x) [H - x(1) - x(2) - B, ...
    x(2) - (mole_gas*R*temp_eos*PR_EOS_Z(0.052*mud_den*x(1)*psi2si ...
    + pchoke*psi2si,temp_eos)/(cap*bbl2si*(0.052*mud_den*x(1)*psi2si+...
    pchoke*psi2si)))];

cc0 = [5000,0];
[c(i,:), feval(i,:), exitflag(i)] = fsolve(F2,cc0,options);

if (exitflag(i) ~= 1)||(c(i,1)<0)
    t1 = i-1;
    break;
end
end
%%

cc1 = zeros(5000,2);
exitflag1 = zeros(5000,1);
dp_fric = zeros(5000,1);
vel=2;  %ft/s
dia = 0.48; %m
for i=1:5000
    B = (i-1)*vel;
    if i>1
        dp_fric(i) = (32*mu_mud*(cc1(i,1)*ft2si-...
            cc1(i-1,1)*ft2si)^2)/(dia^2); %Pa
        dpf = dp_fric(i);
    else
        dp_fric(i) = 0;
        dpf = dp_fric(i);
    end
F6 = @(x) [H - x(1) - x(2) - B , ...
    x(2) - (mole_gas*R*temp_eos*PR_EOS_Z(0.052*mud_den*x(1)*psi2si...
    + vel*dpf*1e-3 + pchoke*psi2si,temp_eos)/(cap*bbl2si*...
    (0.052*mud_den*x(1)*psi2si+ pchoke*psi2si + vel* dpf*1e-3)))];

[cc1(i+1,:),~,exitflag1(i)] = fsolve(F6, cc0,options);
if (exitflag(i) ~= 1)||(c(i,1)<0)
    t2 = i-1;
    break;
end
end
%%

cc3 = zeros(5000,2);
exitflag2 = zeros(5000,1);
dp_fric = zeros(5000,1);
dp_acc = zeros(5000,1);

for i=1:5000
    B = (i-1)*vel;
    if i>1
        dp_fric(i) = (32*mu_mud*(cc3(i,1)*ft2si-cc3(i-1,1)...
            *ft2si)^2)/(dia^2); %Pa
        dpf = dp_fric(i);
    else
```

```
123         dp_fric(i) = 0;
124         dpf = dp_fric(i);
125     end
126
127     if i>5
128         dp_acc(i) = (mud_den/2)*abs((cc3(i,1)*ft2si - ...
129             cc3(i-1,1)*ft2si)^2 - (cc3(i-1,1)*ft2si - ...
130             cc3(i-2,1)*ft2si)^2)/(dia^2); %Pa
131         dpa = dp_acc(i);
132     else
133         dp_acc(i) = 0;
134         dpa = dp_acc(i);
135     end
136
137 F8 = @(x) [H - x(1) - x(2) - B , ...
138     x(2) - (mole_gas*R*temp_eos*PR_EOS_Z(0.052*mud_den*x(1)*psi2si ...
139     + pchoke*psi2si + vel*dpf*1e-3 + dpa*1e-3,temp_eos)/(cap*bbl2si...
140  *(0.052*mud_den*x(1)*psi2si+pchoke*psi2si + vel*dpf*1e-3+ dpa*1e-3)))];
141
142
143 [cc3(i+1,:),~,exitflag2(i)] = fsolve(F8, cc0,options);
144 if (exitflag2(i) ~= 1)||(c(i,1)<0)
145     t3=i-1;
146     break;
147 end
148 end
149
150
151 %%
152 plot(time(1:t1)./60, c(1:t1,2))
153 hold on
154 plot(time(4:t2)./60,cc1(4:t2,2))
155 plot(time(4:t3)./60,cc3(4:t3,2),'-.m')
156 legend 'without' 'with' 'acc'
```

A.3 Implicit formulation for OBM

```
% OIL BASED MUD
% IMPLICIT CALCULATIONS
% REAL GAS BEHAVIOUR
% COMPARISON OF VARIOUS PRESSURE LOSSES

close all;
clear all;
clc;

global Pc Tc R omega

% Setup inputs
H = 10000;              % riser height, ft
cap = 0.35;             % riser annular capacity, bbl/ft


% Mud parameters
temp = 194;             % temperature, F (90 deg C)
mud_den = 11;           % density of mud, ppg from ref A
sg_oil = 0.7825;        % sp. gravity of C7+ of diesel oil,
                        % which is used as base oil at 90 degc
M_oil = 199;            % molecular weight of of DIESEL OIL, kg/kmol
M_water = 18.02;        % mol wt of water, Kg/Kmol
rho_water = 1000;   % density of water at 4 deg c for sp gr calcn
api_oil = (141.5/sg_oil)-131.5; % API gravity of base oil

% Gas parameters
mole_gas = 10;          % amount of methane, Kmol
Mg = 16.04;             % molecular wt of methane, kg/kmol
sg_gas = Mg/28.97;      % specific gravity of gas at 1 atm and 60F
mass_methane = mole_gas*Mg; %kg

% critical parameters of methane

Pc = 667.8;             % critical pressure, psia
Pc = Pc * 6.894757;     % " " ,KPa
Tc = 343;               % critical temperature, R
Tc = Tc/1.8;            % " " ,K
omega = 0.0115;         % acentric factor
R = 8.314;              % universal gas constant (KPa, m3, K, Kg)
temp_sc = 60;           % standard temperature, F
press_sc = 14.7;        % standard pressure, psia

% unit conversion factors
ppg2si = 119.8264;      % density - ppg to kg/m3
bbl2si = 0.1589873;     % volume - bbl to m3
cuft2si = 0.02831685;   % volume - cu.ft to m3
psi2si = 6.894757;      % pressure - psia to KPa
ft2si = 0.3048;         % length - ft to m
in2si = 0.0254;         % length - in to m

% calculating densities in SI units
rho_air = 1.205; % kg/m3 at 1 atm and 60F
rho_mud = mud_den*ppg2si;
rho_oil = sg_oil*rho_water;
rho_gas = sg_gas*rho_air;
mu_mud = 5e-2;              % mud viscosity, Pa.s
% unit convertions for EOS calculations
temp_eos = (temp + 459.67)/1.8;     % temperature in K
B0 = 1.7; % assumption - take the average
```

```
pchoke = 234.4; %psi
options = optimset('Display','off');
time = 1:1:5000;

%% bubble point
F1 = @(x) (100*(37.589*exp(3.4446*mole_gas/(mole_gas + ...
    (rho_oil.*x*cap*bbl2si/(M_oil*B0)))))/psi2si - ...
    (0.052*mud_den*(H-x)+pchoke));
C = fsolve(F1,20,options);
mole_liq = C*cap*bbl2si*rho_oil/(M_oil*B0); %Kmol
c = zeros(5000,3);
feval = zeros(5000,3);
exitflag = zeros(5000,1);
for i=1:5000
    B = i*2;

F2 = @(x) [H - x(1) - x(2) - B - C, ...
    x(2) - ((mole_gas - (mole_liq*x(3)/(1-x(3))))*R*temp_eos*...
    PR_EOS_Z(0.052*mud_den*x(1)*psi2si + pchoke*psi2si,temp_eos)/...
    (cap*bbl2si*(0.052*mud_den*x(1)*psi2si+ pchoke*psi2si))), ...
    100*(37.589*exp(3.4446*x(3)))/psi2si - (0.052*mud_den*x(1)+ pchoke)];

cc0 = [9000,100,6];
[c(i,:), feval(i,:), exitflag(i)] = fsolve(F2,cc0,options);

if exitflag(i) == 0
    t1 = i-1;
    break;
end
end
%%
cc1 = zeros(5000,3);
feval1 = zeros(5000,3);
exitflag1 = zeros(5000,1);
dp_fric = zeros(5000,1);
vel=2;  %ft/s
dia = 0.48; %m
for i=1:5000
    B = i*vel;
    if i>1
        dp_fric(i) = (32*mu_mud*(cc1(i,1)*ft2si-cc1(i-1,1)*...
            ft2si)^2)/(dia^2); %Pa
        dpf = dp_fric(i);
    else
        dp_fric(i) = 0;
        dpf = dp_fric(i);
    end
F6 = @(x) [H - x(1) - x(2) - B - C, ...
    x(2) - ((mole_gas - (mole_liq*x(3)/(1-x(3))))*R*temp_eos*...
    PR_EOS_Z(0.052*mud_den*x(1)*psi2si + vel*dpf*1e-3 +...
    pchoke*psi2si,temp_eos)/(cap*bbl2si*(0.052*mud_den*x(1)*psi2si+ ...
    pchoke*psi2si + vel* dpf*1e-3))), ...
    100*(37.589*exp(3.4446*x(3)))/psi2si - (0.052*mud_den*x(1)...
    + pchoke + vel*dpf/psi2si)];

cc2 = [9000, 100, 6];
[cc1(i+1,:),feval1(i,:),exitflag1(i)] = fsolve(F6, cc2,options);
if exitflag1(i) == 0
    t2=i-1;
    break;
end
end
```

```
%%
cc3 = zeros(5000,3);
feval1 = zeros(5000,3);
exitflag1 = zeros(5000,1);
dp_fric = zeros(5000,1);
dp_acc = zeros(5000,1);
vel=2;  %ft/s
dia = 0.48; %m
for i=1:5000
    B = i*vel;
    if i>1
        dp_fric(i) = (32*mu_mud*(cc3(i,1)*ft2si-cc3(i-1,1)*...
            ft2si)^2)/(dia^2); %Pa
        dpf = dp_fric(i);
    else
        dp_fric(i) = 0;
        dpf = dp_fric(i);
    end

    if i>5
        dp_acc(i) = (mud_den/2)*abs((cc3(i,1)*ft2si - cc3(i-1,1)...
    *ft2si)^2 - (cc3(i-1,1)*ft2si - cc3(i-2,1)*ft2si)^2)/(dia^2); %Pa
        dpa = dp_acc(i);
    else
        dp_acc(i) = 0;
        dpa = dp_acc(i);
    end

F8 = @(x) [H - x(1) - x(2) - B - C, ...
    x(2) - ((mole_gas - (mole_liq*x(3)/(1-x(3))))*R*temp_eos*...
    PR_EOS_Z(0.052*mud_den*x(1)*psi2si + pchoke*psi2si + vel*dpf*1e-3...
    + dpa*1e-3,temp_eos)/(cap*bbl2si*(0.052*mud_den*x(1)*psi2si+...
    pchoke*psi2si + vel*dpf*1e-3+ dpa*1e-3))), ...
    100*(37.589*exp(3.4446*x(3)))/psi2si - (0.052*mud_den*x(1)...
    + pchoke +vel*dpf/psi2si+ dpa/psi2si)];
cc2 = [5000, 100, 6];
[cc3(i+1,:),feval1(i,:),exitflag1(i)] = fsolve(F8, cc2,options);
if exitflag1(i) == 0
    t3=i-1;
    break;
end
end


%%
figure(1)
plot(time(1:t1-6)./60, c(1:t1-6,2))
hold on
plot(time(6:t2-6)./60,cc1(6:t2-6,2))
plot(time(14:t3-6)./60,cc3(14:t3-6,2),'-.m')
legend 'without' 'with' 'acc'
figure(2)
hold on
plot(time(14:t3-6)./60,cc3(14:t3-6,2),'LineWidth',1.25)
figure(3)
hold on
plot(time(14:t3-6)./60,cc3(14:t3-6,1),'LineWidth',1.25)
```

A.4 Drift Flux model for WBM

```
% DRIFT FLUX MODEL
% WATER BASED MUD SYSTEM

clear all;
close all;
clc;

global nstates ncell ag al rhol0 p0 alphag_out rhog_out alphal_out...
rhol_out p_choke alphag_in rhog_in velg_int dx ...
alphal_in rhol_in vell_int mu_l mu_g g C0 v_slip dia temp total_mole...
MMgas R

ag = 446; %m/s for methane
al = 1000; %m/s for water
rhol0 = 1000; % kg/m3
p0 = 1e5; % reference pressure for rhol0
temp = 90+273; % temperaute, K
R = 8.314;  % universal gas constant (KPa, m3, K, Kg)
g=9.81; %m/s2

depth = 3048; %10000'
C0 = 1.2;
total_mole = 10;   % kmol
cap = 0.35;   %bbl/ft
bbl2si = 0.1589873;
ft2si = 0.3048;
riser_area = cap*bbl2si/ft2si;     % m2, area
dia = 0.1;  %m
MMgas = 16.04; %kg/kmol

ncell = 3;
nstates = 6;
dx = depth/ncell;
plotl = depth:-dx:0;

mu_l = 5e-2; % assumed from ref:T6
mu_g = 1.35e-5;% methane visc at 90C
Tend = 250;

%Initial and boundary condition

p_in = rhol0*g*depth; %Pa
p_choke = 100e5; %Pa

alphag_in = 0.3;
alphal_in = 1-alphag_in;
rhog_in = p_in /ag^2;
rhol_in = rhol0;

alphag_out = 0.8;
alphal_out = 1-alphag_out;
rhog_out = p_choke/ag^2;
rhol_out = rhol0;
v_slip = 0.35*sqrt(g*(rhol0 - rhog_in)*dia/rhol0); % m/s ref:1

alpha_g = alphag_in;
alpha_l = 1-alpha_g;
vel_l = 0.1;
vel_g = (C0*alpha_l*vel_l+v_slip)/(1-C0*alpha_g);
vell_int = vel_l;
```

```
velg_int = vel_g;

%Set up state
x0=[
    alpha_g*rhog_in
    alpha_l*rhol_in
    alpha_g*rhog_in*vel_g+alpha_l*rhol_in*vel_l
    vel_l
    vel_g
    alpha_g
    ];

x_int=x0*ones(1,ncell);

% generate jacobian pattern
II=eye(ncell);
m=diag([1 1 1 0 0 0]);
M=kron(II,m);
M=sparse(M);
Tri=diag(ones(ncell,1)) + diag(ones(ncell-1,1),1)+...
    diag(ones(ncell-1,1),-1);
Jpatt=kron(Tri,ones(nstates));
Jpatt=sparse(Jpatt);
opt=odeset('mass',M,'jpattern',Jpatt,'reltol',1e-12);
[T,xx]=ode15s(@flx,[0 Tend],x_int, opt);

for i=1:length(T)
    [~,UUL(i,:),UUG(i,:),AAL(i,:),AAG(:,i),PP(i,:)] = flx(T(i),xx(i,:)');
end
%%
figure(1)
plot(T,UUL,T,UUG)

title('Plot of time evolution of phase velocities of liquid and gas')
xlabel('Time, s')
ylabel('Phase velocities, m/s')
legend velL-cell:1 velL-cell:2 velL-cell:3 velG-cell:1 ...
    velG-cell:2 velG-cell:3
grid
figure(2)
plot(T,AAL,T,AAG)
title('Plot of time evolution of volume fractions of liquid and gas')
xlabel('Time,s')
ylabel('Volume fractions')
legend \alphaL-cell:1 \alphaL-cell:2 \alphaL-cell:3 ...
    \alphaG-cell:1 \alphaG-cell:2 \alphaG-cell:3
grid
figure(3)
plot(T,PP)
title('Plot of time evolution of pressure')
xlabel('Time, s')
ylabel('Pressure, Pa')
legend Press-cell:1 Press-cell:2 Press-cell:3
grid
```

A.4.1 User defined function for DF - WBM

```
function [xdot,vl,vg,aal,aag,pp]=flx(t,x)
global nstates ncell ag al rhol0 p0 alphag_out rhog_out...
    alphal_out rhol_out p_choke alphag_in rhog_in velg_int dx ...
    alphal_in rhol_in vell_int mu_l mu_g g C0 v_slip dia

```

```
X = zeros(nstates,ncell);
X(:) = x(:);
aag = X(6,:);
aal = 1-aag;
rrhog = X(1,:)./aag;
pp = ag^2*rrhog;
rrhol = rhol0+(pp-p0)/al^2;
vl = X(4,:);
vg = X(5,:);

I = 1:ncell;

a = (vg>0);
b = (vl>0);

ag_aug = [aag alphag_out];
rhog_aug = [rrhog rhog_out];

aghat = a.*ag_aug(I) + (1-a).*ag_aug(I+1);
rhoghat = a.*rhog_aug(I) + (1-a).*rhog_aug(I+1);

al_aug = [aal alphal_out];
rhol_aug = [rrhol rhol_out];

alhat = b.*al_aug(I) + (1-b).*al_aug(I+1);
rholhat = b.*rhol_aug(I) + (1-b).*rhol_aug(I+1);

ppaug = [pp p_choke];

%Gas
gasflux = aghat.*rhoghat.*vg;
gasflux = [alphag_in*rhog_in*velg_int gasflux];
rhs1=-diff(gasflux)/dx; % right hand side 1

%Liquid
liqflux = alhat.*rholhat.*vl;
liqflux = [alphal_in*rhol_in*vell_int liqflux];
rhs2=-diff(liqflux)/dx;

%Momentum
flux_g=aghat.*rhoghat.*vg.*vg;
flux_g=[alphag_in*rhog_in*velg_int*velg_int flux_g];

flux_l=alhat.*rholhat.*vl.*vl;
flux_l=[alphal_in*rhol_in*vell_int*vell_int flux_l];

rhs3=(-diff(flux_g)/dx) + (-diff(flux_l)/dx)+ (-diff(ppaug)/dx)...
-(32*(aal.*vl+aag.*vg).*(mu_l*aal+mu_g*aag)/dia^2)+ g*(X(1,:)+X(2,:));

Xdot=[
    rhs1
    rhs2
    rhs3
    vg.*(1-C0*aag)-(C0*aal.*vl+v_slip); %res1
    X(2,:)-aal.*rrhol; %res2
    X(3,:)-(aghat.*rhoghat.*vg+alhat.*rholhat.*vl) %res3
    ];
xdot=Xdot(:);
end
```

A.5 Drift Flux model for OBM

```
% DRIFT FLUX MODEL
% OIL BASED MUD SYSTEM

clear all;
close all;
clc;

global nstates ncell ag al rhol0 p0 alphag_out rhog_out alphal_out...
rhol_out p_choke alphag_in rhog_in velg_int dx ...
alphal_in rhol_in vell_int mu_l mu_g g C0 v_slip dia temp total_mole...
riser_area MMgas R

ag = 446;
al = 1000;
rhol0 = 782.5; %ref:density of diese
p0 = 1e5;
temp = 90+273; % temperaute, K
R = 8.314;     % universal gas constant (KPa, m3, K, Kg)

depth = 3048;
dia = 0.1;%0.022;
C0 = 1.2;
total_mole = 10;   % kmol
cap = 0.35;
bbl2si = 0.1589873;
ft2si = 0.3048;
riser_area = cap*bbl2si/ft2si; % m2, area
MMgas = 16.04; %kg/kmol

ncell = 3;
nstates = 6;
dx = depth/ncell;
plotl = depth:-dx:0;
g=9.81;

mu_l = 5e-2;
mu_g = 1.35e-5;%5e-6;
Tend = 250;

%Initial and boundary condition

p_in = rhol0*g*depth;%100e5; %Pa
p_choke =100e5;

alphag_in = 0.3;
alphal_in = 1-alphag_in;
% rhog_in = p_in /ag^2;
rhog_in = p_in*1e-3*MMgas/(1.0097*R*temp);
p_in = p_in*1e-6; %MPa
B = (774) + (22.9)*p_in + (0.433)*p_in^2 + (-0.0188)*p_in^3; %MPa
p_in = p_in*1e6; %Pa
B = B*1e6; %Pa
rhol_in = rhol0+((p_in-p0)*rhol0)/B;
% rhol_in = rhol0;
v_slip = 0.35*sqrt(g*(rhol0 - rhog_in)*dia/rhol0); % m/s ref:1;


alphag_out = 0.8;
alphal_out = 1-alphag_out;
rhog_out = p_choke*1e-3*MMgas/(1.0097*R*temp);
```

```
61  rhol_out = rhol0;
62
63  alpha_g = alphag_in;
64  alpha_l = 1-alpha_g;
65  vel_l = 0.1;
66  vel_g = (C0*alpha_l*vel_l+v_slip)/(1-C0*alpha_g);
67
68  vell_int =vel_l;
69  velg_int=vel_g;
70
71
72  %Set up state
73  x0=[
74      alpha_g*rhog_in
75      alpha_l*rhol_in
76      alpha_g*rhog_in*vel_g+alpha_l*rhol_in*vel_l
77      vel_l
78      vel_g
79      alpha_g
80      ];
81
82  x_int=x0*ones(1,ncell);
83
84  % generate jacobian pattern
85  II=eye(ncell);
86  m=diag([1 1 1 0 0 0]);
87  M=kron(II,m);
88  M=sparse(M);
89  Tri=diag(ones(ncell,1)) + diag(ones(ncell-1,1),1)+ ...
90      diag(ones(ncell-1,1),-1);
91  Jpatt=kron(Tri,ones(nstates));
92  Jpatt=sparse(Jpatt);
93  opt=odeset('mass',M,'jpattern',Jpatt,'reltol',1e-12);
94  [T1,xx1]=ode15s(@flxmt,[0 Tend],x_int, opt);
95
96  for i=1:length(T1)
97      [~,UUL1(i,:),UUG1(i,:),AAL1(i,:),AAG1(:,i),PP1(i,:)...
98          ,gasr(i,:)] = flxmt(T1(i),xx1(i,:)');
99  end
100 %Plotting
101 figure(4)
102 plot(T1,UUL1,T1,UUG1)
103 title('Plot of time evolution of phase velocities of liquid and gas')
104 xlabel('Time, s')
105 ylabel('Phase velocities, m/s')
106 legend velL-cell:1 velL-cell:2 velL-cell:3 velG-cell:1 ...
107     velG-cell:2 velG-cell:3
108 grid
109
110 figure(5)
111 plot(T1,AAL1,T1,AAG1)
112 title('Plot of time evolution of volume fractions of liquid and gas')
113 xlabel('Time, s')
114 ylabel('Volume fractions')
115 legend \alphaL-cell:1 \alphaL-cell:2 \alphaL-cell:3 \alphaG-cell:1...
116      \alphaG-cell:2 \alphaG-cell:3
117 grid
118
119 figure(6)
120 plot(T1,PP1)
121 title('Plot of time evolution of pressure')
122 xlabel('Time, s')
```

```
ylabel('Pressure, Pa')
legend Press-cell:1 Press-cell:2 Press-cell:3
grid

figure(7)
plot(T1,gasr)
title('Plot of time evolution of gas exchange rate')
xlabel('Time,s')
ylabel('gas exchange rate, mol/s')
legend Gasrate-cell:1 Gasrate-cell:2 Gasrate-cell:3
grid
```

A.5.1 User defined function for DF - OBM

```
function [xdot,vl,vg,aal,aag,pp,gasrate]=flxmt(t,x)
global nstates ncell rhol0 p0 alphag_out rhog_out alphal_out...
    rhol_out p_choke alphag_in rhog_in velg_int dx ...
    alphal_in rhol_in vell_int mu_l mu_g g C0 v_slip dia ...
    temp total_mole riser_area MMgas R

X = zeros(nstates,ncell);
X(:) = x(:);
aag = X(6,:);
aal = 1-aag;
rrhog = X(1,:)./aag;
pp = (rrhog*R*temp*1.0097/MMgas)*1e-3; %MPa
B = (774) + (22.9)*pp + (0.433)*pp.^2 + (-0.0188)*pp.^3; %MPa
pp = pp*1e6; %Pa
B = B*1e6; %Pa
rrhol = rhol0+((pp-p0).*rhol0)./B;
vl = X(4,:);
vg = X(5,:);

ak = 13.6;
bk = -0.05108;
ck = 12.17;
dk = -0.04063;
ek = -0.01888;
pk = pp*1e-6; %MPa
pbar = pp*1e-5;    % bar
Kc = 1e-4*(ak + bk*temp + ck*pk + dk*pk*temp + ek*(pk.^2));
massfrac_diss = 3e-07*(pbar).^2 + 0.0002*pbar + 0.0068;
mass_liq = rrhol*dx*riser_area;
mass_gas_diss = mass_liq.*massfrac_diss./(1-massfrac_diss);
mass_gas_left = total_mole*MMgas - mass_gas_diss;
diff_massgas = mass_gas_left-mass_gas_diss;
gasrate = Kc.*diff_massgas./(aag*dx);

I = 1:ncell;

a = (vg>0);
b = (vl>0);

ag_aug = [aag alphag_out];
rhog_aug = [rrhog rhog_out];

aghat = a.*ag_aug(I) + (1-a).*ag_aug(I+1);
rhoghat = a.*rhog_aug(I) + (1-a).*rhog_aug(I+1);

al_aug = [aal alphal_out];
rhol_aug = [rrhol rhol_out];

```

```
alhat = b.*al_aug(I) + (1-b).*al_aug(I+1);
rholhat = b.*rhol_aug(I) + (1-b).*rhol_aug(I+1);

ppaug = [pp p_choke];

%Gas
gasflux = aghat.*rhoghat.*vg;
gasflux = [alphag_in*rhog_in*velg_int gasflux];
rhs1=-diff(gasflux)/dx + gasrate;

%Liquid
liqflux = alhat.*rholhat.*vl;
liqflux = [alphal_in*rhol_in*vell_int liqflux];
rhs2=-diff(liqflux)/dx - gasrate;

%Momentum
flux_g=aghat.*rhoghat.*vg.*vg;
flux_g=[alphag_in*rhog_in*velg_int*velg_int flux_g];

flux_l=alhat.*rholhat.*vl.*vl;
flux_l=[alphal_in*rhol_in*vell_int*vell_int flux_l];

rhs3=(-diff(flux_g)/dx) + (-diff(flux_l)/dx)+ (-diff(ppaug)/dx) -...
    (32*(aal.*vl+aag.*vg).*(mu_l*aal+mu_g*aag)/dia^2)+ g*(X(1,:)+X(2,:));

Xdot=[
    rhs1
    rhs2
    rhs3
    vg.*(1-C0*aag)-(C0*aal.*vl+v_slip); %res1
    X(2,:)-aal.*rrhol; %res2
    X(3,:)-(aghat.*rhoghat.*vg+alhat.*rholhat.*vl) %res3
    ];
xdot=Xdot(:);
end
```